Bulk Separation of Binary Gas Mixtures By Pressure Swing Adsorption

by

Mohammad Arshad Sheikh

A Thesis Presented to the

FACULTY OF THE COLLEGE OF GRADUATE STUDIES

KING FAHD UNIVERSITY OF PETROLEUM & MINERALS

DHAHRAN, SAUDI ARABIA

In Partial Fulfillment of the
Requirements for the Degree of

MASTER OF SCIENCE

In

CHEMICAL ENGINEERING

December, 1995

INFORMATION TO USERS

This manuscript has been reproduced from the microfilm master. UMI films the text directly from the original or copy submitted. Thus, some thesis and dissertation copies are in typewriter face, while others may be from any type of computer printer.

The quality of this reproduction is dependent upon the quality of the copy submitted. Broken or indistinct print, colored or poor quality illustrations and photographs, print bleedthrough, substandard margins, and improper alignment can adversely affect reproduction.

In the unlikely event that the author did not send UMI a complete manuscript and there are missing pages, these will be noted. Also, if unauthorized copyright material had to be removed, a note will indicate the deletion.

Oversize materials (e.g., maps, drawings, charts) are reproduced by sectioning the original, beginning at the upper left-hand corner and continuing from left to right in equal sections with small overlaps. Each original is also photographed in one exposure and is included in reduced form at the back of the book.

Photographs included in the original manuscript have been reproduced xerographically in this copy. Higher quality 6" x 9" black and white photographic prints are available for any photographs or illustrations appearing in this copy for an additional charge. Contact UMI directly to order.

UMI

A Bell & Howell Information Company
300 North Zeeb Road, Ann Arbor MI 48106-1346 USA
313/761-4700 800/521-0600

BULK SEPARATION OF BINARY GAS MIXTURES BY PRESSURE SWING ADSORPTION

BY

MOHAMMAD ARSHAD SHEIKH

A Thesis Presented to the

FACULTY OF THE COLLEGE OF GRADUATE STUDIES

KING FAHD UNIVERSITY OF PETROLEUM & MINERALS

DHAHRAN, SAUDI ARABIA

In Partial Fulfillment of the
Requirements for the Degree of

MASTER OF SCIENCE

In

CHEMICAL ENGINEERING

December, 1995

UMI Number: 1378709

UMI Microform 1378709
Copyright 1996, by UMI Company. All rights reserved.

This microform edition is protected against unauthorized
copying under Title 17, United States Code.

UMI
300 North Zeeb Road
Ann Arbor, MI 48103

KING FAHD UNIVERSITY OF PETROLEUM & MINERALS
DHAHRAN, SAUDI ARABIA

This Thesis written by

Mohammad Arshad Sheikh

under the direction of his Thesis Advisor, and approved by his Thesis Committee, has been presented to and accepted by the Dean, College of Graduate Studies, in partial fulfillment of the requirements for the degree of

MASTER OF SCIENCE IN CHEMICAL ENGINEERING

Thesis Committee:

Kevin F. Loughlin

Chairman (Dr. Kevin F. Loughlin)

Co-Chairman (Dr. Ashraf. I. Fatehi)

Mirza Mamin Hassan

Member (Dr. Mirza. M. Hassan)

Dr. Dulaihan K. Al-Harbi
Department Chairman

Dr. Ala H. Rabeh
Dean, College of Graduate Studies

Date : 10.4.96

ACKNOWLEDGMENTS

I will always remain indebted to my thesis committee chairman Dr. Kevin F. Loughlin who has always helped and guided me in his usual cheerful way. He would arrange all the books — chemical engineering or others — I demand throughout my stay at this university.

I cannot overemphasize the amount of gratitude I owe to Dr. Mirza M. Hassan for his advice throughout the course of this research. I am specially thankful to him for his patience in navigating through all those lengthy computer programs and for his making the course on adsorptive separations so interestingly informative.

Thanks are also due to Dr. A. I. Fatehi for his help and guidance. Support of King Fahd University of Petroleum & Minerals for this research is gratefully acknowledged. Also, I thank my friends who would provide me all kinds of support I am ever in need of.

CONTENTS

Acknowledgments..... ii
Contents..... iii
List of Figures..... vi
List of Tables..... x
Thesis Abstract (English)..... xii
Thesis Abstract (Arabic)..... xiii

Chapter 1 INTRODUCTION AND BACKGROUND..... 1

1.1 Pressure Swing Adsorption and Separation of Methane-Nitrogen Mixture..... 1
1.2 A Binary Linear Driving Force Equation..... 5
1.3 Pressure Swing Adsorption Reactor..... 6
1.4 Goals of the Present Research..... 9
References..... 12

Chapter 2 DETERMINATION OF EQUILIBRIUM AND KINETIC PARAMETERS..... 15

2.1 Equilibrium Isotherm by Volumetric Method..... 15
2.2 Kinetic and Equilibrium Data from Chromatography..... 26
2.3 Binary Breakthrough Experiments..... 40
Nomenclature..... 49
References..... 51

Chapter 3 PSA SEPARATION OF METHANE AND NITROGEN..... 52

3.1 Apparatus..... 52
3.2 PSA Cycles..... 57
3.3 Results and Discussion (PSA Experiments)..... 61
3.4 Mathematical Modeling..... 80
3.5 Results and Discussion (PSA Modeling)..... 96
3.6 Conclusion..... 102
Nomenclature..... 105
References..... 107

Chapter 4 MODIFICATION OF THE LDF EQUATION FOR CONCENTRATION DEPENDENT DIFFUSIVITY..... 109

4.1 Theoretical Formulation..... 109
4.2 Comparison of Distributed and Lumped Parameter Models..... 114
4.3 Conclusion..... 146
Nomenclature..... 148
References..... 150

Chapter 5 SIMULATION OF A PRESSURE SWING ADSORPTION REACTOR PROCESS..... 151

5.1 Reaction System..... 151
5.2 Mathematical Modeling..... 152
5.3 Discussion..... 159
Nomenclature..... 164

References..... 167

Chapter 6 CONCLUSIONS AND RECOMMENDATIONS..... 168

6.1 Summary of Conclusions..... 168

6.2 Recommendations for Further Work..... 171

APPENDIX..... 174

A) Calibration factors for flow meters..... 175

B) Typical calculations for a PSA run..... 176

C) Experimental data for PSA runs..... 178

D) Computer programs..... 208

VITAE..... 211

LIST OF FIGURES

Figure		Page
2.1	Schematic diagram of the volumetric apparatus used for the measurement of adsorption equilibria	17
2.2	Virial model for methane and nitrogen on MAXSORB at 300 K	24
2.3	Pure gas isotherms of methane and nitrogen on MAXSORB at 300 K	25
2.4	Schematic diagram of the chromatographic apparatus	27
2.5	Typical output of a chromatographic experiment (Run 3)	30
2.6	First chromatographic moment versus $1/v$ for the two gases	33
2.7	Van Deemter plot for methane and nitrogen on MAXSORB at 300 K	36
2.8	γ versus $1 / v^2$ from the chromatographic experiments	37
2.9	Results of binary breakthrough experiments for Run 1	43
2.10	Results of binary breakthrough experiments for Run 2	44
3.1	A simplified schematic diagram of the PSA apparatus employed in the present work for runs 1 to 17	53
3.2	Valve sequencing and pressure profile for an adsorption bed	56
3.3	A simplified schematic diagram of the PSA apparatus employed for runs 1N to 6N operating with cocurrent depressurization	62
3.4	Effect of pressure ratio on purity and recovery of methane	67
3.5	Effect of pressure ratio on purity and recovery of nitrogen	68
3.6	Effect of cycle duration on purity and recovery of methane	70
3.7	Effect of raffinate velocity on nitrogen in raffinate	71
3.8	Graph between purity and methane recovery of the bottom product	72

3.9 Effect of cocurrent depressurization time on purity of top and bottom products 75
3.10 Effect of cocurrent depressurization time on recovery of methane and nitrogen 76
3.11 Methane recovery in bottom and extract products as a function of the cocurrent depressurization time 78
3.12 Graph of purity versus recovery for modified cycle 79
3.13 Schematic of the Skarstrom cycle used for modeling the PSA process 81
3.14 Gas phase concentration profiles in the beds at the end of cycle at cyclic steady state (Run 2) 98
3.15 Theoretical approach to cyclic steady state with different initial conditions (Run 4) 99
3.16 Theoretical approach to cyclic steady state with frozen solid phase during pressurization and blowdown steps (Run 4) 101
4.1 Comparison of three models for single component uptake. Case 1 117
4.2 Comparison of three models for single component uptake. Case 2 118
4.3 Comparison of three models for single component uptake. Case 3 119
4.4 Comparison of three models for single component uptake. Case 4 120
4.5 Comparison of three models for single component uptake. Case 5 121
4.6 Comparison of three models for single component uptake. Case 6 122
4.7 Comparison of the new binary LDF equation with the detailed model for binary diffusion. Case 7. (1 and 3 detailed model, 2 and 4 new LDF model; species A plots 1 and 2, species B plots 3 and 4) 127
4.8 Comparison of the new binary LDF equation with the detailed model for binary diffusion. Case 8. (1 and 3 detailed model, 2 and 4 new LDF model; species A plots 1 and 2, species B plots 3 and 4) 128
4.9 Comparison of the new binary LDF equation with the detailed

model for binary diffusion. Case 9. (1 and 3 detailed model, 2 and 4 new LDF model; species A plots 1 and 2, species B plots 3 and 4)..... 129

4.10 Comparison of the new binary LDF equation with the detailed model for binary diffusion. Case 10. (1 and 3 detailed model, 2 and 4 new LDF model; species A plots 1 and 2, species B plots 3 and 4)..... 130

4.11 Comparison of the new binary LDF equation with the detailed model for binary diffusion. Case 11. (1 and 3 detailed model, 2 and 4 new LDF model; species A plots 1 and 2, species B plots 3 and 4)..... 131

4.12 Comparison of the new binary LDF equation with the detailed model for binary diffusion. Case 12. (1 and 3 detailed model, 2 and 4 new LDF model; species A plots 1 and 2, species B plots 3 and 4)..... 132

4.13 Comparison of the new binary LDF equation with the detailed model for binary diffusion. Case 13. (1 and 3 detailed model, 2 and 4 new LDF model; species A plots 1 and 2, species B plots 3 and 4)..... 133

4.14 Comparison of the new binary LDF equation with the detailed model for binary diffusion. Case 14. (1 and 3 detailed model, 2 and 4 new LDF model; species A plots 1 and 2, species B plots 3 and 4)..... 134

4.15 Comparison of the new binary LDF equation with the detailed model for binary diffusion. Case 15. (1 and 3 detailed model, 2 and 4 new LDF model; species A plots 1 and 2, species B plots 3 and 4)..... 135

4.16 Comparison of the new binary LDF equation with the detailed model for binary diffusion. Case 16. (1 and 3 detailed model, 2 and 4 new LDF model; species A plots 1 and 2, species B plots

3 and 4)..... 136
4.17 Comparison of the new binary LDF equation with the detailed model for binary diffusion. Case 17. (1 and 3 detailed model, 2 and 4 new LDF model; species A plots 1 and 2, species B plots 3 and 4)..... 137
4.18 Comparison of the new binary LDF equation with the detailed model for binary diffusion. Case 18. (1 and 3 detailed model, 2 and 4 new LDF model; species A plots 1 and 2, species B plots 3 and 4)..... 138
4.19 Comparison of the new binary LDF equation with the detailed model for binary diffusion. Case 19. (1 and 3 detailed model, 2 and 4 new LDF model; species A plots 1 and 2, species B plots 3 and 4)..... 139
4.20 Comparison of the new binary LDF equation with the detailed model for binary diffusion. Case 20. (1 and 3 detailed model, 2 and 4 new LDF model; species A plots 1 and 2, species B plots 3 and 4)..... 140
4.21 Comparison of the new binary LDF equation with the detailed model for binary diffusion. Case 21. (1 and 3 detailed model, 2 and 4 new LDF model; species A plots 1 and 2, species B plots 3 and 4)..... 141
4.22 Comparison of the new binary LDF equation with the detailed model for binary diffusion. Case 22. (1 and 3 detailed model, 2 and 4 new LDF model; species A plots 1 and 2, species B plots 3 and 4)..... 142
5.1 Schematic of the cycle steps used for simulation of PSA reactor process..... 153

LIST OF TABLES

Table		Page
2.1	Properties of MAXSORB activated carbon	19
2.2	Helium calibration of the volumetric apparatus	19
2.3	Isotherm data of methane on MAXSORB at 300 K	21
2.4	Isotherm data of nitrogen on MAXSORB at 300 K	22
2.5	Data on the chromatographic column	28
2.6	Results of chromatographic experiments of methane on MAXSORB at 300 K using helium as the carrier gas	31
2.7	Results of chromatographic experiments of nitrogen on MAXSORB at 300 K using helium as the carrier gas	32
2.8	Parameters on system dynamics from chromatography (Methane)	38
2.9	Parameters on system dynamics from chromatography (Nitrogen)	39
2.10	Data on the breakthrough column	42
2.11	Parametric values used for the solution of the binary breakthrough equations	48
3.1	Summary of results of PSA experiments with Skarstrom cycle	63
3.2	Summary of results of PSA experiments with modified cycle	74
3.3	Parametric values used in the simulations of equilibrium PSA system with Skarstrom cycle	94
3.4	Velocity, cycle time, and other parameters input to PSA simulations	95
3.5	Summary of PSA simulation results (at the end of a cycle) at cyclic steady state	97
4.1	Parameter values used for comparison of different models for single component uptake	116

4.2 Parameter values used for comparison of distributed and lumped parameter models for binary uptake..... 124
4.3 Summary of conclusions from the results of binary uptake cases..... 144
5.1 Parametric values used in the simulations of PSAR..... 160
5.2 Summary of results of PSAR simulation..... 161

ABSTRACT

NAME OF STUDENT	Mohammad Arshad Sheikh
TITLE OF STUDY	Bulk Separation of Binary Gas Mixtures by Pressure Swing Adsorption
MAJOR FIELD	Chemical Engineering
DATE OF DEGREE	December 1995

Pressure swing adsorption separation of a 60% methane-40% nitrogen mixture is carried out on a high-specific-surface area activated carbon MAXSORB in a dual-bed unit. Pure gas isotherms on MAXSORB are linear with an equilibrium separation factor of 3.0 in favor of methane. The kinetics is very rapid for both the gases and, consequently, the current PSA is equilibrium controlled. A Skarstrom cycle and a modified cycle with cocurrent depressurization step are used to obtain a stream of up to 88% methane. Mathematical modeling of the Skarstrom experiments is also performed successfully.

A new linear driving force expression for single-component and binary diffusion is theoretically derived for a concentration dependent diffusivity system. The results of the new equations match fairly well with the exact distributed parameter model solution.

Simulation of a pressure swing adsorption reactor is also performed and the results compared with a catalytic reactor with no adsorption capacity for a sample reaction of ethane dehydrogenation on a cadmium catalyst impregnated on 4A zeolite.

خلاصة الرسالة

اسم الطالب الكامل : محمد أرشد شيخ

عنوان الرسالة : الفصل المجملي لخليط الغاز ثنائي العنصر بالإدمصاص المضغوط المزدوج

التخصص : هندسة كيميائية

تاريخ الشهادة : ديسمبر ١٩٩٥م

تم الفصل بالإدمصاص المضغوط المزدوج لخليط ٦٠٪ ميثان - ٤٠٪ نيتروجين باستخدام الكربون المنشط ماكسورب ذا المساحة السطحية النوعية العالية في وحدة الحوض الثنائي . خط التحاور للغاز النقي على الماكسورب خط خطي بمعامل إتزان ٣٫٠ لصالح الميثان . الكينائيكية سريعة جداً لكلى الغازين لذلك كان الإدمصاص المضغوط المزدوج محكوم بالإتزان . إستعملت حلقة سكاستروم وحلقة أخرى معدله بوحدة نزع الضغط ذات الإتجاه الواحد للحصول على ناتج يحتوي على ٨٨٪ ميثان . أجرى تمثيل رياضي لتجارب السكاستروم بنجاح . هناك علاقة خطية قائدة القوة لوحيد العنصر وثنائي العنصر أشتقت نظرياً لنظام التركيز المتعلق بالإنتشارية . نتائج المعادلات الجديدة تتفق بشكل مرضي مع الحل الدقيق لموديل المقدار المنتشر .

أجريت مماسات لمفاعل الإدمصاص الضاغط المزدوج وتم مقارنة النتائج بمفاعل محفز عديم سعة الإمصاص لتفاعل نزع الهيدروجين من الإيثان فوق سطح حافز الكادميوم العشرّب على الزيولايت 4A .

درجة الماجستير في العلوم

جامعة الملك فهد للبترول والمعادن

الظهران ، المملكة العربية السعودية

ديسمبر ١٩٩٥

CHAPTER 1

INTRODUCTION AND BACKGROUND

Adsorption of fluid molecules on the solid surface results from a change in potential field of the fluid in the vicinity of the solid adsorbent. This gives rise to a solid-fluid interaction which varies with the nature of the fluid and the solid; hence two gases will exhibit different adsorption affinity for an adsorbent. It is this phenomenon of selective adsorption which is utilized in gas separation and purification processes. Reviews of fundamentals of adsorption and adsorption separation processes are given, among many others, by Ruthven (1984) and Yang (1987). In this chapter a brief introduction to the topics discussed in this research thesis is given and the relevant literature or previous work on these topics is summarized.

1.1 PRESSURE SWING ADSORPTION AND SEPARATION OF METHANE-NITROGEN MIXTURE

Pressure Swing Adsorption (PSA) is characterized by adsorption at a high pressure to produce purified raffinate and desorption at a lower pressure to produce purified extract and regenerate the adsorbent bed. The steps involved in a single cycle are pressurization of the bed, adsorption of the strongly adsorbed component at high

pressure, reduction of pressure to a lower level, and desorption of the adsorbed component at the low pressure. This desorption is aided by a further reduction in the gas phase partial pressure of the strongly adsorbed species by passing the nonadsorbed species through the bed. The steps listed above constitute the basic PSA cycle named after Skarstrom. To obtain near continuous products, two beds are operated in tandem; one going through the adsorption and the other through the desorption step. Several modifications of the Skarstrom cycle have been commercialized to enhance the efficiency of PSA separation. Reviews of PSA technology and its applications have been given by Ruthven *et al.*. (1994) and Yang (1987). Extensive research and development in PSA has made the process a relatively well-established tool for trace component removal as well as for fractionation of a gas mixture. A list of general features of a PSA process is presented below as formulated by Ruthven *et al.* (1994). These features to a large extent determine advantages and limitations of the PSA technology for a given separation.

Product purity. Using the most simple PSA cycle the raffinate product can be generally recovered in a very pure form. If an improvement in the extract product purity is desired more complex cycle schemes can be employed.

Recovery. The recovery of purified product in a PSA process is generally low as compared to other separation processes such as distillation. Hence, a PSA process is suitable where the feed is relatively inexpensive so that a lower recovery does not render the overall process infeasible. However, with improved cycle schemes this disadvantage can be largely overcome.

Energy efficiency. The energy efficiency of a PSA process is relatively low as compared to distillation which requires heat whereas PSA requires mechanical energy as pressure.

However, when feed is available at an elevated pressure the energy requirement of a PSA process can be greatly reduced. As a general rule a PSA separation is cheaper than cryogenic distillation.

Scaleup. As opposed to other separation processes the capital cost of a PSA process increases linearly with throughput. Hence a PSA process is economically more feasible than other separation processes up to a certain throughput. However, over the past few years the growth of commercial PSA processes indicates the balance favors PSA except for extremely large throughputs. PSA air separation plants of up to 170 tons of nitrogen per day have been reported (Simonet, 1990).

Pressure of the products. Since the pressure is lowered for desorption in a PSA process the extract product is obtained at a lower pressure while the raffinate is available at the adsorption pressure. Therefore when the extract product is desired at an elevated pressure, additional cost of recompression of the extract is involved.

Blowdown losses. A part of the feed is lost to the blowdown gas when the bed pressure is reduced in preparation for the desorption step. When the raffinate is the desired product this loss may represent a significant reduction in recovery of weak sorbate and a reduction in extract purity.

Methane content of underground natural gas varies from one reservoir to another with nitrogen being the largest impurity. It is therefore desirable to upgrade the methane content of different methane-nitrogen mixtures to achieve a natural gas of pipeline quality. Presently, cryogenic distillation is used in some places to upgrade the natural gas for increased heating value. PSA can be a feasible alternative separation process because

of its economic superiority over cryogenic distillation. Recently, there has been a couple of attempts to effect methane-nitrogen separation through PSA. Ackley (1991) studied kinetic separation of a 50-50% methane-nitrogen mixture with carbon molecular sieves (CMS) as the sorbent in a single-bed process. Using vacuum desorption and a range of cycle times, Ackley obtained up to 79.2% methane at 48.3% recovery as the raffinate product. The highest recovery obtained was 75% with methane purity limited 60.2%. Fatehi (1992) studied the same system using a dual-bed PSA apparatus based on the Skarstrom cycle with 60% methane and 40% nitrogen as the feed. The highest methane concentration achieved in the raffinate product was 75.8%. Besides the usual diffusion and film resistances, an additional barrier resistance was also observed to be present in the CMS.

Both the above attempts do not seem to represent a satisfactory separation due to the following reasons. The difference in kinetic diameters of methane and nitrogen molecules is small which limits the diffusional time constant ratio to a low value. Absolute values of diffusivity for both components in CMS are also low. Furthermore, kinetic and equilibrium effects are in opposition to each other (Farooq and Ruthven, 1992); that is, equilibrium favors the slow diffusing methane. This makes the applicable cycle times limited to a narrow range which is difficult to control practically.

1.2 A BINARY LINEAR DRIVING FORCE EQUATION

Adsorptive separation and purification are carried out in a packed column in most processes. Since the number of interacting parameters in an adsorption process is large, it is common to solve a mathematical model rather than perform a large number of experiments to find an optimal range of operating conditions. This is especially true for the PSA processes. Except for the cases where the local equilibrium theory is applicable it is necessary to solve an equation for mass transfer resistance between fluid and the solid together with material balance equations for an adsorption column. A partial differential equation based on material balance of the adsorbed species in the sorbent particle represents this material balance. The solution of this distributed parameter system gives the adsorbed phase concentration profile in the particle as a function of time. To simplify the solution of the differential equations for the column, an ordinary differential equation, *i.e.*, a lumped parameter approximate equation is usually used instead of the distributed parameter model. This is known as the linear driving force approximation (LDF) and was first suggested by Glueckauf and Coates (1947). Since a knowledge of the solid phase concentration profile is not generally useful in a PSA model, replacing the distributed parameter system by the LDF equation does not reduce the utility of the model results and does have other advantages too. That is, a significant saving in computational effort is achieved and the mass transfer resistances can be linearly added into a single equivalent mass transfer coefficient.

However, the LDF expression as developed by Glueckauf and Coates (1947) is based on a constant diffusivity and is not available for binary systems with coupled isotherms where diffusivity is a strong function of sorbate concentration. Using single component LDF equations for such binary systems reduces the model accuracy. These disadvantages preclude the use of the Glueckauf LDF equation for most kinetically controlled bulk PSA separation processes. The alternative is to use the full pore diffusion model, *i.e.*, the binary diffusion partial differential equations given by Round *et al.* (1966) who have used chemical potential gradient as the driving force for adsorptive mass transfer. Complete PSA models using this approach have been given by Yang and Doong(1985), Farooq and Ruthven (1991), and Farooq *et al.* (1993). Derivation of a new binary LDF equation with concentration dependent diffusivity will combine the advantages of computational efficiency of an LDF equation and accuracy of a variable diffusivity model

1.3 PRESSURE SWING ADSORPTION REACTOR

In recent years, the idea of combined reaction and separation has gained popularity due to its economic attractiveness. Practical applications of the concept are well known in the field of reactive distillation and membrane reactors (Fogler, 1992) and chromatographic reactors (Petroulas *et al.*, 1985). Recently there has been some interest in combining PSA with chemical reaction. With a better understanding and relatively well established mathematical modeling of PSA processes the idea of combining chemical

reaction and physical adsorption has attracted some attention. There are many advantages to such a coupling of adsorptive separation and catalytic chemical reaction as compared to conventional chemical reactors. The products of the desired forward reaction can be removed from the reaction zone by adsorption on a solid thus enhancing the conversion by suppressing the backward reaction step. This allows the chemical reaction to run at a lower temperature for a given equilibrium conversion or achieve a higher conversion for a given reaction temperature. Furthermore, separation of the reaction products can be effected in the hybrid Pressure Swing Adsorption Reactor (PSAR) which makes the process economically favorable.

In practice a PSA system of any configuration and cyclic steps can be coupled with chemical reaction. For example, sections of active catalyst and selective adsorbent may follow each other or PSA beds may be filled with a mixture of catalyst and adsorbent.

Pressure swing adsorption with chemical reaction is a field of recent interest and there is a paucity of experimental results on the process. Only a very few theoretical and modeling studies have been performed which are briefly reviewed here. The first theoretical investigation of a PSAR system seems to have been carried out by Vaporciyan and Kadlec (1987). They considered a single rapid PSA column filled with a mixture of adsorbent and catalyst with extremely fast reaction and instantaneous adsorption equilibrium and concluded that a PSAR system operates between the two extreme limits of a pure PSA system or a pure reactor system. Later on, they reported some experimental

results (Vaporciyan and Kadlec, 1989) using platinum/alumina beads as the catalyst and 5A zeolite as the adsorbent in a rapid PSA process for oxidation of carbon monoxide. They found that under certain operating conditions equilibrium yields higher than a conventional packed bed reactor could be achieved. Another mathematical modeling attempt has been reported by Lu and Rodrigues (1994). They considered catalytic dehydrogenation of ethane on a supported 4A catalyst and studied the effect of various parameters and showed that a PSAR system gives better conversion than a simple packed bed reactor. They used an equilibrium model for adsorption (*i.e.*, no mass transfer resistance) as well as for the reaction with an axially dispersed plug flow model for a single bed PSAR. Kirkby and Morgan (1994) used the method of characteristics to solve their model equations for cases of hypothetical reactions.

In a recent publication (Alpay *et al.*, 1995) experimental efforts to find a suitable adsorbent for dehydrogenation of methylcyclohexane to toluene on Pt/Al_2O_3 catalyst have been reported. The authors have also given a detailed account of some theoretical aspects of the PSAR process and have qualitatively compared a PSAR with chromatographic and membrane reactor systems.

1.4 GOALS OF THE PRESENT RESEARCH

This research thesis has three basic goals. First, to determine the extent to which methane purity and recovery can be achieved with 60% methane and 40% nitrogen mixture as feed using a pressure swing adsorption process. The adsorbent is a high surface area activated carbon (generic name MAXSORB) and both Skarstrom cycle and a modified Skarstrom cycle are used. Secondly, a binary linear driving force expression is developed using the gradient of chemical potential as the driving force for diffusion. Thirdly, modeling simulation of a pressure swing adsorption reactor for a dual-bed, four-step process is carried out. Below, a brief discussion of each of these goals is presented.

As noted in section 1.1 there is need of a better PSA process for methane and nitrogen separation. Due to its active polarizability methane is adsorbed in priority to nonpolar nitrogen on all commercially available sorbents. Kinetic separation of the methane-nitrogen mixtures has not been very successful. The present research explores the option of obtaining enriched methane as the extract product using activated carbon as the adsorbent. As indicated in section 1.1, PSA can be used to obtain purified extract product if proper modifications in the cycle are made. Many successful attempts have been reported in the literature for obtaining the extract as the desired product (Yang and Doong, 1985 and Cen and Yang, 1986). In these works a hydrogen-methane and a carbon monoxide-methane mixture were separated on active carbon. Both extract and the raffinate

were obtained as high purity (90% +) and high recovery (~ 85%) streams using a modified Skarstrom cycle and vacuum desorption.

In the present work a new high specific surface area (2200 m^2/g), high capacity activated carbon MAXSORB (by Kansai Coke and Chemical Company, Japan) is utilized. An account of synthesis procedure and adsorption characteristics of MAXSORB has been given by Otowa *et al.* (1993). Properties of MAXSORB and results of sorption and diffusion of methane and nitrogen will be given in the next chapter. The volumetric method is applied to determine the equilibrium isotherms of the two components. To determine the kinetic parameters for methane and nitrogen on MAXSORB, pulse chromatography and breakthrough curve analysis are employed. A 60-40 % methane-nitrogen mixture is used as the feed in a dual-bed PSA apparatus. Different values of cycle time and adsorption pressure are employed with desorption at the atmospheric pressure. Two types of cycles are used: (*i*) Skarstrom cycle, and (*ii*) a modified Skarstrom cycle comprised of six steps with cocurrent depressurization prior to the countercurrent blowdown.

The second objective of this work is to derive a binary linear driving force (LDF) equation and extend it to the binary diffusion case taking into account the concentration dependence of diffusivity using chemical potential gradient as the driving force for diffusion. This is important for binary systems for which the concentration dependence of diffusivity is more pronounced as the uptake rate of a component is influenced by the presence of each of the two components. The new binary LDF equation, a lumped

parameter model, is compared to the exact distributed parameter model of Round *et al.* (1966) for binary diffusion in a sphere. The range of applicability of the model is investigated, for different step sizes of the sorbate concentration for both codiffusion and counterdiffusion.

The third objective of this work is to model a two-bed PSAR process with a reversible catalytic dehydrogenation reaction. A comparison of performance of a PSAR with a conventional packed bed reactor is also carried out. As indicated above, a single-bed PSAR process has been modeled by some investigators; but there is no attempt in the literature to simulate a dual-bed pressure swing adsorption reactor process. Lu and Rodrigues (1994) have used instantaneous adsorption equilibrium in their axially dispersed plug flow model for a catalytic dehydrogenation reaction. In the current research mass transfer resistance has been added to the catalytic dehydrogenation reaction of Lu and Rodrigues (1994) and a dual-bed process has been modeled with realistic parametric values.

References

Ackley, M. W., Separation of Nitrogen and Methane by Adsorption: Pressure Swing Adsorption Modelling, PhD Dissertation, University of New York at Buffalo, USA, 1991.

Alpay, E., D. Chatsiriwech, L. S. Kreshenbaum, C. P. Hull and N. F. Kirkby, Combined Reaction and Separation by Pressure Swing Adsorption, *Chem. Eng. Sci.*, 49, 5845-5864, 1995.

Cen, P. L. and R. T. Yang, Separation of Binary Gas Mixtures into Two High-Purity Products by a New Pressure Swing Cycle, *Sep. Sci. Technol.*, 2, 845-865, 1986.

Farooq, S. and D. M. Ruthven, Numerical Simulation of a Kinetically Controlled Pressure Swing Adsorption Bulk Separation Process Based on a Diffusion Model, *Chem. Eng. Sci.*, 46, 2213-2229, 1991.

Farooq, S. and D. M. Ruthven, Effect of Equilibrium Selectivity in a Kinetically controlled PSA Separation, *Chem. Eng. Sci.*, 47, 2093-2094, 1992.

Farooq, S., M. N. Rathor and K. Hidajat, A Predictive Model for a Kinetically Controlled Pressure Swing Adsorption Separation Process, *Chem. Eng. Sci.*, 48, 4129-4141, 1993.

Fatehi, A. I., Binary Separations by Pressure Swing Adsorption Processes, PhD Dissertation, King Fahd University of Petroleum & Minerals, Dhahran, Saudi Arabia, 1992.

Fogler, H. S., *Elements of Chemical Reaction Engineering*, Prentice Hall, New York, 1992.

Glueckauf, E. and J. I. Coates, Theory of Chromatography. IV. The Influence of Incomplete Equilibrium on the Front Boundary of Chromatograms and on the Effectiveness of Separation, J. Chem. Soc., 1315-1327,1947.

Kirkby, N. F. and J. E. P. Morgan, A Theoretical Investigation of Pressure Swing Reaction, *Trans. I. Chem.*, 72 (A), 541-550, 1994.

Lu, Z. P. and A. E. Rodrigues, Pressure Swing Adsorption Reactors: Simulation of a Three-Step One-Bed Process, *AIChE J*, 40, 1118-1137, 1994.

Otowa, T., R. Tanibata and M. Itoh, Production and Adsorption Characteristics of MAXSORB: High-surface-area Active Carbon, *Gas Sep. Purif.*, 7, 241-245, 1993.

Petroulas, T., R. Aris and R. W. Carr Jr., Analysis and Performance of a Countercurrent Moving-Bed Chromatographic Reactor, *Chem. Eng. Sci.*, 40, 2223-2240, 1985

Round, G. F. , H. E. Habgood and R. Newton, Numerical Analysis of Surface Diffusion in Binary Adsorbed Film, *Sep. Sci.*, 1, 219-244, 1966

Ruthven, D. M., *Principles of Adsorption and Adsorption Processes*, John Wiley, New York, 1984.

Ruthven, D. M., S. Farooq and K. S. Knaebel, *Pressure Swing Adsorption*, VCH, New York 1994.

Simonet, G., referred to in *Chemical Abstracts*, 113: 100346n, 1990.

Vaporciyan, G. G. and R. H. Kadlec, Equilibrium-Limited Periodic Separating Reactors, *AIChE J*, 33, 1334-1343, 1987.

Vaporciyan, G. G. and R. H. Kadlec, Periodic Separating Reactors: Experiments and Theory, *AIChE J*, 35, 831-844, 1989.

Yang, R. T., *Gas Separation by Adsorption Processes*, Butterworths, Boston, 1987.

Yang, R. T. and S. J. Doong, Gas Separation by Pressure Swing Adsorption: A Pore-diffusion Model for Bulk Separation, *AIChE J*, 31, 1829-1842, 1985.

CHAPTER 2

DETERMINATION OF EQUILIBRIUM AND KINETIC PARAMETERS

To design a pressure swing adsorption separation of a gas mixture equilibrium and kinetic data must be available. The commonly used methods to measure adsorption equilibrium and rate parameters are gravimetric, volumetric, and chromatographic. The choice among these methods is based on convenience since precisely the same information can be extracted from each. In this study, system equilibrium and kinetics are measured by the volumetric method. The parameters obtained by the volumetric technique are confirmed using pulse chromatography and breakthrough experiments.

2.1 EQUILIBRIUM ISOTHERM BY VOLUMETRIC METHOD

Volumetric method is the most widely used technique to determine adsorption equilibrium isotherms. Figure 2.1 shows a schematic sketch of the volumetric apparatus used in the present work to determine the isotherm of methane and nitrogen on MAXSORB at a temperature of 300 K. Gas from the cylinder is admitted to chamber B which is isolated from chambers D and E. The volume of chamber B is known to be 982.47 cm^3 (Al Baghli, 1994). Temperature and pressure of the gas in B are measured

and an appropriate equation of state applied to calculate the number of moles of gas contained in B. The valve between B and the gas cylinder is closed and the control valve between chambers B and D is opened for some time and some gas is allowed to enter the chamber D. A weighed and regenerated sample of adsorbent is placed in chamber E, the void volume of which is determined by helium calibration method. Then the valve between chambers D and E is opened and adsorption of the gas takes place until equilibrium is established. From a knowledge of number of moles of gas entered in E and moles of gas present in free volume of E when the equilibrium is established, the number of moles of gas adsorbed are calculated. The procedure is repeated at different pressure levels and an isotherm is measured at a temperature controlled by a thermostat. Further details of the volumetric method for the determination of adsorption equilibrium have been given by Al Baghli (1994). Some properties of MAXSORB activated carbon are listed in Table 2.1.

Adsorbent Regeneration

A weighed adsorbent sample is regenerated to desorb any adsorbed atmospheric gases and moisture. The regeneration is carried out under a vacuum of less than 2×10^{-3} torr at a temperature of 83 °C for a period of 18 hours. This is accomplished by connecting a flask containing a sorbent sample to a vacuum pump (Edwards Model KC-3) and the temperature is controlled by a Thermolyne Furnatrol temperature controller (Model CP-13315). At the end of regeneration, the sample is weighed again and the weight of dry, raw MAXSORB sample determined. Then the sample is transferred to

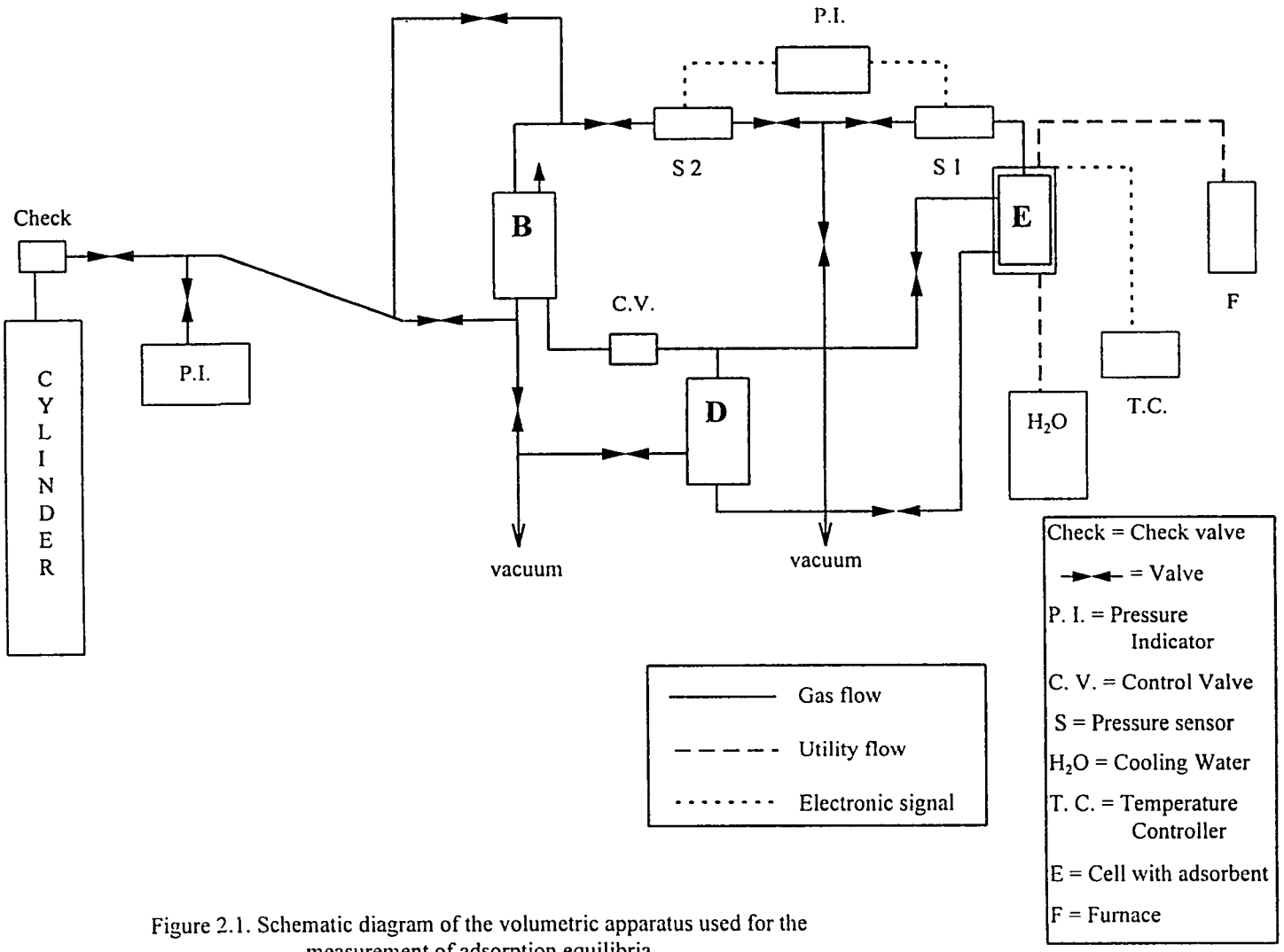

Figure 2.1. Schematic diagram of the volumetric apparatus used for the measurement of adsorption equilibria

chamber E and the chamber is sealed and pressure tested. The adsorbent sample enclosed in E is regenerated again at 85 ^{o}C and 2 x 10^{-3} torr for 10 hours.

Calibration of Volume of chamber E

The volume of chamber D and free volume of chamber E are determined using the helium calibration method. The procedure has been outlined above. From the knowledge of moles of helium admitted to chamber E and under the assumption that no helium is adsorbed, the free volume of E is calculated. The procedure is repeated 8 times at different pressure levels to get a reproducible value of free volume of E within 0.1%. The virial equation of state with virial coefficients taken from Daymond and Smith (1980) is applied to helium at 300 K. Results of the volume calculation by the helium calibration method are summarized as Table 2.2.

Adsorption Isotherm of Methane and Nitrogen

Single gas isotherms of methane and nitrogen are determined separately at a temperature of 300 K. The apparatus is shown in Figure 2.1 and the procedure of isotherm measurement given above. The pressure is measured by two 0-200 psi differential pressure transducers (Model 570 D-200 P-2AI-VIX) and a Datametrics electronic manometer (Type 1014 A) with a null offset adapter (Type 1056). The manometer is accurate up to 0.001 psi. The Redlich-Kwong equation of state is used to calculate the PVT behavior of both methane and nitrogen. Adsorbent regeneration is carried out when the sorbate gas is switched to nitrogen from methane.

Table 2.1. Properties of MAXSORB activated carbon

Appearance	Pellets (cylindrical)
BET surface area *	2250 m^2/g
Total pore volume *	1.15 cm^3/g
Bulk density	0.322 g/cm^3
Particle density	0.604 g/cm^3
Particle diameter	0.115 cm

* data reported by Kansai Coke and Chemical Company

Table 2.2. Helium calibration of the volumetric apparatus

Weight of dry, raw MAXSORB filled in cell E	49.50 g
Regeneration conditions	83 °C, 2 x 10^{-3} mm Hg
Regeneration time	16 hours
Helium calibration temperature	300 K
Volume of chamber B	982.47 cm^3
Volume of chamber D	381.51 cm^3
Free volume of chamber E	616.20 cm^3

The need for the determination of mixed gas isotherm is eliminated because pure component isotherms for both methane and nitrogen are found to be linear in the pressure range of interest for the present PSA separation (0-70 psia).

Results of Volumetric Method

The data of pure gas isotherms of methane and nitrogen is presented in Tables 2.3 and 2.4 respectively. To determine the Henry constant for each gas the virial adsorption isotherm model (Ruthven, 1984) is used:

$$p = \frac{q}{K_H} \exp\left(A_1 q + A_2 q^2 + \ldots\ldots A_n q^n \right) \tag{2.1}$$

This implies that

$$\ln p = \ln q - \ln K_H + \left(A_1 q + A_2 q^2 + \ldots\ldots + A_n q^n \right) \tag{2.2}$$

In the low concentration region, the terms with higher powers of q can be dropped to obtain the following linear form:

$$\ln \frac{p}{q} = -\ln K_H + A_1 q \tag{2.3}$$

Equation (2.3) gives $-\ln K_H$ as the intercept of a plot of ln p/q on the ordinate and q on the abscissa. The units of K_H are mmole per gram of MAXSORB / psia.

Table 2.3. Isotherm data of methane on MAXSORB at 300 K

Methane			
Pressure (psia)	Concentration (mmol/g)	Pressure (psia)	Concentration (mmol/g)
0.0	0.0	28.636	1.527
3.358	0.244	34.770	1.775
6.132	0.418	45.042	2.157
8.458	0.548	56.00	2.601
10.976	0.685	69.090	2.938
13.908	0.845	79.154	3.216
21.560	1.211	88.270	3.461

Table 2.4. Isotherm data of nitrogen on MAXSORB at 300 K

Nitrogen			
Pressure (psia)	Concentration (mmol/g)	Pressure (psia)	Concentration (mmol/g)
0.0	0.0	81.746	1.534
1.82	0.042	93.814	1.684
3.608	0.091	105.510	1.842
10.486	0.258	118.416	1.991
21.748	0.479	126.594	2.084
32.906	0.681	138.968	2.247
56.672	1.053	146.832	2.339
69.236	1.385		

Plots of virial isotherm (2.3) for methane and nitrogen on MAXSORB at 300 K are shown in Figure 2.2 and single gas isotherms of both methane and nitrogen are shown in Figure 2.3. From Figure 2.3 it can be seen that the isotherm for each gas deviates only slightly from linearity in the pressure range of 0 - 75 psia. Hence, up to a pressure of 5 atm — the highest pressure of PSA experiments of chapter 3 — isotherm of each gas is approximated as linear with the following dimensionless Henry's constants calculated from the virial isotherm:

$$K_{CH_4} = 18.8712$$

$$K_{N_2} = 6.2817$$

The above values give an equilibrium separation factor of 3.0 in favor of methane on MAXSORB. Before a PSA separation scheme can be devised, the data on system dynamics must be available. Single gas isotherms of both methane and nitrogen are shown in Figure 2.3 . In the volumetric experiments the rate of uptake of both methane and nitrogen on MAXSORB activated carbon is observed to be so rapid that no reliable information on system dynamics can be extracted. Hence, the kinetics of the system is measured by pulse chromatography and confirmed by breakthrough experiments. The equilibrium isotherm of both the gases determined by the volumetric method is confirmed by pulse chromatography and breakthrough analysis.

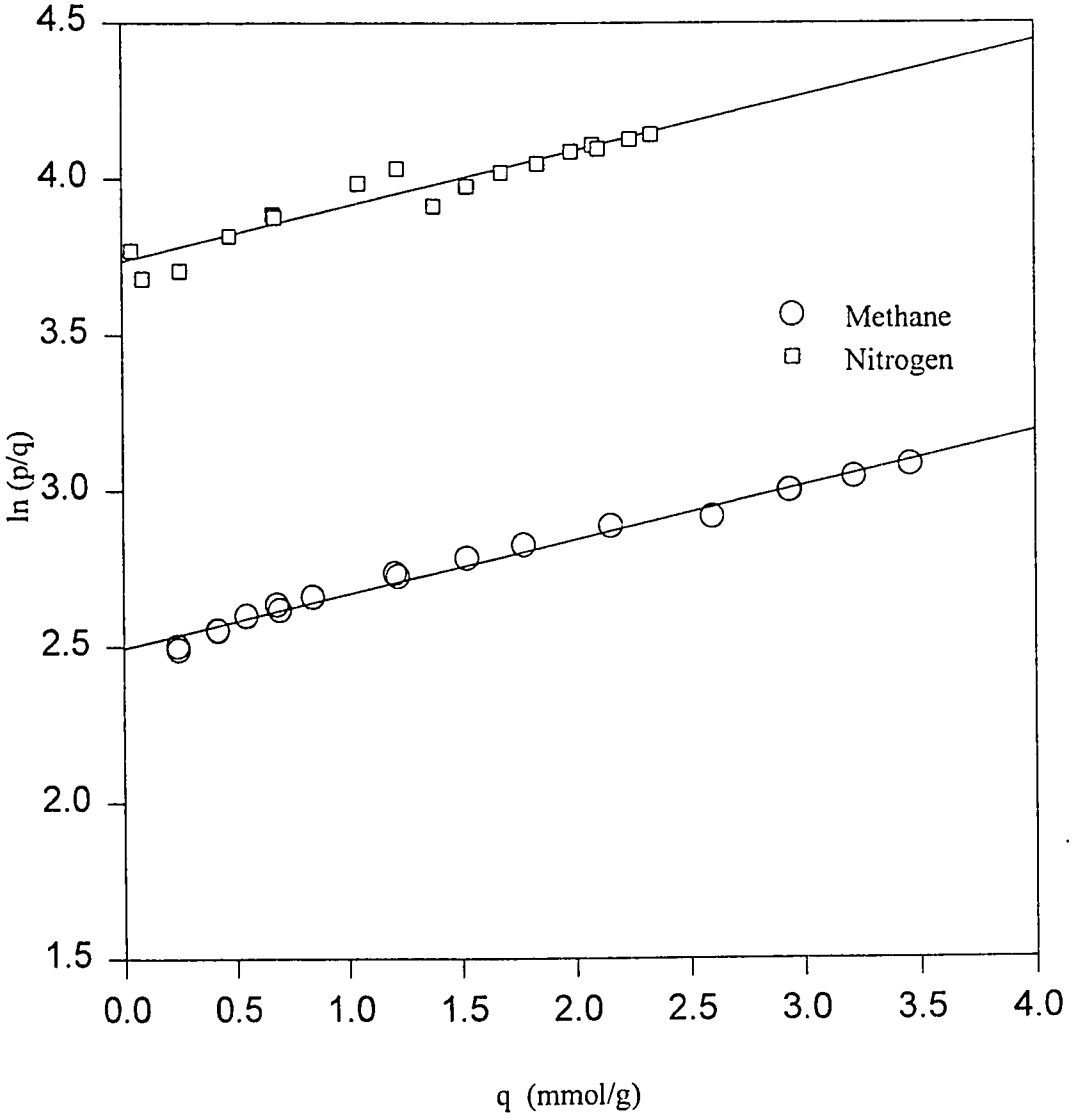

Figure 2.2. Virial model for methane and nitrogen on MAXSORB at 300 K

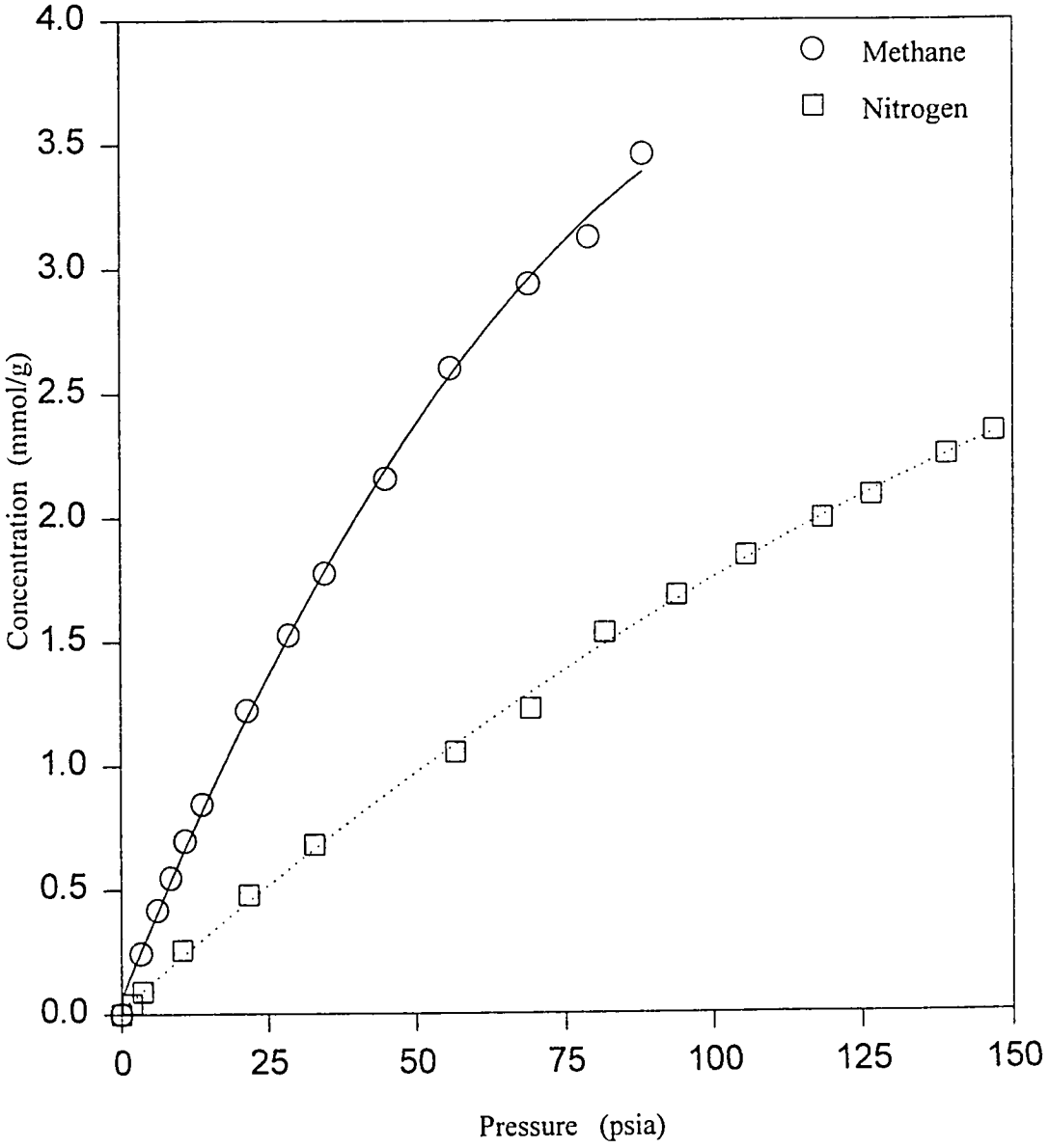

Figure 2.3. Pure gas isotherms of methane and nitrogen on MAXSORB at 300 K

2.2 KINETIC AND EQUILIBRIUM DATA FROM CHROMATOGRAPHY

Experimental Apparatus and Procedure

An account of determination of rate and isotherm data from moments analysis of pulse response and plate theory of chromatography is given by Ruthven (1984) and Kärger and Ruthven (1992). In the present work equilibrium and kinetics parameters are extracted from the first and second moments of pulse chromatographic response respectively. A pulse of sorbate gas is injected into a stream of carrier gas and the mixture is passed through a regenerated adsorbent sample contained in a packed column. At the outlet of the column containing the sample the pulse chromatographic response is recorded on a strip chart recorder.

The experimental setup used in the present work for chromatographic experiments is shown in Figure 2.4. A known weight of MAXSORB is packed in a column placed in an oven for overnight regeneration. Details of chromatographic column are summarized in Table 2.5. The carrier gas used in this work is helium and a pulse of pure methane is injected from the sampling loop and the mixture is fed to the packed column. The outlet stream of the adsorbent bed is passed through a thermal conductivity detector GOWMAC 10-454. A Linseis (Model LS 51) chart recorder is used to record the output of the GOWMAC detector. The recorded response is analyzed for its first and second moments which are matched with the theoretical solution to find equilibrium and kinetic

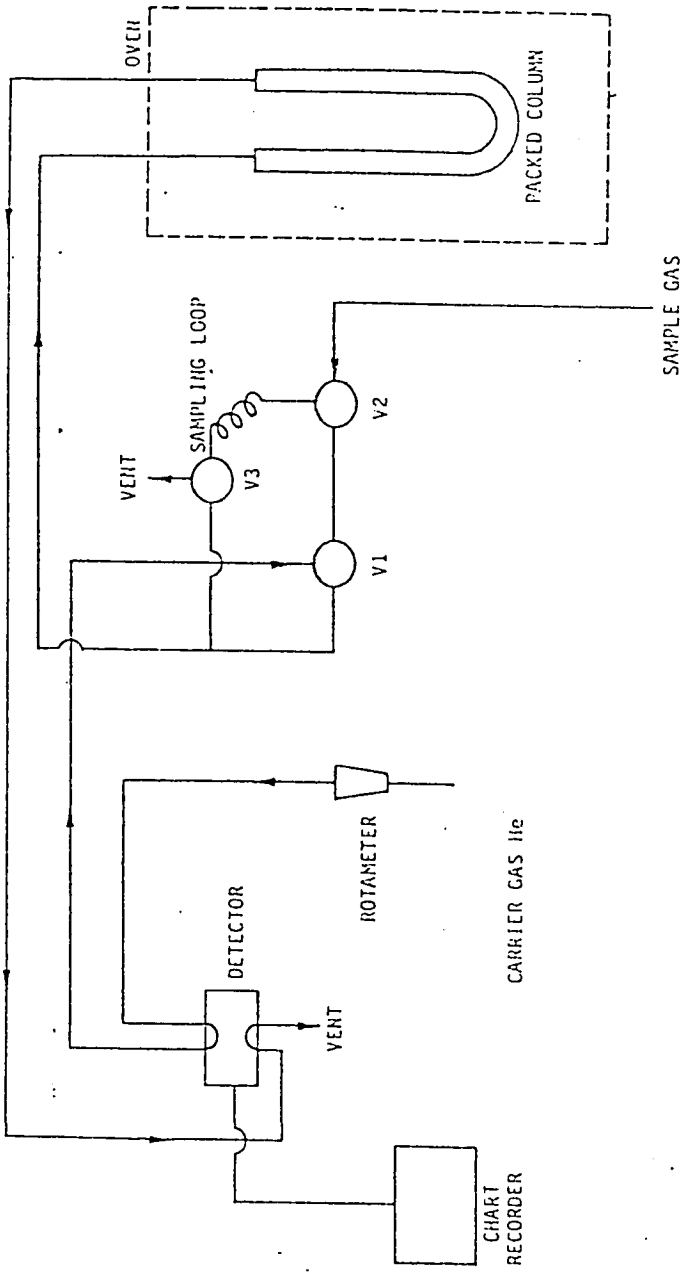

Figure 2.4. Schematic diagram of the chromatographic apparatus

Table 2.5. Data on the chromatographic column

Column length	44.5 cm
Inside diameter	1.04 cm
Weight of MAXSORB	12.40 g
Voidage	0.456
Regeneration temperature	80 °C
Gas for the regeneration	Helium at 1 atm.

parameters. The velocity through the packed column is determined by measuring the volumetric flow rate of the gas after the thermal conductivity detector unit. Several measurements of flow rate are made for each run using a soap bubble meter to ensure that the measured flow rate represents an accurate value. The interstitial velocity through the packed column is obtained by dividing the measured volumetric flow rate by the area and voidage of chromatographic column from Table 2.5. The same procedure is repeated for pure nitrogen at different velocities after the adsorbent is regenerated. Figure 2.5 shows a typical single component chromatographic pulse response for each of methane and nitrogen on MAXSORB at 300 K for one of the several runs for each sorbate.

Moments Analysis

Equilibrium and kinetic parameters of the methane-nitrogen-MAXSORB system are determined by moments analysis of the pulse chromatographic data by equations provided by Ruthven from the work of Haynes and Sarma (1973). The first moment is given by

$$\mu = \frac{L}{v}\left[1 + \left(\frac{1-\varepsilon}{\varepsilon}\right)K\right] \qquad (2.4)$$

For different runs (see Tables 2.6 and 2.7) the interstitial velocity through the packed adsorbent column is varied. The Henry constant K is given by equation (2.4) as the slope of the plot of μ versus 1 / v. Such a plot for the two components is shown in Figure 2.6. The equation for the second moment of a chromatographic response is (provided $K >> \varepsilon$ for the particle)

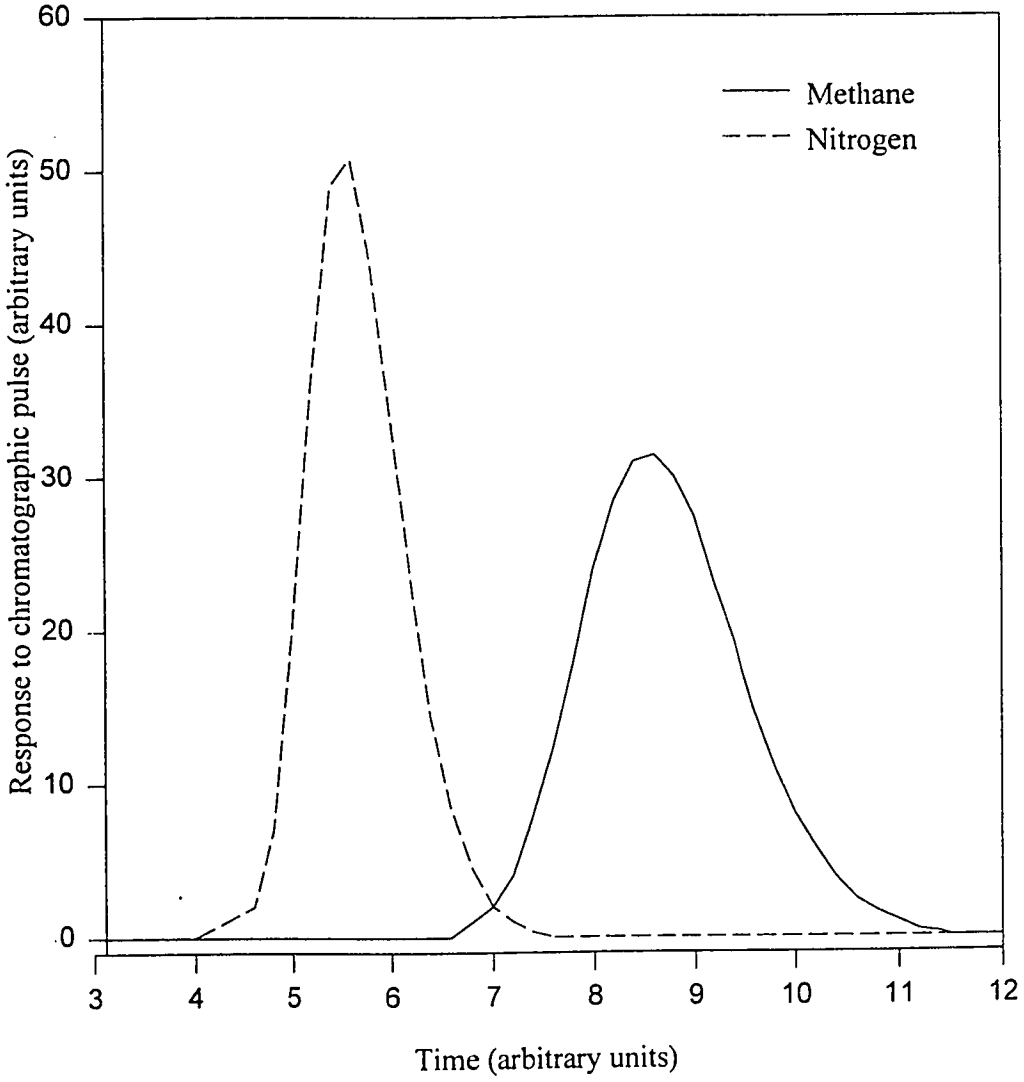

Figure 2.5. Typical output of a chromatographic experiment (Run 3)

Table 2.6. Results of chromatographic experiments of methane on MAXSORB at 300 K using helium as the carrier gas

Run No.	Chart Speed [cm/min]	Volumetric Flow Rate [cm^3 STP/ min]	Interstitial Velocity [cm/sec]	1st Moment [sec]	2nd Moment [sec]	γ [sec]	HETP [cm]
1	1	114.31	4.39	223.0	579.0	0.0524	0.516
2	1	200.68	8.65	129.0	129.0	0.0200	0.346
3	4	199.58	8.60	131.0	138.0	0.0208	0.358
4	4	96.40	4.15	267.0	578.0	0.0436	0.362
5	4	68.25	2.94	373.0	1390.0	0.0758	0.446
6	2	204.63	8.82	130.0	143.0	0.0212	0.374

Table 2.7. Results of chromatographic experiments of nitrogen on MAXSORB at 300 K using helium as the carrier gas

Run No.	Chart Speed [cm/min]	Volumetric Flow Rate [cm^3 STP/ min]	Interstitial Velocity [cm/sec]	1st Moment [sec]	2nd Moment [sec]	γ [sec]	HETP [cm]
1	4	77.96	3.36	119.0	113.0	0.0572	0.354
2	4	296.08	12.8	39.6	10.9	0.0121	0.308
3	4	48.61	2.09	190.0	366.0	0.108	0.452
4	4	107.41	4.63	85.2	50.7	0.0336	0.311
5	4	261.00	11.2	359.0	10.0	0.0154	0.345

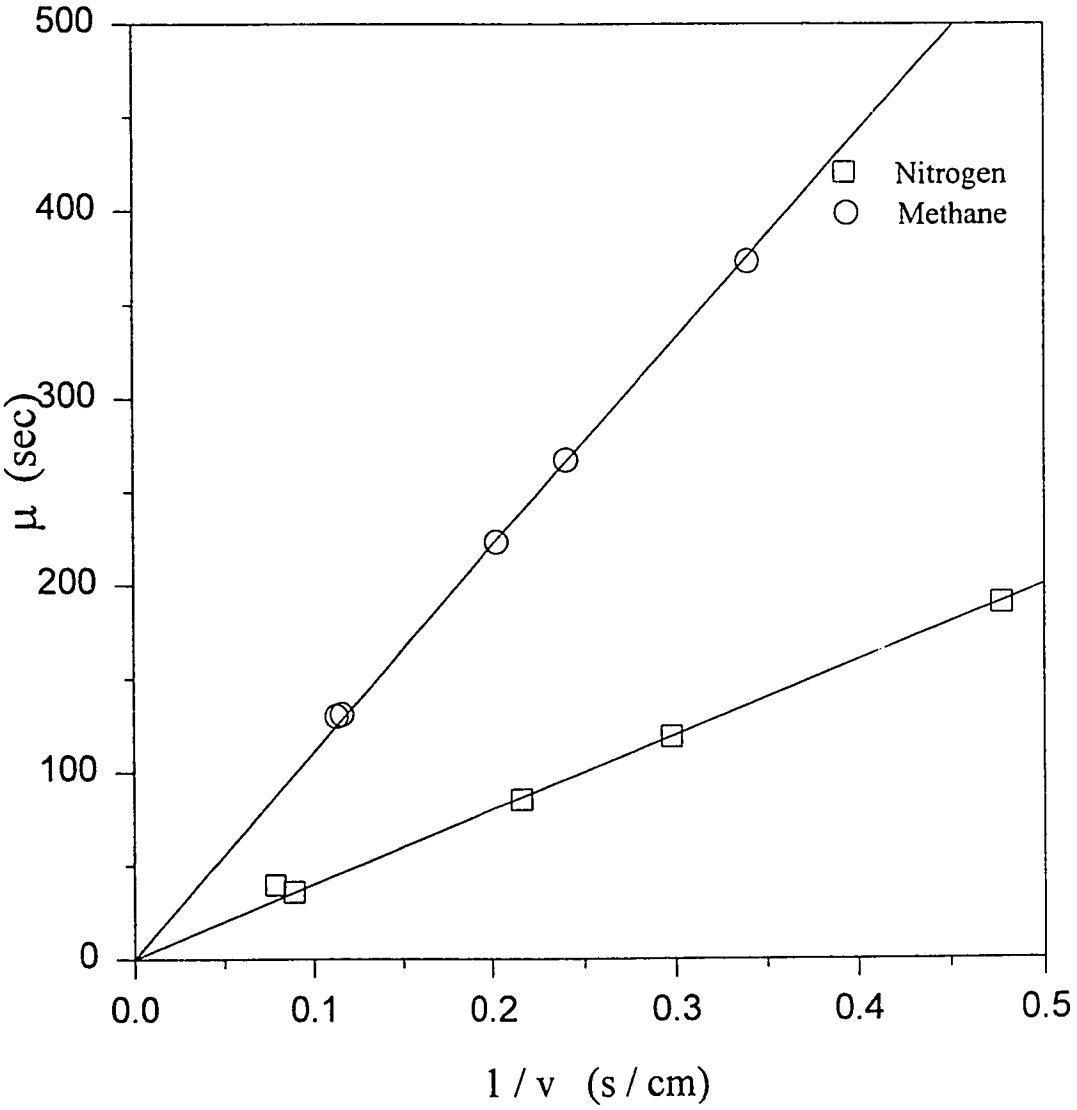

Figure 2.6. First chromatographic moment versus $1/v$ for the two gases

$$\frac{\sigma^2}{2\mu^2} = \frac{D_L}{vL} + \left(\frac{v}{L}\right)\left(\frac{1-\varepsilon}{\varepsilon}\right)\left(\frac{R_p}{3k_f} + \frac{R_p^2}{15\varepsilon_p D_p} + \frac{r_c^2}{15KD_c}\right)\left(1 + \frac{\varepsilon}{(1-\varepsilon)K}\right)^{-2} \qquad (2.5)$$

For the case where the linear driving force expression is used to account for the uptake by the solid phase the equation corresponding to (2.5) is

$$\frac{\sigma^2}{2\mu^2} = \frac{D_L}{vL} + \left(\frac{v}{L}\right)\left(\frac{1-\varepsilon}{\varepsilon}\right)\frac{1}{kK}\left(1 + \frac{\varepsilon}{(1-\varepsilon)K}\right)^{-2} \qquad (2.6)$$

Multiplication of both sides of the above equation by L/v yields

$$\frac{\sigma^2}{2\mu^2}\frac{L}{v} = \frac{D_L}{v^2} + \left(\frac{1-\varepsilon}{\varepsilon}\right)\frac{1}{kK}\left(1 + \frac{\varepsilon}{(1-\varepsilon)K}\right)^{-2} \qquad (2.7)$$

According to this equation the slope of a plot of γ versus $1 / v^2$ is the axial dispersion coefficient, where γ is given by

$$\gamma = \frac{\sigma^2}{2\mu^2}\frac{L}{v} \qquad (2.8)$$

The intercept of this plot corresponds to the total mass transfer resistance

$$\left(\frac{1-\varepsilon}{\varepsilon}\right)\frac{1}{kK}\left(1 + \frac{\varepsilon}{(1-\varepsilon)K}\right)^{-2}$$

Moreover, Van Deemter plots, *i.e.*, the height equivalent to a theoretical plate (HETP) versus the interstitial velocity through the chromatographic column, are

developed for both methane and nitrogen. The Van Deemter equation is the following (Ruthven, 1984)

$$HETP = \frac{\sigma^2}{\mu^2} L = 2\frac{D_L}{v} + 2v\left(\frac{\varepsilon}{1-\varepsilon}\right)\frac{1}{k\,K}\left[1+\frac{\varepsilon}{(1-\varepsilon)K}\right]^{-2} \qquad (2.9)$$

The information on system dynamics is, however, not extracted from plate theory analysis of chromatographic response because the parameters furnished by this method are less accurate than those determined by the moments analysis. The general shape of the Van Deemter plot is seen to be reproduced for the present system (Figure 2.7).

The plots of γ versus $1 / v^2$ are presented in Figure 2.8 and the information on the system dynamics has been summarized in Tables 2.8 and 2.9. The values of Henry's constant predicted by the chromatographic method agree within 7% to the corresponding values determined from the volumetric method (see Section 2.1). The chromatographic Henry constants are larger than the volumetric values for both the components. This may be attributable to an additional delay in the response to the sorbate pulse due to dead volumes present in the chromatographic apparatus. The values of LDF coefficient k from the chromatographic response analysis reflect very low mass transfer resistance for both methane and nitrogen. Although the ratio of the mass transfer coefficients of nitrogen to methane is about 2.8, the absolute value of each mass transfer coefficient is high enough to indicate a near absence of mass transfer resistance. The effect of axial dispersion coefficient, D_L is not expected to be significant if the length to diameter ratio of the PSA column is large with a high interstitial velocity.

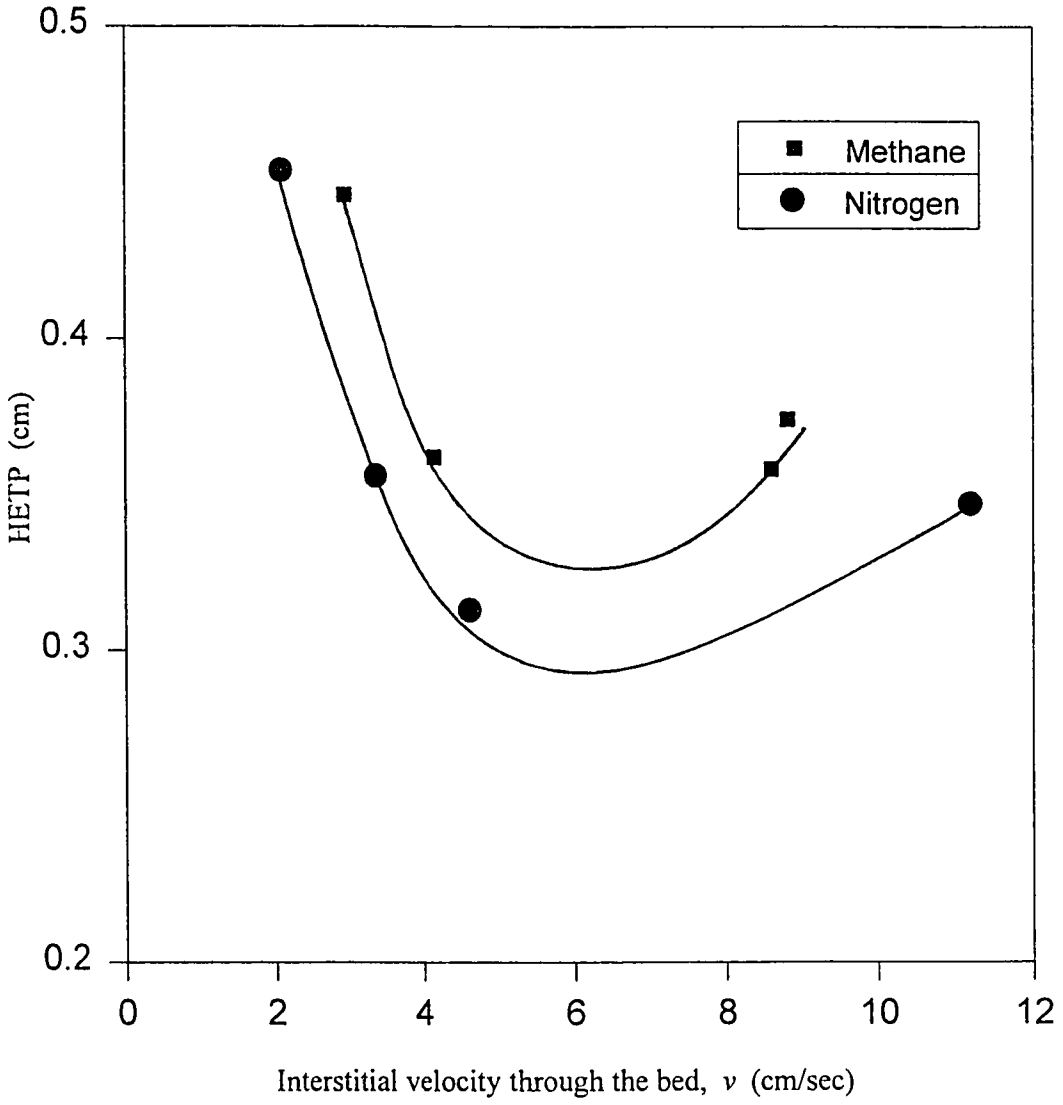

Figure 2.7. Van Deemter plot for methane and nitrogen on MAXSORB at 300 K

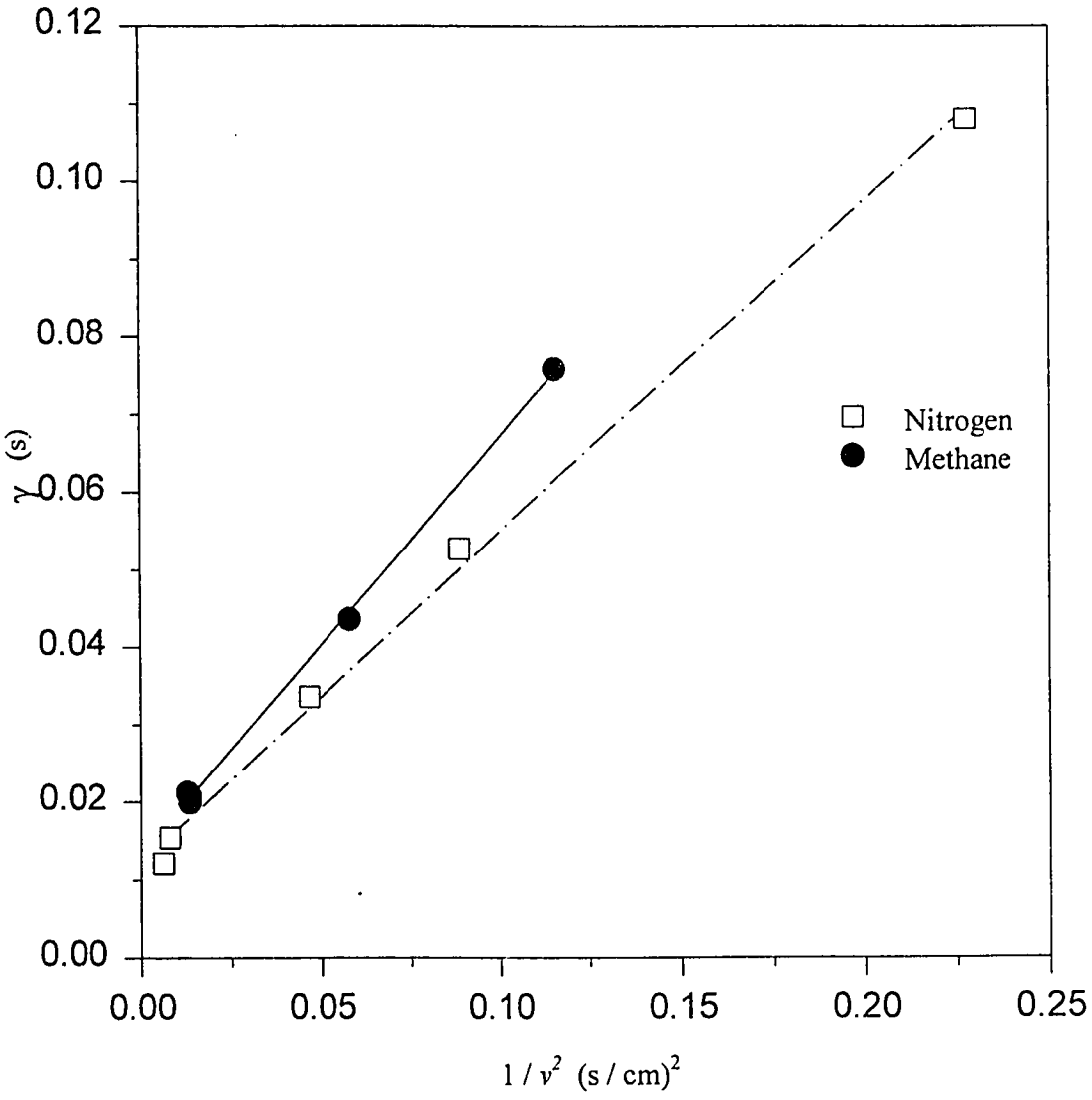

Figure 2.8. γ versus $1 / v^2$ from the chromatographic experiments

Table 2.8. Parameters on system dynamics from chromatography (Methane)

Henry's constant	20.1855
Slope of γ vs. $1 / v^2$ plot	0.5365
Intercept	0.013
D_L (CH_4 in He)	0.5365 cm^2/sec
D_m (CH_4 in He) at 1 atm.	0.6786 cm^2/sec
Bed porosity, ε	0.456
Mass transfer coefficient k_{CH4}	2.947 sec^{-1}

Table 2.9. Parameters on system dynamics from chromatography (Nitrogen)

Henry's constant	6.6867
Slope of γ vs. $1 / v^2$ plot	0.4266
Intercept	0.012
D_L (N_2 in He)	0.4266 cm^2/sec
D_m (N_2 in He) at 1 atm.	0.5050 cm^2/sec
Bed porosity, ε	0.456
Mass transfer coefficient k_{N_2}	8.255 sec^{-1}

With equilibrium constants, LDF constants, and axial dispersion coefficients for the present system of methane and nitrogen on MAXSORB at hand a rough configuration of the PSA separation scheme can be set. The equilibrium isotherm is linear with a separation factor of 3.0 in favor of methane and there are no significant mass transfer resistances. Hence the planned PSA separation is equilibrium-based with methane being the strongly adsorbed component. The methane rich stream is obtained as the extract product. A higher pressure ratio is expected to favor the efficiency of the separation. Moreover, longer cycle times may lead to better adsorption and a better utilization of the bed length. But methane breakthrough in the raffinate product, which leads to a loss in terms of methane recovery, dictates the cycle time. Other aspects of the methane-nitrogen separation are discussed in the next chapter.

2.3 BINARY BREAKTHROUGH EXPERIMENTS

As mentioned earlier in this chapter the results of volumetric and chromatographic method are verified using breakthrough experiments. Hence binary breakthrough experiments are performed with a 60/40 CH_4/N_2 mixture as the feed. The equilibrium and kinetic parameters as determined from the pulse chromatography are used in breakthrough modeling without any adjustments.

In the present study a packed column containing a weighed quantity of MAXSORB is regenerated using a stream of pure helium for 20 hours and is equilibrated with pure nitrogen flowing through the column at a pressure of 1 atm. Table 2.10 lists details of the column used for the breakthrough studies. At time t=0, the feed at the column inlet (z=0) is switched to 60% methane - 40% nitrogen mixture and the output response is measured for its volume percent methane using a SERVOMEX (Series 1400) online paramagnetic methane analyzer. The feed flow rate is measured using a MATHESON (Series 8200) flow indicator and controller. This flow meter is calibrated prior to breakthrough experiments using a soap bubble meter. For precisely the same flow rate of two gases of different compositions, the flow meter does not give the same reading due to a difference in heat capacities of the two gaseous mixtures. Therefore, a composition correction must be applied to all flow rate readings. For the present case the base composition is taken to be 60% methane and 40% nitrogen. Correction factor for any other methane percentage is determined using the conversion factors based on the heat capacity provided by Matheson Gas Products Inc., USA.

When the breakthrough with the 60/40 mixture is complete, the feed gas is switched back to pure nitrogen and flow and composition at the column outlet are measured until pure nitrogen breaks through the column. This completes one run with methane adsorption and nitrogen desorption in the first half (Step A) and the reverse in the second half (Step B). Three such runs are performed experimentally but only two are modeled due to limitations of computer time required for simulation of the low velocity run 3. Figures 2.9 and 2.10 show methane mole fraction versus time for runs 1 and 2.

Table 2.10. Data on the breakthrough column

Column length	51.0 cm
Cross sectional area	9.35 cm^2
Construction	Stainless Steel
Inside diameter	13.45 cm
Weight of MAXSORB	150.0 g
Voidage	0.48

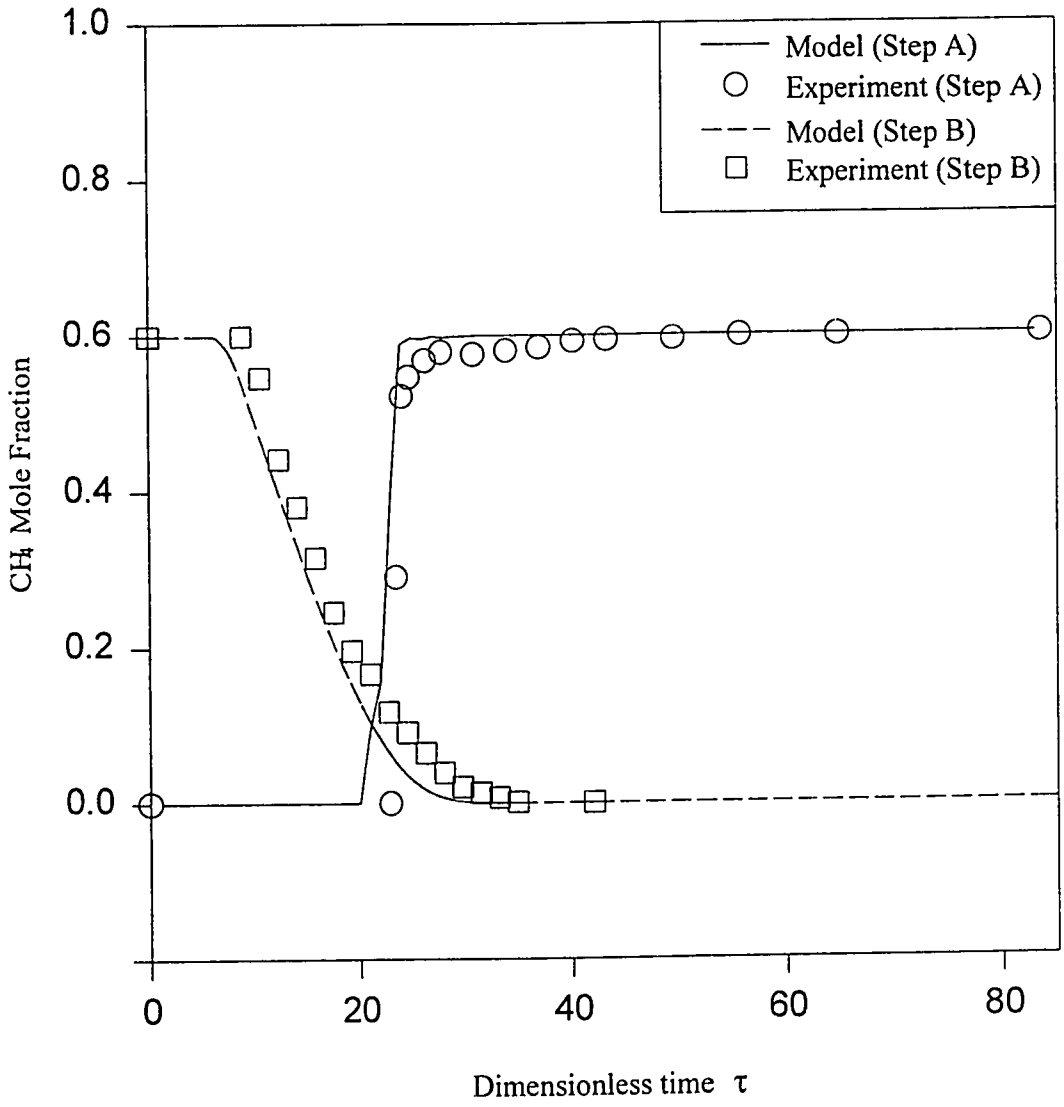

Figure 2.9. Results of the binary breakthrough experiments for Run 1

Mole fraction of nitrogen = 1.0 - (mole fraction of methane)

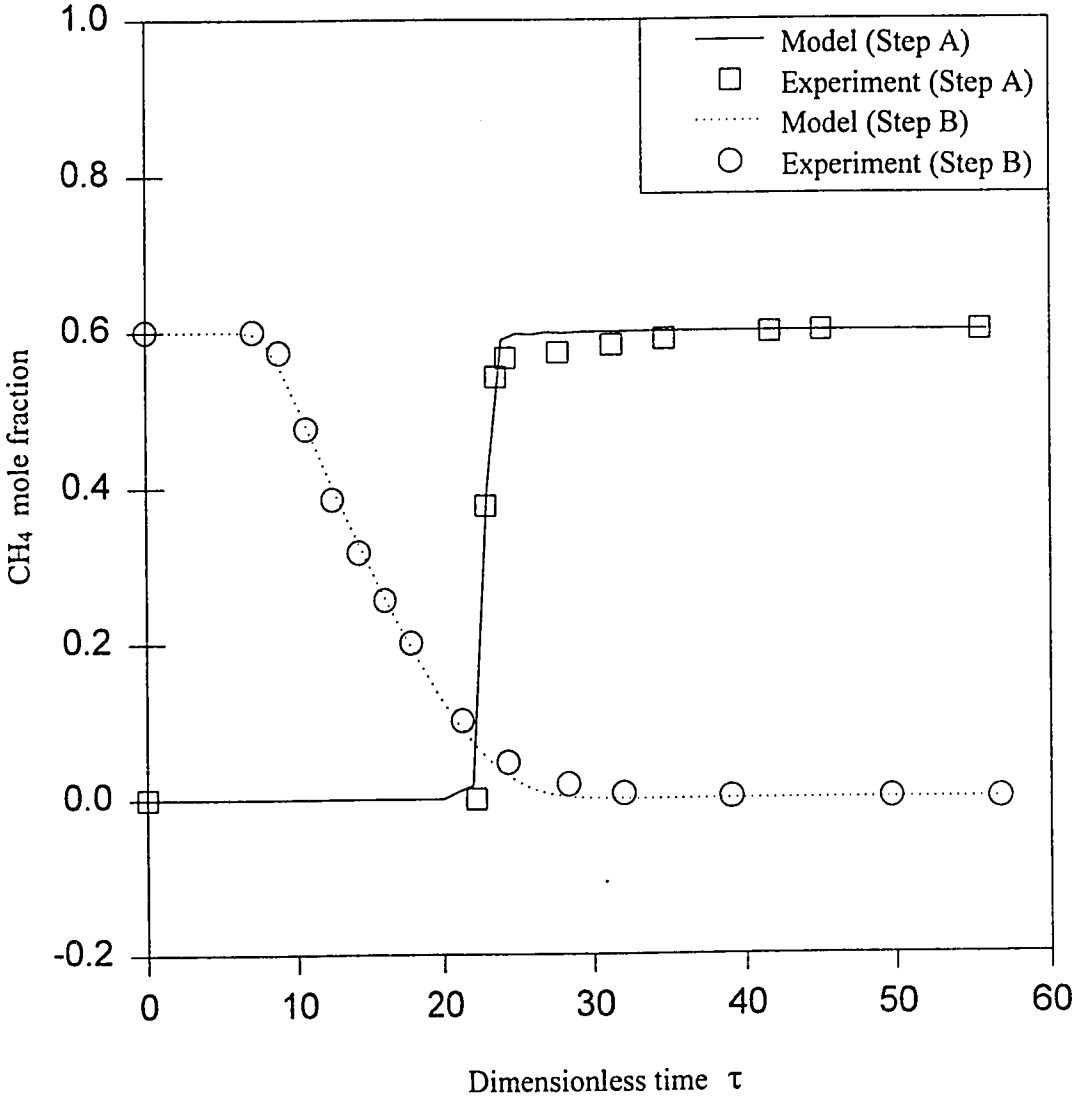

Figure 2.10. Results of binary breakthrough experiments for Run 2

Mole fraction of nitrogen = 1.0 - (mole fraction of methane)

Nitrogen fraction can be determined by difference because the column outlet is a binary methane nitrogen mixture of varying composition.

The equations used for binary breakthrough modeling are listed below. Details of normalization and underlying assumptions are discussed in Chapter 3. In these equations component A denotes methane and B denotes nitrogen.

$$-D_L \frac{\partial^2 c_A}{\partial z^2} + v\frac{\partial c_A}{\partial z} + c_A \frac{\partial v}{\partial z} + \frac{\partial c_A}{\partial t} + \left(\frac{1-\varepsilon}{\varepsilon}\right)\frac{\partial \bar{q}_A}{\partial t} = 0 \tag{2.10}$$

$$-D_L \frac{\partial^2 c_B}{\partial z^2} + v\frac{\partial c_B}{\partial z} + c_B \frac{\partial v}{\partial z} + \frac{\partial c_B}{\partial t} + \left(\frac{1-\varepsilon}{\varepsilon}\right)\frac{\partial \bar{q}_B}{\partial t} = 0 \tag{2.11}$$

Adding the two equations and recognizing that the total pressure is constant implying that the concentration c_T defined as $c_T = c_A + c_B$ is a constant with axial distance and time, we get

$$c_T \frac{\partial v}{\partial z} + \left(\frac{1-\varepsilon}{\varepsilon}\right)\frac{\partial \bar{q}_A}{\partial t} + \left(\frac{1-\varepsilon}{\varepsilon}\right)\frac{\partial \bar{q}_B}{\partial t} = 0 \tag{2.12}$$

The accumulation in the solid phase is represented by the linear driving force expression for each component

$$\frac{\partial \bar{q}_A}{\partial t} = k_A \left(q_A^* - \bar{q}_A\right) \tag{2.13}$$

$$\frac{\partial \bar{q}_B}{\partial t} = k_B \left(q_B^* - \bar{q}_B\right) \tag{2.14}$$

Equilibrium isotherms are linear

$$q_A^{\bullet} = K_A\, c_A \tag{2.15}$$

$$q_B^{\bullet} = K_B\, c_B \tag{2.16}$$

The above system of equations is subject to the following boundary conditions:

Danckwert's boundary conditions,

$$-D_{L_A} \left.\frac{\partial c_A}{\partial z}\right|_{z=0} = v_I \left(c_A\big|_{z=0^-} - c_A\big|_{z=0^+} \right) \tag{2.17}$$

$$\left.\frac{\partial c_A}{\partial z}\right|_{z=L} = 0 \tag{2.18}$$

Velocity boundary condition,

$$v\big|_{z=0} = v_I \tag{2.19}$$

The initial conditions depend on whether the equations are solved for the first step (step A) or the second step (step B). For example, for step A,

$$c_A = 0 \;,\; c_B = c_{B_o} \;,\; \bar{q}_A = 0, \quad \bar{q}_B = K_{N_2}\, c_{B_o}$$

where c_{Bo} is the initial concentration of nitrogen.

The above set of equations is normalized (see Chapter 3) and solved using method of orthogonal collocation to resolve the partial differential equations into a set of simultaneous ordinary differential equations which is solved by standard IMSL subroutines. Note that the overall mass balance equation is resolved into a set of simultaneous linear algebraic equations which is solved by the appropriate IMSL

subroutine. Table 2.11 lists the data used for the solution of the above model equations for runs 1 and 2.

The results of the binary breakthrough simulations have been summarized in Figures 2.9 and 2.10. It can be seen that there is a good accord between the experimental and theoretical predictions of methane and nitrogen. The model is run based on Henry's constants, LDF constants, and axial dispersion coefficient values obtained from chromatographic analysis of single component data for each of the adsorbates. The accuracy of binary breakthrough predictions establishes that the same equilibrium and kinetic parameters can be used to simulate the PSA experiments. This is the subject of the next chapter.

Table 2.11. Parametric values used for the solution of the binary breakthrough equations for Runs 1 and 2

Parameter	Value
Temperature	300 K
Pressure	1 atm
Bed length	51 cm
Bed voidage	0.48
K_{CH4}	20.186
K_{N2}	6.687
k_{CH4}	2.95 s^{-1}
k_{N2}	8.25 s^{-1}
$D_{m\ (CH4\ -\ N2)}$	0.257
$D_{L\ (CH4\ -\ N2)}$	0.335 cm^2/s
Interstitial velocity (step A)	2.63 cm/s (Run 1) 2.95 cm/s (Run 2)
Interstitial velocity (step B)	2.75 cm/s (Run 1) 3.02 cm/s (Run 2)

Axial dispersion coefficient D_L for methane nitrogen systems is calculated theoretically using $D_L = 0.7\,D_m + 0.5\,v\,R_p$, where R_p is the radius of the adsorbent particle. The calculated value is used in the simulations.

Nomenclature

A_n	coefficients of the virial isotherm [$(cm^3\ mole^{-1})^n$]
c	gas phase concentration of sorbate [mole cm^{-3}]
D_L	axial dispersion coefficient [$cm^2\ s^{-1}$]
K	dimensionless Henry's law constant [-]
k	overall effective mass transfer coefficient used in the linear driving force expression [s^{-1}]
k_f	external fluid film mass transfer coefficient [cm s^{-1}]
K_H	Henry's law constant [mmol g^{-1} $psia^{-1}$]
L	length of chromatographic / breakthrough column [cm]
p	sorbate pressure [psia or atm]
q	sorbate concentration [mole cm^{-3}]
$\bar{q}$	sorbate concentration averaged over a particle [mole cm^{-3}]
R_p	radius of the sorbent particle [cm]
t	time [s]
v	interstitial velocity through chromatographic / breakthrough column [cm s^{-1}]
z	axial distance along the length of breakthrough column [cm]

Greek symbols

γ	defined by equation (2.8)

ε	porosity of the chromatographic / breakthrough column [-]
μ	first chromatographic moment [s]
σ	standard deviation of the chromatographic response [s]
τ	dimensionless time [$=t\ v\ /L$]

References

Al Baghli, N. A., Adsorption of Light Gases and Their Mixtures on SR-115 and ETS-10 Zeolites, M.S. Thesis, King Fahd University of Petroleum & Minerals, Dhahran, Saudi Arabia, 1994.

Daymond, J. H. and E. B. Smith, *The Virial Coefficients of Pure Gases and Mixtures: A Critical Compilation*, Clarendon Press, New York, 1980.

Haynes, H. W. Jr., and P. N. Sarma, A Model for the Application of Gas Chromotography to Measurements of Diffusion in Bidisperse Structured Catalysts, *AIChE J*, 19,1043-1049, 1973.

Kärger, J., D. M. Ruthven, *Diffusion in Zeolites and Other Microporous Solids*, John Wiley, New York, 1992.

Ruthven, D. M., *Principles of Adsorption and Adsorption Processes*, John Wiley, New York, 1984.

CHAPTER 3

PSA SEPARATION OF METHANE AND NITROGEN

In this chapter separation of a methane-nitrogen mixture on MAXSORB activated carbon adsorbent by pressure swing adsorption is discussed. Some details of the PSA apparatus employed are given followed by a description of mathematical modeling of the process and a comparison of the experimental and theoretical results.

3.1 APPARATUS

For this study a dual-column laboratory-scale PSA setup is used. A schematic diagram of the apparatus is shown in Figure 3.1. In the breakthrough analysis of chapter 2 one of the two identical PSA columns was used. Data on the breakthrough column as given in Table 2.10 are valid for each of the two PSA columns. Before the PSA operation is started the whole apparatus is purged and maintained under a high pressure of helium (6 atm) for a long period of time to test for any leaks. Any possible leakage is detected and rectified by appropriately tightening the column flanges or replacing the malfunctioning component.

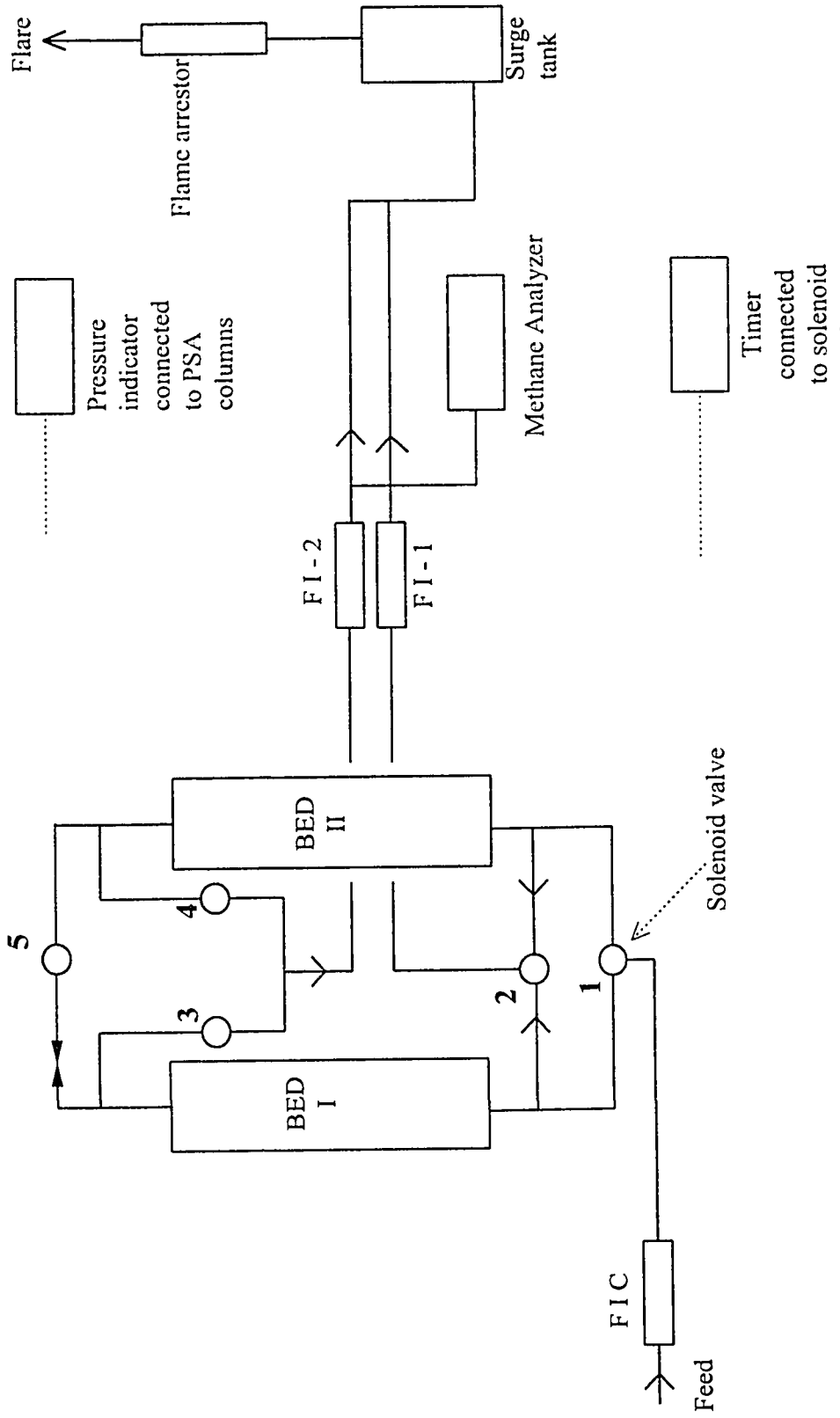

Figure 3.1. A simplified schematic diagram of the PSA apparatus employed in the present work for runs 1 to 17

Feed gas: A mixture of 60 volume percent methane in nitrogen is used as the feed gas. The cylinders of feed gas and other gases are procured from Matheson Gas Products Inc., USA and have a guaranteed purity of 99.95%.

Valves and piping: The two-way solenoid valves (8223 A22) and three-way solenoid valves (8320 A171) used in this work are manufactured by ASCO, Netherlands. Each valve is tested and guaranteed by the manufacturer. Steel piping of 1/4 inch nominal diameter is used. Check valves are also incorporated at proper locations to prevent backflow.

Flow indicators: A pair of Matheson flow indicators FI (Series 8100) and a flow indicator and controller FIC (Series 8200) are used in the present experiments. These devices are linear thermal mass flow meters based on a measurement of amount of heat transferred to the gas passing through a heated conduit. Each of the flow meters is calibrated by passing the feed gas and measuring the flow by a soap-bubble meter. Straight line calibration factors for converting the flow meter reading to mass flow rate are obtained and reproduced using many readings. The same calibration procedure is repeated using pure methane and the calibration factors corresponding to pure methane are obtained. Linear interpolation for methane mole fraction is used to calculate calibration factors for a mixture of methane-nitrogen of any composition. This ensures that the measured flow rates incorporate correction for the gas composition. A summary of the calibration results for the flow indicators is given in the Appendix.

Pressure indicator: A two-channel pressure indicator (Edwards Datametrics 1049) is connected to the top of each PSA column to measure the gauge pressure in the column.

Timer for solenoid valves: A Xanadu Universal Programmable Timer (M78-100) is used to operate the solenoid valves shown in Figure 3.1. It is programmed by shading the appropriate areas on a program card to enter the cycle configuration. Total cycle time in seconds is input directly to the timer. An example of a cycle configuration is given in Figure 3.2 where a Skarstrom cycle is programmed and an approximate pressure profile is shown for one of the PSA columns.

Methane analyzer: A Servomex (Series 1400) online paramagnetic methane analyzer mentioned in chapter 2 is used to measure the composition of raffinate product, extract, and blowdown gas.

Chart recorders: Strip-chart recorders by Linseis (Model LS 51) are connected to each of the flow indicators (FI-1 and FI-2) to monitor the flow rates of the raffinate and extract / blowdown products on a continuous basis. Similar chart recorders are attached to the methane analyzer to continuously monitor the compositions of different streams. A record of FIC reading (*i.e.*, the feed flow rate) is kept only for a few runs with Skarstrom cycle (runs 2 to 8).

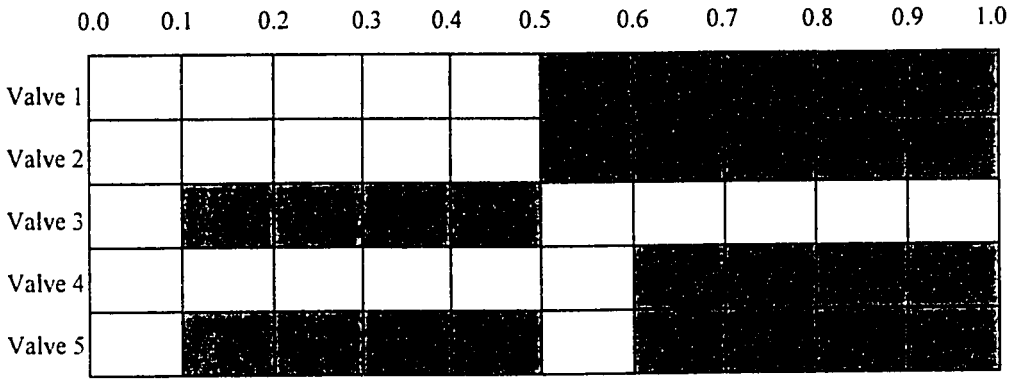

Schematic of valve sequencing for a typical Skarstrom cycle

Shaded = Valve ON, Blank = Valve OFF

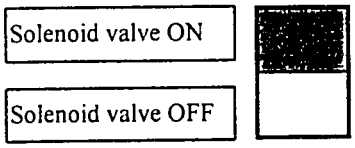

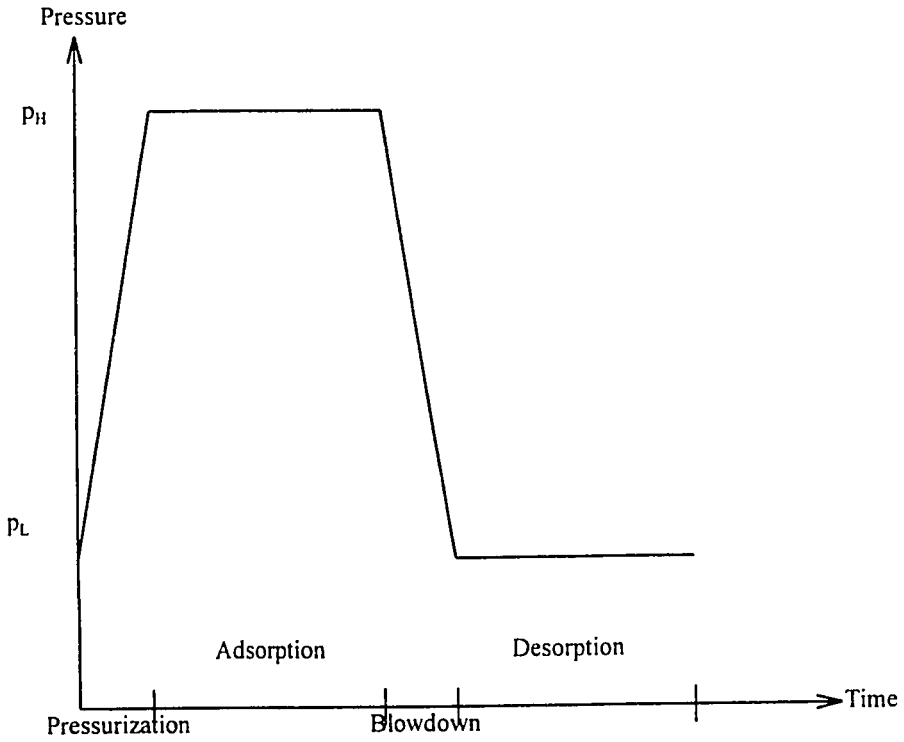

Pressure history of bed 1

Figure 3.2. Valve sequencing and pressure profile for an adsorption bed

Both the adsorbent beds are regenerated before the actual PSA operation is started. Adsorbent regeneration is carried out under a steady flow of helium at a pressure of 1 atm and a temperature of 300 K for a period of approximately 10 hours. This ensures that there are no adsorbed gases or moisture on the adsorbent. Then the feed gas is turned on to pressurize bed 1 as the first step of the Skarstrom cycle. Run 1 is started from initial conditions of clean beds (*i.e.*, all helium). For each of the subsequent runs the initial conditions are approximately the end conditions of the previous run.

3.2 PSA CYCLES

The Skarstrom cycle is the basic PSA cycle and is commonly used to study the operation on a laboratory scale. However, it is rarely used on a large scale where more complex cycle schemes and multiple beds are necessary. In the present work two types of cycle schemes are used: (i) Skarstrom cycle, (ii) A six-step cycle including cocurrent depressurization prior to countercurrent blowdown with rest of the cycle steps same as the Skarstrom cycle.

First the PSA separation with Skarstrom cycle is briefly discussed. As mentioned above the operation is started with fully regenerated beds. The sequence of steps is as follows:

Step 1. Pressurization of bed 1 to the adsorption pressure (or high pressure denoted by p_H) using feed the gas. Countercurrent blowdown of bed 2 from p_H to the desorption pressure or low pressure p_L.

Step 2. Adsorption in bed 1 at p_H to produce the raffinate. Desorption in bed 2 at p_L to produce the extract.

Step 3. Countercurrent blowdown of bed 1 from p_H to p_L. Pressurization of bed 2 from p_L to p_H with the feed gas.

Step 4. Desorption in bed 1. Adsorption in bed 2.

Since the required product in the current work is the extract, the objective is to increase the purity of methane in the extract product. With the Skarstrom cycle, 17 runs are performed at different levels of adsorption pressure, cycle time, and bed length to velocity ratio. The flow rates of the raffinate and the extract products are measured continuously and a permanent record is maintained only when the cyclic steady state is achieved. Due to a low mass transfer resistance in the present system the cyclic steady state is attained quickly, *i.e.*, generally only 4 to 5 cycles are required to reach the cyclic steady state. As will be seen later the mole fraction of methane in the extract product is limited to about 78%. This is not a substantial improvement over the previous attempts as outlined in chapter 1. Therefore other cycle schemes are explored to increase the purity of strongly adsorbed methane in the extract product.

A modified cycle consisting of the following overall steps is resorted to achieve the objective of a richer extract product:

Step 1. Pressurization of bed 1 is commenced from p_L using the feed gas. Cocurrent depressurization (blowdown) of bed 2 from p_H to p_{CD} where the subscript CD denotes the end pressure of the cocurrent depressurization step.

Step 2. Pressurization of bed 1 is continued to p_H. Countercurrent blowdown of bed 2 from p_{CD} to p_L.

Step 3. Adsorption in bed 1 at p_H to produce the raffinate. Desorption in bed 2 at p_L to produce the extract.

Step 4. Cocurrent depressurization of bed 1 from p_H to p_{CD}. Pressurization of bed 2 is commenced from p_L.

Step 5. Countercurrent blowdown of bed 1 from p_{CD} to p_L. Pressurization of bed 2 with feed is continued to p_H.

Step 6. Desorption in bed 1. Adsorption in bed 2.

In the PSA operation the bed utilization during the adsorption step is usually not complete. Therefore the region ahead of the mass transfer zone is richer in the light component — nitrogen. Incorporating the cocurrent depressurization step in the cycle pushes this raffinate-like region out of the bed from the raffinate-end and provides time for the adsorbed methane to desorb. Hence in the subsequent countercurrent blowdown and purge steps there is less nitrogen near the extract-end of the bed. This increases the methane content of both the blowdown gas and the extract product. Moreover, less nitrogen is lost in the blowdown gas which increases the recovery of weakly adsorbed nitrogen. However, the primary objective of the present research is to achieve high purity

and recovery of methane in the extract product. Suh and Wankat (1989) have recommended the following criterion for cocurrent depressurization: If the reciprocal of the separation factor is larger than about 0.01 or the mole fraction of the strongly absorbable component in the feed is less than 80% a combination of cocurrent and countercurrent blowdown increases the recovery of weakly adsorbed species and gives a richer extract product. For the present case this criterion is satisfied as the reciprocal of the separation factor is 0.33 and there is 60% methane in the feed. Therefore, including cocurrent depressurization is expected to improve the quality of the extract product.

There are numerous attempts in the literature where an improvement in the recovery of light component and a better extract product are reported when cocurrent depressurization is used. Yang and Doong (1985) studied an equilibrium PSA process where they separate a 50/50 CH_4/H_2 mixture on activated carbon. They concluded that substantial improvements in CH_4 purity and H_2 recovery are achieved with cocurrent depressurization. Cen and Yang (1986a and 1986b) separated CO/H_2 and CH_4/H_2 mixtures on activated carbon and reported that a better enrichment of CH_4 or CO in the extract product is obtained by incorporating cocurrent depressurization step. They also varied the duration of the cocurrent depressurization step relative to the countercurrent blowdown step and found that a shorter cocurrent depressurization step gave poorer extract purity.

For the present system of CH_4/N_2 on MAXSORB activated carbon, inclusion of cocurrent depressurization step is expected to show some improvement over the

conventional Skarstrom cycle. A parametric study is performed where the cocurrent depressurization time is varied with all other parameters held at the same values. Six runs (labeled as 1N to 6N) are performed with the modified cycle. A cycle configuration of, for instance, 2-3-45-2-3-45 means 3% of the total cycle time is cocurrent depressurization, 2% of the total cycle time is for countercurrent blowdown, and 45% is for adsorption or desorption. The pressurization time is 5% of the total cycle time. To run the PSA apparatus on the modified cycle some changes in the setup used for the Skarstrom cycle are necessary. The flow of raffinate is directed through a flow indicator and controller (FIC). The flow controller is kept fully open during cocurrent blowdown to obtain a reduction in the pressure of the column. To achieve the desired raffinate flow the flow controller is kept partially adjusted during the adsorption step. The new equipment scheme is as shown in Figure 3.3. The sequence timer is programmed accordingly to achieve the desired cycle steps by opening or closing the appropriate solenoid valves. For one of the runs with modified cycle (labeled as 4N) there is no cocurrent depressurization time; hence, this run corresponds to the Skarstrom cycle.

3.3 RESULTS AND DISCUSSIONS (PSA EXPERIMENTS)

Table 3.1 summarizes the experimental conditions and results of PSA experimental runs at the cyclic steady state for CH_4 / N_2 / MAXSORB system with Skarstrom cycle. For Run 1 detailed calculations are not performed because of some uncertainty in the output of strip-chart recorders. As mentioned before methane mole

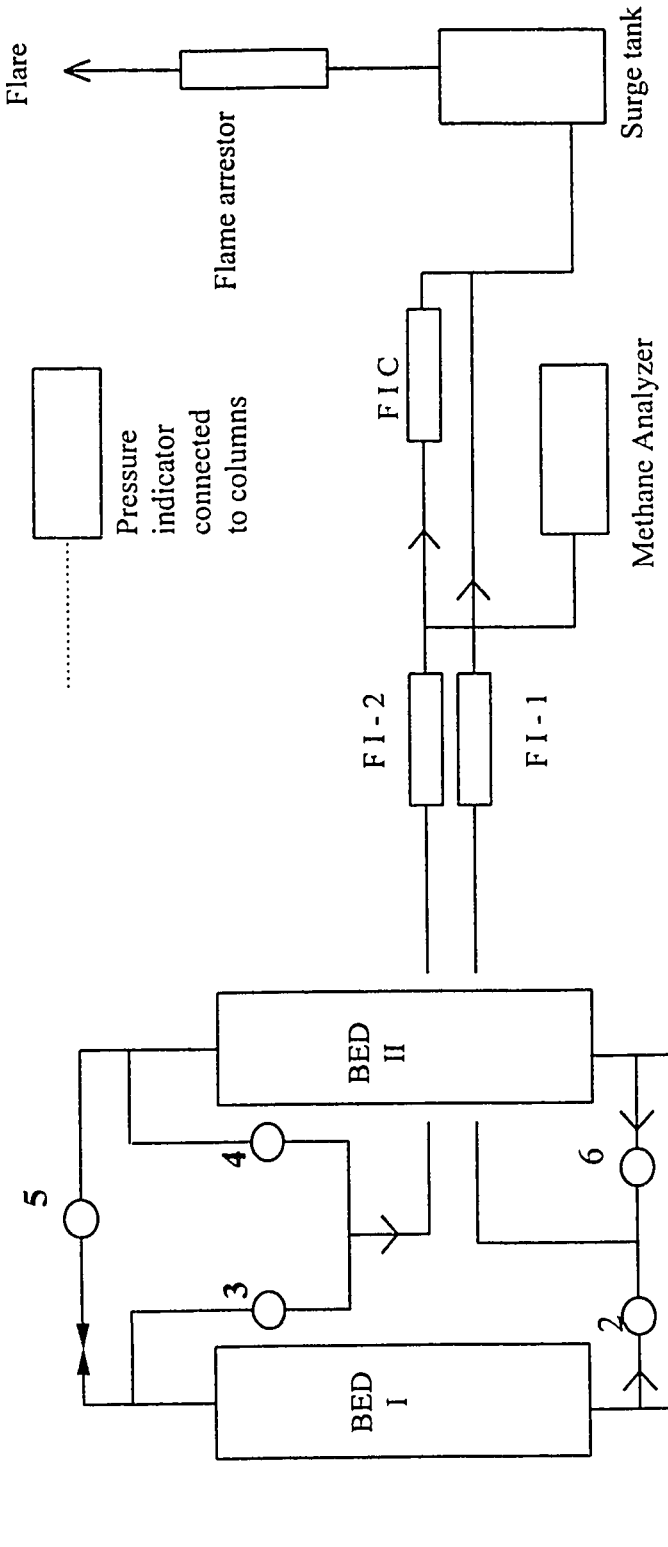

Figure 3.3. A simplified schematic diagram of the PSA apparatus employed for runs 1N to 6N operating with cocurrent depressurization

Table 3.1. Summary of results of PSA experiments with Skarstrom cycle. All values are averages over a full cycle at cyclic steady state

Run No.	p_H [1]	Total cycle time	Cycle configuration	**Extract product**		**Raffinate product**			**Bottom product**	
			pressurization/ blowdown - adsorption /desorption [2]	Interstitial velocity	Methane recovery	Interstitial velocity	Nitrogen purity [3]	Nitrogen recovery	Methane purity	Methane recovery
	[atm]	[s]	[% total cycle time]	[cm/s]	%	[cm/s]	%	%	%	%
1	4.05	300	5 - 45 [4]	[5]	-	-	-	-	-	-
2	4.08	200	10 - 40	6.211	60.42	0.228	80.05	18.18	69.37	97.61
3	4.06	150	20 - 30	4.880	36.07	0.181	79.71	12.23	68.49	98.40
4	4.06	400	7 - 43	2.933	43.23	0.293	83.81	35.81	72.56	96.08
5	4.06	500	7 - 43	2.566	41.85	0.258	85.87	44.37	74.39	96.75
6	4.06	600	5 - 45	2.533	51.33	0.270	86.72	44.55	74.98	96.06
7	4.06	540	5 - 45	2.967	52.04	0.256	86.33	40.40	76.00	96.72

8	5.00	540	5 - 45	4.681	64.43	0.209	93.88	33.25	72.63	98.79
9	3.00	540	5 - 45	(6)	-	0.535	63.11	53.88	76.37	82.55
10	3.00	420	5 - 45	2.754	48.18	0.444	65.51	41.15	73.09	88.07
11	3.00	600	5 - 45	-	-	0.410	80.55	41.40	73.99	94.34
12	3.00	600	5 - 45	-	-	0.319	83.69	37.08	74.00	96.12
13	5.00	540	5 - 45	-	-	0.290	92.28	45.35	73.08	97.51
14	5.00	540	5 - 45	-	-	0.132	99.25	0.25	71.95	99.9
15	5.00	300	7 - 43	-	-	0.314	66.82	27.21	78.32	93.49
16	5.00	480	5 - 45	-	-	0.394	69.66	52.62	78.01	88.00
17	5.00	480	5 - 45	-	-	0.353	72.22	48.22	79.08	91.34

All values are averages over a full cycle at cyclic steady state.

(1) p_L = 1.0 atm for all runs
(2) For Skarstrom cycle Pressurization time of one bed = Blowdown time of the other
Adsorption time of one bed = Desorption time of the other
(3) Obtaining by subtracting the measured methane mole percent from 100.0
(4) Duration of Step I and III = 15 s, duration of Step II and IV = 135 s
(5) For run 1 calculations not performed
(6) Extract product not calculated separately for some runs

percent and flow rate are monitored for the raffinate and the extract product. There are minor variations in the column pressure (about 5%) during the high-pressure adsorption step. These are ignored in the second column of the table. From the output of the chart recorders data is read-off with a time interval of 5 or 10 seconds. The flow indicator readings are converted to mass flow rates using calibration factors obtained for each flow meter (see Appendix). The values of methane purity and interstitial velocity given in Table 3.1 are calculated average values for the whole cycle. These are calculated using Simpson's rule for numerical integration in the following formulas:

$$\overline{Q} = \frac{\int Q\,dt}{\int dt} \tag{3.1}$$

$$\overline{c} = \frac{\int Q c'\,dt}{\int Q\,dt} \tag{3.2}$$

where Q and c are the instantaneous values of flow rate in cm^3 STP/s and methane mole fraction respectively and are read-off the experimental output with a small time interval of 5 seconds. In the above equations the limit of integration corresponds to the range of cycle time applicable for a particular calculation. For example, for the averaging of the raffinate product flow and composition, the limits of integration are taken to be the duration of the adsorption step.

For the present PSA separation the purity of the blowdown gas is high enough to make it suitable as a methane-rich product. This is illustrated in Appendix for a particular

run where detailed calculations are presented. The composition and recovery of the strongly adsorbed component are averaged for both blowdown and extract product considered as a single mixed product. This stream which is a combination of extract and blowdown products is called the bottom product. For runs 2 to 8 methane recovery only in the extract product has been calculated and is presented in Table 3.1. The interstitial velocities appearing in the table are based on the average flow calculated for the whole cycle and on the column cross sectional area and porosity. The following definition of the recovery of a component in a product stream P is used for recovery calculations:

$$\text{Recovery} = \frac{\bar{c}_P \, \bar{Q}_P}{\bar{c}_{Feed} \, \bar{Q}_{Feed}} \tag{3.3}$$

The effect of pressure ratio on the raffinate and the bottom-product is shown in Figures 3.4 and 3.5 respectively. For the runs shown in these figures other parameters such as the cycle time, cycle configuration, feed and product flow rates *etc.*, have the same values. With increasing pressure ratio there is an increase in purity of nitrogen in the raffinate product. This is because more methane is adsorbed at a higher adsorption pressure. This also reduces the methane lost to the raffinate and results in an increased methane recovery in the bottom product. However, purging of the bed in the desorption step is carried out with a purer nitrogen stream. Due to axial dispersion, some of the nitrogen-rich purge gas appears in the extract product thus lowering the methane purity of the extract. Hence as the pressure ratio increases a richer raffinate product is obtained with a lower nitrogen recovery. All the unrecovered nitrogen appears in the bottom product.

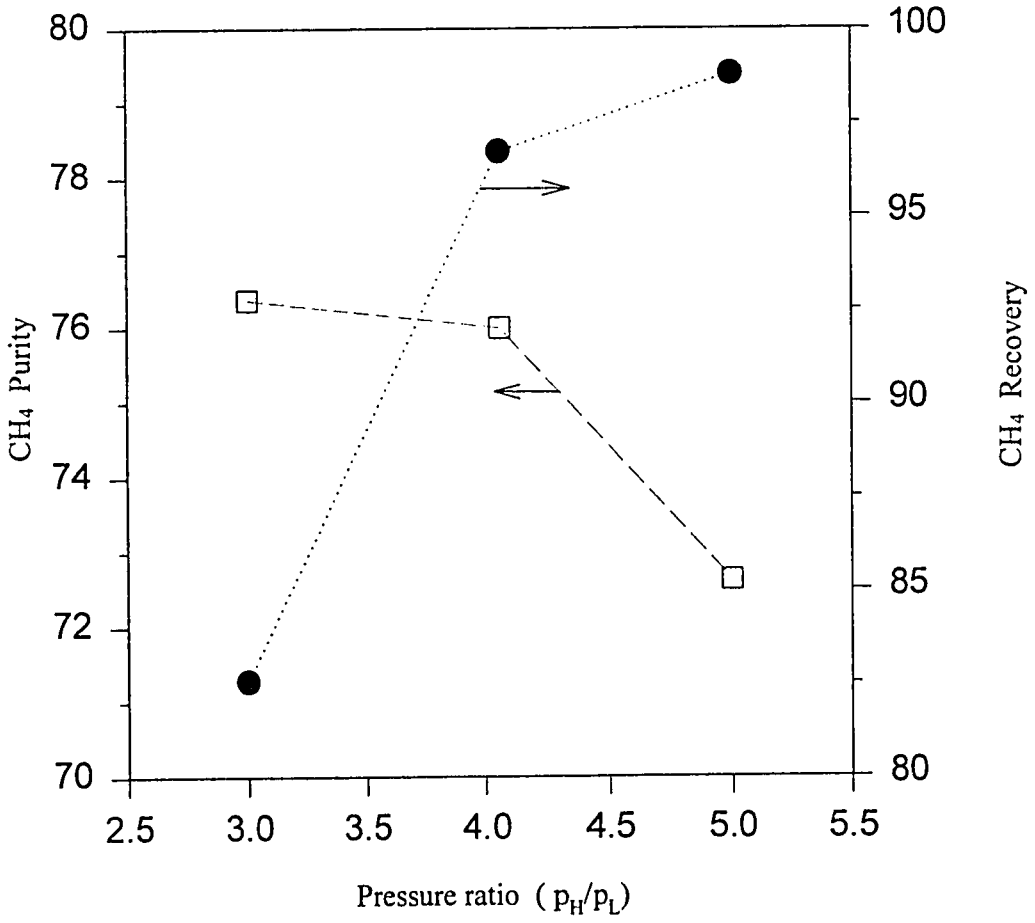

Figure 3.4. Effect of pressure ratio on purity and recovery of methane

(Experimental, Skarstrom cycle)

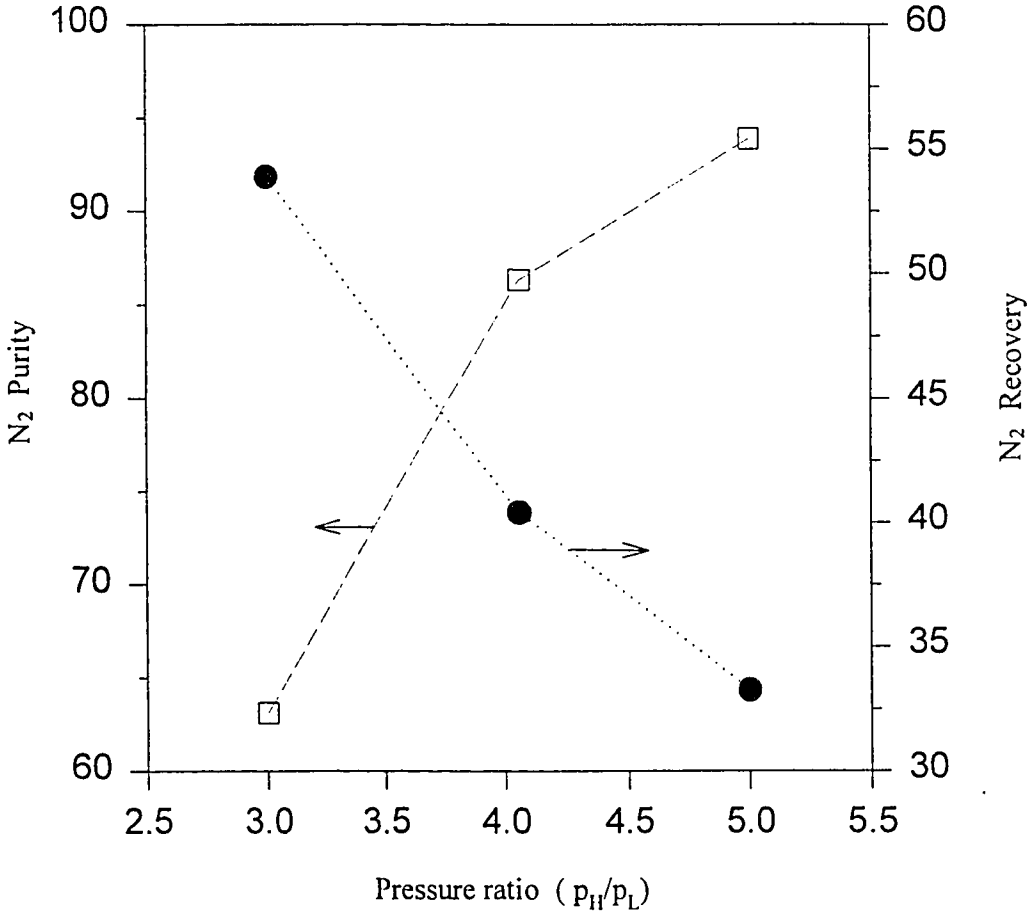

Figure 3.5. Effect of pressure ratio on purity and recovery of nitrogen

(Experimental, Skarstrom cycle)

Similarly the influence of cycle time on purity and recovery of methane in the bottom product is shown in Figure 3.6. This is represented as runs 9 to 11 in Table 3.1. The effect of cycle time on the bottom product quality is subject to other parameteric values such as the cycle configuration and feed flow rate *etc.* The extent of methane purity for a cycle time of 540 seconds appears to be higher than that for other values of cycle times in Figure 3.6. However, the recovery of methane for a cycle time of 540 seconds shows the expected reverse trend with increasing purity.

In Figure 3.7 the effect of raffinate flow rate on purity and recovery of nitrogen in the raffinate product is illustrated. With a higher raffinate velocity the mass transfer zone extends closer to the raffinate-end. Hence some methane appears in the raffinate thus reducing the nitrogen purity of the raffinate. The same opposing trend of purity and recovery is demonstrated by the raffinate product in Figure 3.7.

Finally, a graph of purity versus recovery of methane in the bottom product is shown is Figure 3.8. The overall trend is a low recovery with higher methane purity. The straight line fitted by least squares regression does not imply a linear relationship but is shown only to reflect the overall trend of purity and recovery. The best value in Figure 3.8 is a trade-off between purity and recovery and is dictated by economic and other operational factors.

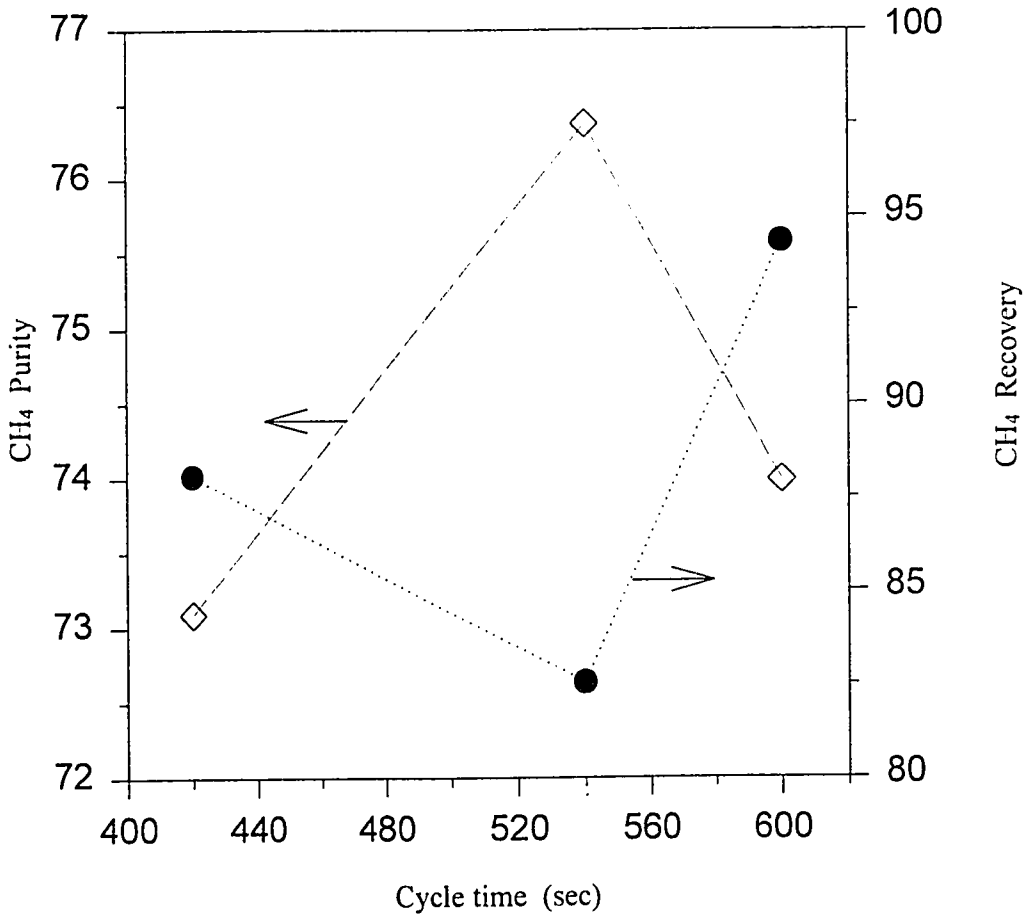

Figure 3.6. Effect of cycle duration on purity and recovery of methane
(Experimental, Skarstrom cycle)

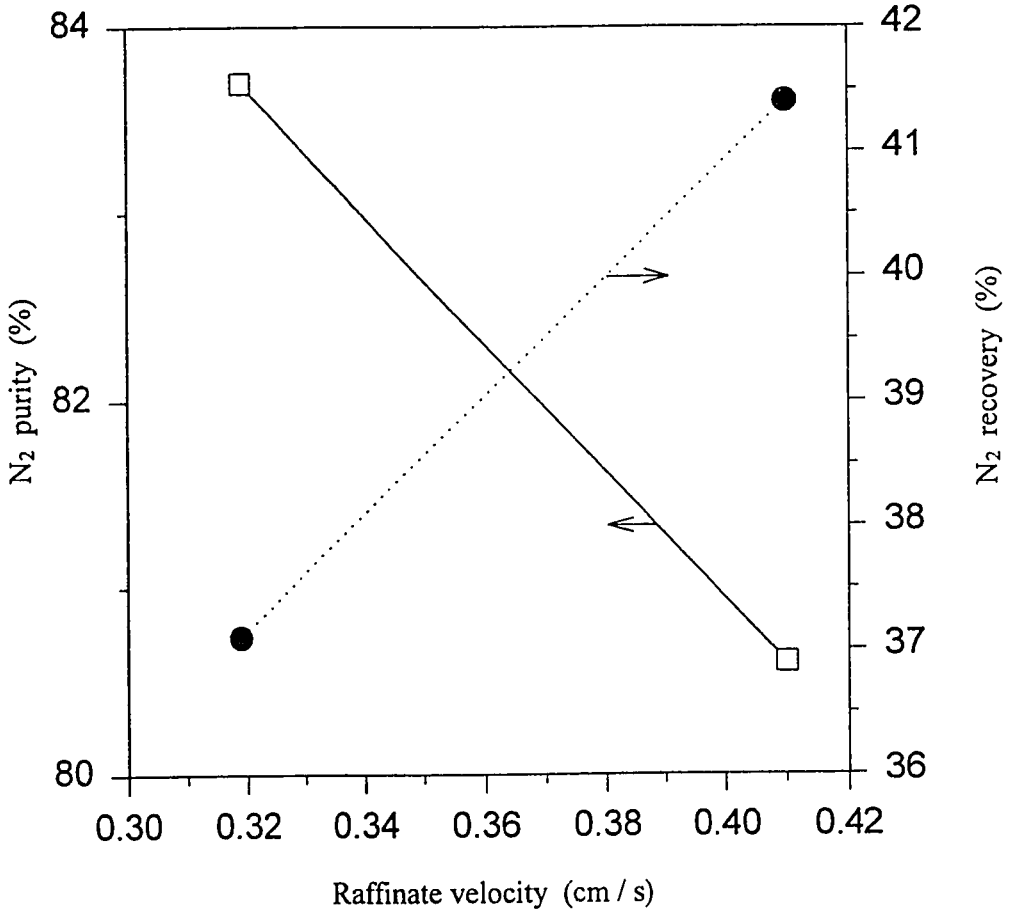

Figure 3.7. Effect of raffinate velocity on nitrogen in raffinate

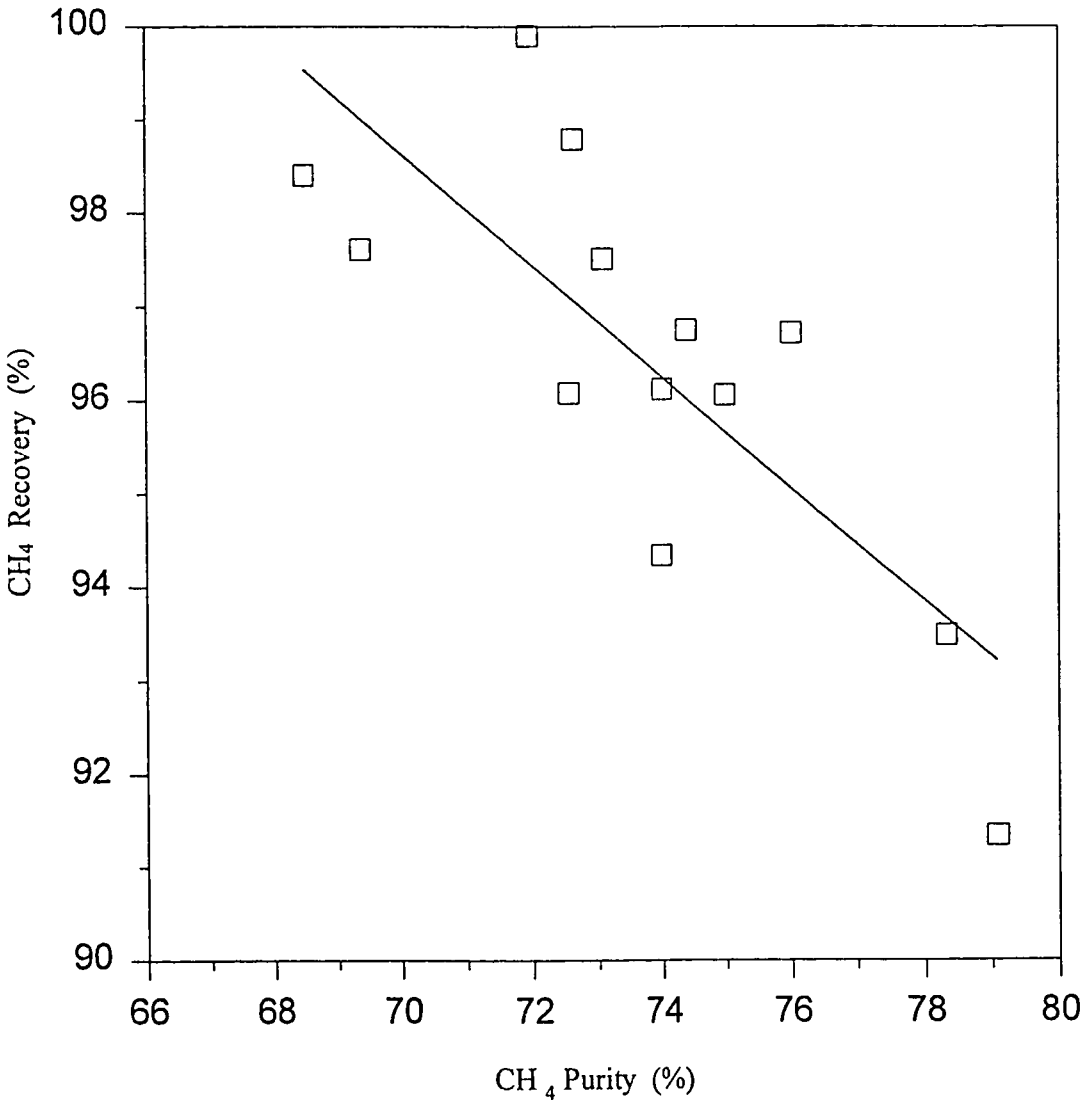

Figure 3.8. Graph between purity and methane recovery of the bottom product (Experimental, Skarstrom cycle).
Regressed straight line is drawn only to show the overall trend

The results of PSA runs with the modified cycle are summarized as Table 3.2 which also shows the experimental conditions. For all these runs the total cycle time is 360 seconds and the adsorption pressure is 5 atm. Only the mode of depressurization is varied to investigate the effect of incorporating cocurrent depressurization step in the PSA cycle. It should be noted that the stream at the bed outlet during the cocurrent depressurization step is considered as a part of the product and the term top-product is used to refer to a mixture of cocurrent depressurization stream and the raffinate product.

Predictably, there is an increase in methane content of the bottom product when the modified cycle is used. A discussion of the cocurrent depressurization step with reference to concentration wavefront movement was given in section 3.2. It can also be observed from Table 3.2 that with increasing cocurrent depressurization time more and more methane is lost to the top-product. However, major advantages are gained in nitrogen recovery in the top-product and the purity of the bottom product. This is demonstrated in Figures 3.9 and 3.10 where purities of the two products and methane and nitrogen recovery are plotted as functions of the cocurrent depressurization time. Methane content of the bottom product and nitrogen recovery in the top-product are seen to increase as the cocurrent depressurization time represents a larger fraction of the total cycle time. This is also in accordance with the trend expected from the discussion of the cocurrent depressurization time in terms of wavefront movement. That is, less nitrogen is present in the bed during blowdown and the region near the extract-end during the purge step is richer in methane. Hence, a lesser amount of nitrogen appears in the bottom-

Table 3.2. Summary of results of PSA experiments with modified cycle

Run no. [1]	Cocurrent depressurization time [s]	Countercurrent blowdown time [2] [s]	Top product			Extract product		Bottom product	
			Interstitial velocity [cm/s]	N_2 purity[3] %	N_2 recovery %	Interstitial velocity [cm/s]	CH_4 recovery %	CH_4 purity %	CH_4 recovery %
4N [4]	0.0	18.0	0.407	81.60	51.25	5.586	73.80	77.20	93.46
1N	3.6	14.4	0.286	82.94	44.21	6.356	81.76	79.51	95.97
3N	7.2	10.8	0.409	78.67	57.71	6.528	76.38	85.00	93.87
5N	10.8	7.2	0.405	73.25	61.70	6.188	86.22	85.62	91.01
6N	14.4	3.6	0.410	70.00	66.28	6.124	87.88	87.36	89.14

(1) Run numbers are sequenced according to increasing cocurrent depressurization time.

(2) Sum of the two modes of depressurization time is 5% of the total cycle time in all cases.

(3) 100.0 – (measured methane mole percent).

(4) Note that this is Skarstrom cycle.

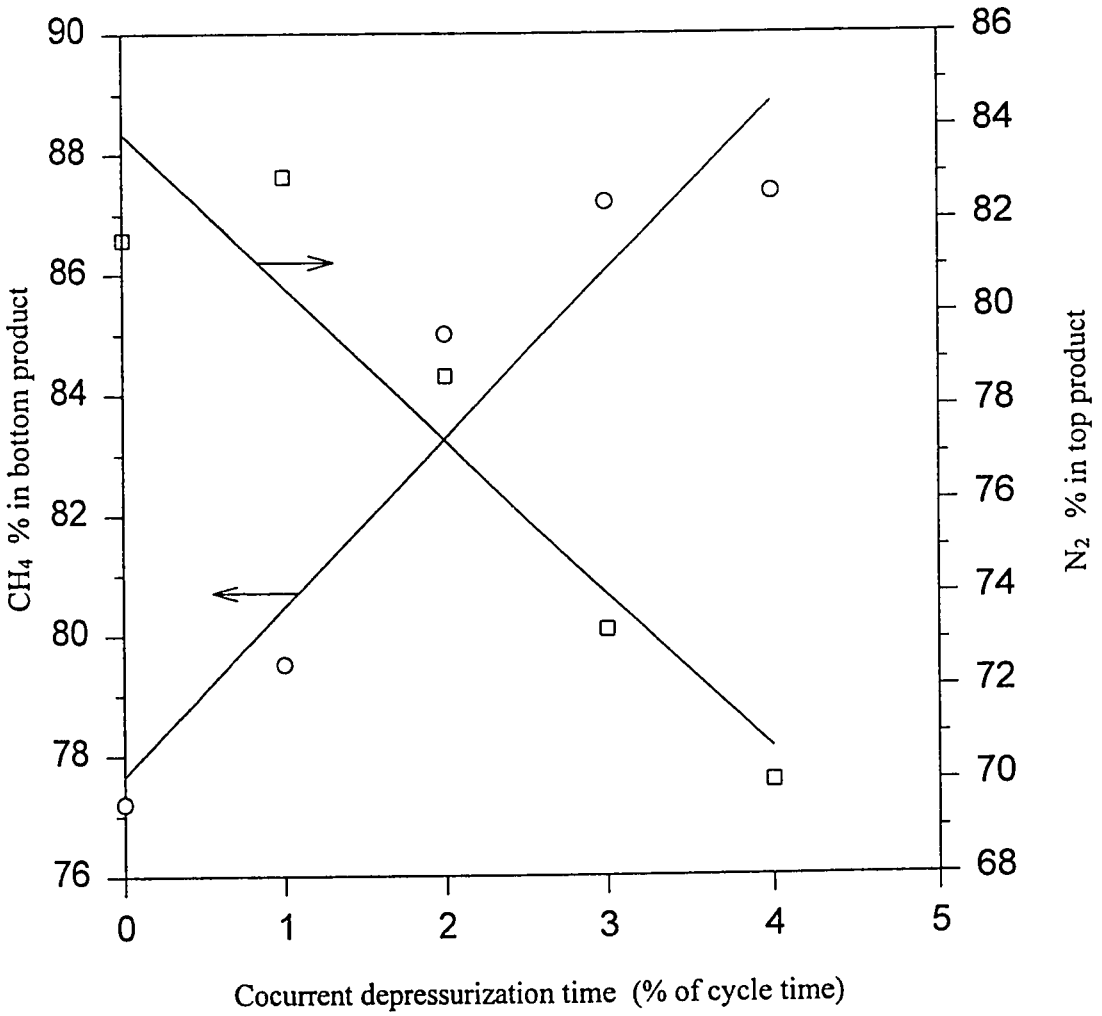

Figure 3.9. Effect of cocurrent depressurization time on purity of top and bottom-products

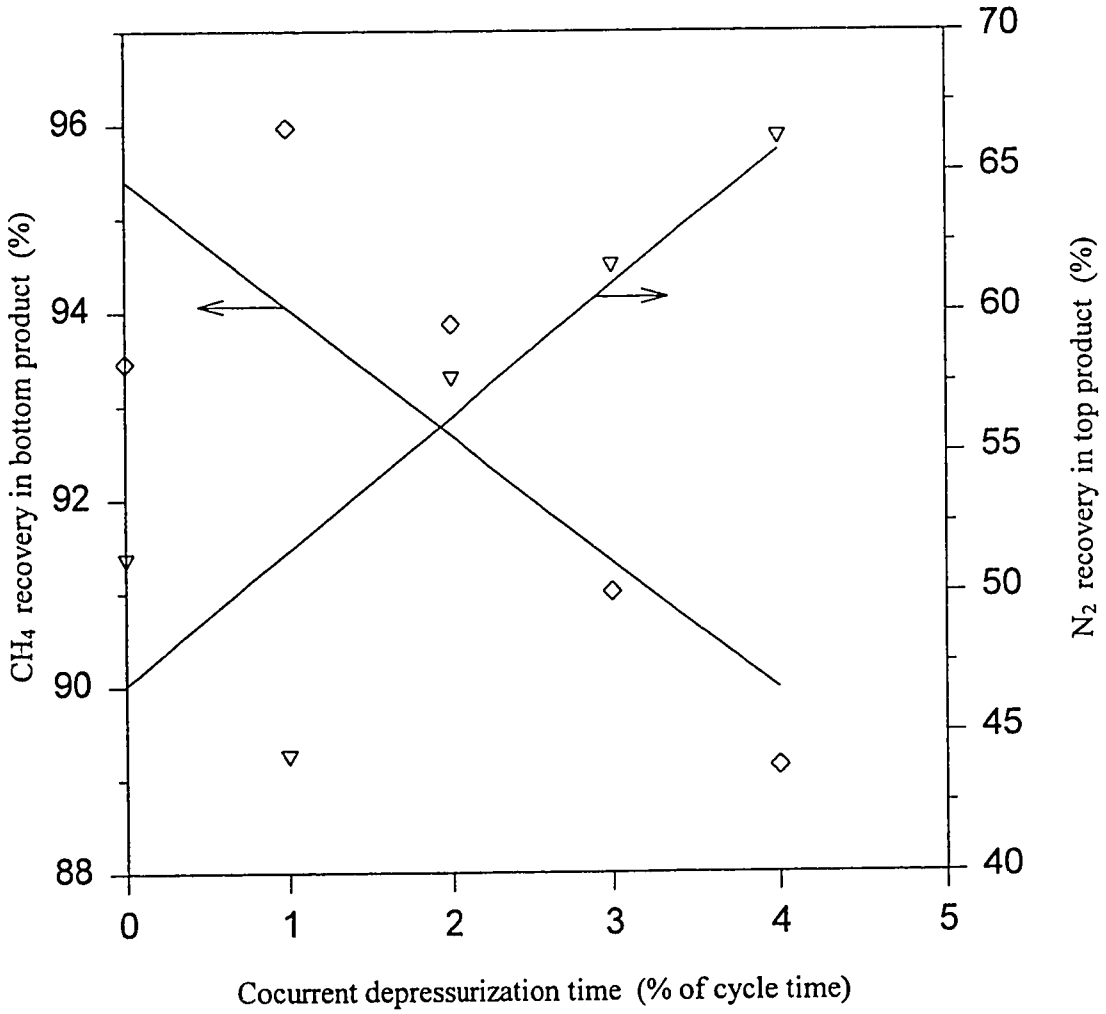

Figure 3.10. Effect of cocurrent depressurization time on recovery of methane and nitrogen

product. Consequently the bottom product is richer in methane and a higher fraction of nitrogen in the feed is recovered in the top-product.

The quantity of countercurrent blowdown product reduces as the cocurrent depressurization time represents a larger portion of the total depressurization time. This is illustrated in Figure 3.11 which is a graph of methane recovery in the top-product and the extract product as a function of cocurrent depressurization time. It is seen that the difference in methane recovery in the bottom product and pure extract product decreases as the cocurrent depressurization is increased. This stems from the fact that the end pressure of the cocurrent depressurization step is closer to the desorption pressure when the time of this step is long. Then very little gas is lost in countercurrent blowdown due to a lower column pressure and a shorter duration of blowdown step. This shows up as the diminished difference between methane recovery in bottom and extract products. A graph between methane purity versus methane recovery in the bottom-product is shown as Figure 3.12. Here again, the choice of proper cocurrent depressurization time depends upon economic factors and operational constraints. The general trend, however, is the same as for all PSA separation processes; *i.e.*, lower recovery for a higher purity and *vice versa*.

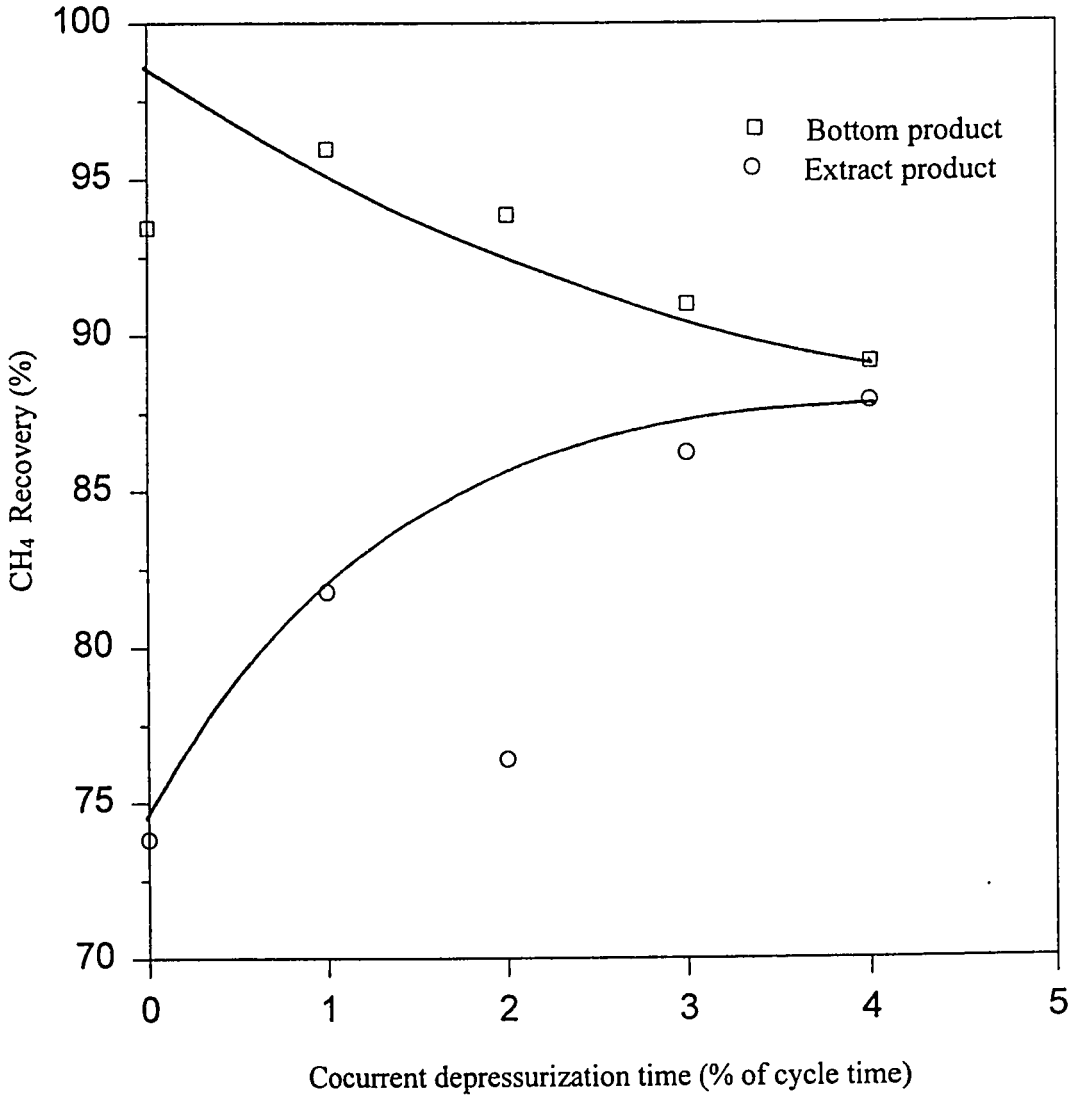

Figure 3.11. Methane recovery in bottom and extract products as a function of the cocurrent depressurization time

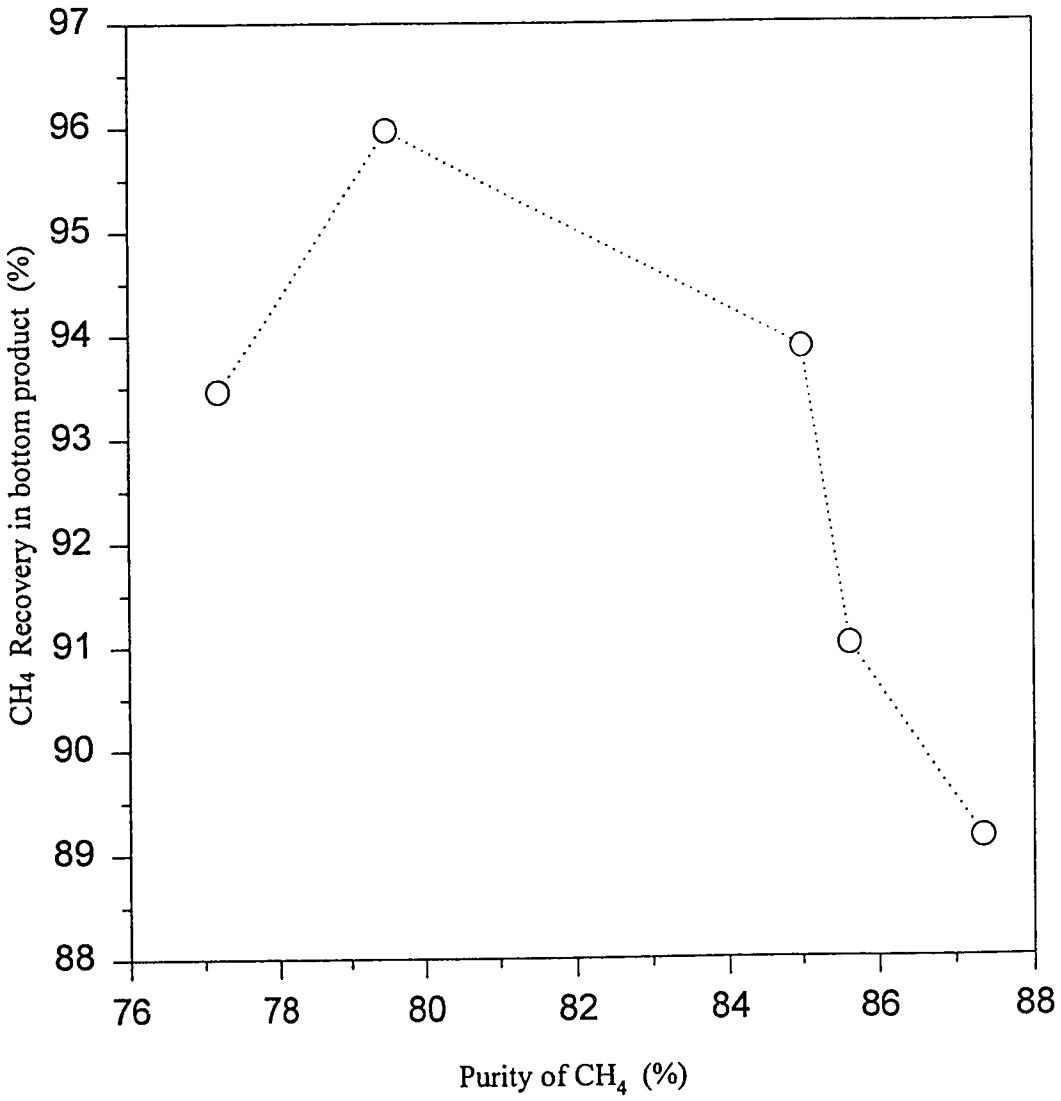

Figure 3.12. Graph of purity versus recovery for the modified cycle (Experimental)

3.4 MATHEMATICAL MODELING

A general overview of mathematical modeling of PSA processes has been given by Ruthven *et al.* (1994). For the present system the dynamic model with linear driving force expression is used to simulate some of the experimental Skarstrom cycle PSA runs described in section 3.2. The configuration of the beds is as shown in Figure 3.13.

The model is based on the following assumptions:

(1) The ideal gas law is applicable to the gas phase. The maximum pressure involved in the PSA experiments is 5 atm and the temperature is 300 K. At these conditions mixtures of methane and nitrogen are not expected to deviate too strongly from ideal gas behavior.

(2) Mass transfer between the gas and adsorbed phase is accounted for in all four cycle steps. For equilibrium controlled PSA systems with low kinetic resistance, assumption of frozen solid phase during pressurization and blowdown steps is not accurate. However, for one of the PSA experimental runs the effect of assuming frozen solid phase concentration profile during the two steps is investigated. When the frozen solid assumption is made, the gas phase concentration profile during blowdown is assumed to remain the same as that at the end of adsorption step with total pressure reduced from p_H to p_L. During pressurization the gas phase concentration profile is assumed to be pushed forward in the column by a distance ratio equal to the pressure ratio. Gas composition behind this distance is same as

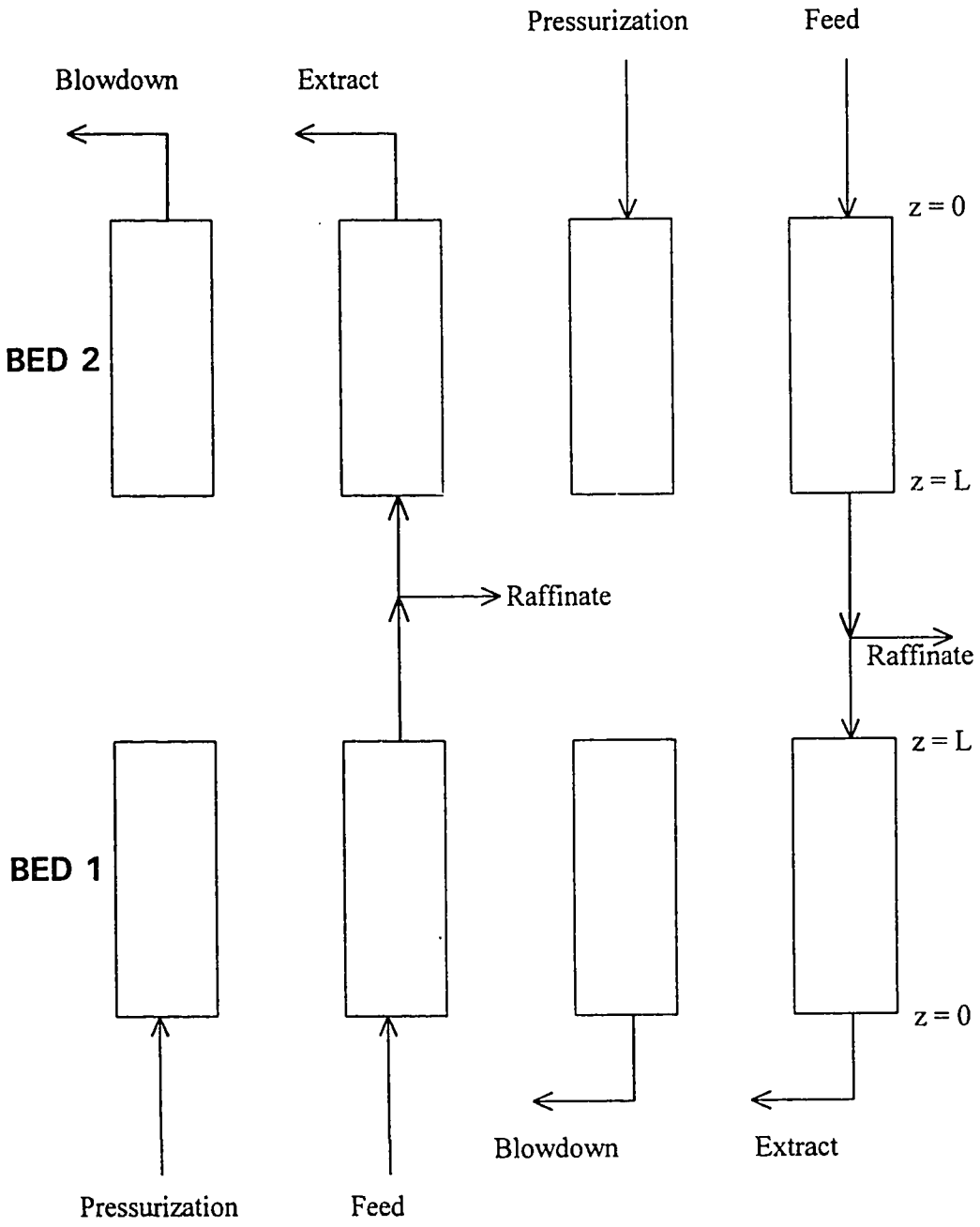

Figure 3.13. Schematic of the Skarstrom cycle used for modeling the PSA process

the feed composition and the composition ahead of this distance is equal to the average of gas phase composition at the end of the purge step. The comparison of the results will be discussed later in this chapter.

(3) The frictional pressure drop through the bed is neglected.

(4) The PSA separation system is taken to be isothermal. The heat of adsorption of CH_4 on activated carbon is less than 5 kcal/mole and does not vary with coverage (Yang and Doong, 1985). The maximum temperature gradient is expected to be not more than 5 to 8°C. Moreover only axial variations in gas and solid concentration in the bed are modeled with radial and tangential variations ignored.

(5) Variation in the velocity of the fluid along the column length, as determined by the overall mass balance equation for the present bulk separation process, is accounted for.

(6) The flow pattern is represented by the axial dispersed plug flow model. For each run the Peclet number is calculated using the axial dispersion coefficient D_L, the feed velocity, and the bed length. Danckwerts' boundary conditions are used in conjunction with the axial dispersion model.

(7) The equilibrium isotherm for each component is linear with Henry's constant as determined in chapter 2.

(8) Since the CH_4 / N_2 / MAXSORB system is equilibrium-driven and mass transfer resistance is of secondary importance, usage of the linear driving force model is preferable over the comprehensive pore diffusion model. This reduces the computational load by a substantial degree. A comparison of the LDF model and

the pore diffusion model for a kinetic PSA air separation process has been given by Farooq and Ruthven (1990).

(9) The LDF coefficient, k is taken to be independent of the pressure. An order of magnitude calculation of different mass transfer resistances for the present system reveals that the dominant mass transfer resistances are micropore and/or Knudsen diffusion. Hence using the same LDF coefficient for high and low pressure steps is justified as the ratio of the effective diffusivities for the two steps is equal to unity (Hassan *et al.*, 1985).

(10) The total pressure during adsorption and desorption steps is taken to be constant at p_H and p_L respectively.

(11) The pressure profile during pressurization and blowdown steps is taken to be a square-wave change for computational convenience. As observed in actual experiments the pressure changes nearly linearly during pressurization and blowdown for the present PSA separation. A comparison of the two approaches, *i.e.*, linear or square-wave pressure change, shows that there is practically no difference in predicted exit concentrations for an equilibrium PSA system by using either type of the pressure profile (Farooq *et al.*, 1989).

(12) In all PSA simulations the initial conditions in the beds are taken to be clean solid phase and all nitrogen in the gas phase although experimentally the initial conditions for each run correspond to the final conditions of the previous run. Therefore the approach to the cyclic steady state as predicted by the theoretical model do not represent the actual approach to steady state. However the same cyclic steady state concentration profiles are obtained with any initial conditions

for the present equilibrium based PSA process. A comparison of approach to cyclic steady state with different initial conditions will be presented below.

(13) The resulting model equations are solved using the method of orthogonal collocation which has been shown to be computationally much superior than finite difference method. (Hassan *et al.*, 1987)

(14) Finally, the usage of the detailed dynamic model over simple equilibrium theory is justifiable as the raffinate product is not pure nitrogen and some degree of mass transfer resistance and axial dispersion are present in the system.

Subject to the above assumptions the model equations for the PSA system are as follows:

[A = methane, B = nitrogen]

Step I :

Bed 1 (Pressurization)

$$-D_L \frac{\partial^2 c_{A1}}{\partial z^2} + \frac{\partial (v_1 c_{A1})}{\partial z} + \frac{\partial c_{A1}}{\partial t} + \left(\frac{1-\varepsilon}{\varepsilon}\right)\frac{\partial \bar{q}_{A1}}{\partial t} = 0 \qquad (3.4)$$

$$-D_L \frac{\partial^2 c_{B1}}{\partial z^2} + \frac{\partial (v_1 c_{B1})}{\partial z} + \frac{\partial c_{B1}}{\partial t} + \left(\frac{1-\varepsilon}{\varepsilon}\right)\frac{\partial \bar{q}_{B1}}{\partial t} = 0 \qquad (3.5)$$

The overall material balance is obtained by adding equations (3.4) and (3.5) and recognizing that the total concentration c_{T1} defined as $c_{T1} = c_{A1} + c_{B1}$ is a function of time and is not a function of z (due to negligible pressure drop in the bed)

$$c_{T1}\frac{\partial v_1}{\partial z} + \frac{\partial c_{T1}}{\partial t} + \left(\frac{1-\varepsilon}{\varepsilon}\right)\frac{\partial \bar{q}_{A1}}{\partial t} + \left(\frac{1-\varepsilon}{\varepsilon}\right)\frac{\partial \bar{q}_{B1}}{\partial t} = 0 \qquad (3.6)$$

Sorption kinetics are represented by the LDF expression for each of the two components

$$\frac{\partial \bar{q}_{A\,l}}{\partial t} = k_A \left(q^*_{A\,l} - \bar{q}_{A\,l} \right) \tag{3.7}$$

$$\frac{\partial \bar{q}_{B\,l}}{\partial t} = k_B \left(q^*_{B\,l} - \bar{q}_{B\,l} \right) \tag{3.8}$$

Adsorption equilibrium isotherm is linear

$$q^*_{A\,l} = K_A \, c_{A\,l} \tag{3.9}$$

$$q^*_{B\,l} = K_B \, c_{B\,l} \tag{3.10}$$

The boundary conditions are (Danckwert's boundary conditions)

$$-D_L \left. \frac{\partial c_{A\,l}}{\partial z} \right|_{z=0} = v_l \Big|_{z=0} \left[\, c_{A\,l} \Big|_{z=0^-} - c_{A\,l} \Big|_{z=0^+} \, \right] \tag{3.11}$$

$$\left. \frac{\partial c_{A\,l}}{\partial z} \right|_{z=L} = 0 \tag{3.12}$$

Similar boundary conditions apply to component B.

Boundary condition for velocity

$$v_l \Big|_{z=L} = 0 \tag{3.13}$$

Note that the differential equation (3.6) is first order in velocity and hence requires only one boundary condition (3.13). The velocity at $z = 0$ appearing in equation (3.11) is calculated by solving the overall mass balance equation (3.6).

Bed 2 (Blowdown)

$$-D_L \frac{\partial^2 c_{A2}}{\partial z^2} + \frac{\partial (v_2 c_{A2})}{\partial z} + \frac{\partial c_{A2}}{\partial t} + \left(\frac{1-\varepsilon}{\varepsilon}\right) \frac{\partial \bar{q}_{A2}}{\partial t} = 0 \tag{3.14}$$

$$-D_L \frac{\partial^2 c_{B2}}{\partial z^2} + \frac{\partial (v_2 c_{B2})}{\partial z} + \frac{\partial c_{B2}}{\partial t} + \left(\frac{1-\varepsilon}{\varepsilon}\right) \frac{\partial \bar{q}_{B2}}{\partial t} = 0 \tag{3.15}$$

The overall material balance is obtained by adding equations (3.14) and (3.15) and recognizing that the total concentration c_{T2} defined as $c_{T2} = c_{A2} + c_{B2}$ is a function of time and is not a function of z (due to negligible pressure drop in the bed)

$$c_{T2} \frac{\partial v_2}{\partial z} + \frac{\partial c_{T2}}{\partial t} + \left(\frac{1-\varepsilon}{\varepsilon}\right) \frac{\partial \bar{q}_{A2}}{\partial t} + \left(\frac{1-\varepsilon}{\varepsilon}\right) \frac{\partial \bar{q}_{B2}}{\partial t} = 0 \tag{3.16}$$

Sorption kinetics are represented by LDF expression for each of the two components

$$\frac{\partial \bar{q}_{A2}}{\partial t} = k_A \left(q^*_{A2} - \bar{q}_{A2}\right) \tag{3.17}$$

$$\frac{\partial \bar{q}_{B2}}{\partial t} = k_B \left(q^*_{B2} - \bar{q}_{B2}\right) \tag{3.18}$$

Adsorption equilibrium isotherm is linear

$$q^*_{A2} = K_A c_{A2} \tag{3.19}$$

$$q^*_{B2} = K_B c_{B2} \tag{3.20}$$

The boundary conditions are (Danckwert's boundary conditions)

$$-D_L \left.\frac{\partial c_{A2}}{\partial z}\right|_{z=L} = v_2\big|_{z=L}\left[c_{A2}\big|_{z=L^+} - c_{A2}\big|_{z=L^-} \right] \tag{3.21}$$

But since $v_2 = 0$ at the inlet of the column, z = L , we have

$$-D_L \left.\frac{\partial c_{A2}}{\partial z}\right|_{z=L} = \left.\frac{\partial c_{A2}}{\partial z}\right|_{z=0} = 0 \tag{3.22}$$

Similar boundary conditions apply to component B.

Boundary condition for velocity

$$v_2\big|_{z=L} = 0 \tag{3.23}$$

Step 2:

Bed 1 (Adsorption)

$$-D_L \frac{\partial^2 c_{A1}}{\partial z^2} + \frac{\partial (v_1 c_{A1})}{\partial z} + \frac{\partial c_{A1}}{\partial t} + \left(\frac{1-\varepsilon}{\varepsilon}\right)\frac{\partial \bar{q}_{A1}}{\partial t} = 0 \tag{3.24}$$

$$-D_L \frac{\partial^2 c_{B1}}{\partial z^2} + \frac{\partial (v_1 c_{B1})}{\partial z} + \frac{\partial c_{B1}}{\partial t} + \left(\frac{1-\varepsilon}{\varepsilon}\right)\frac{\partial \bar{q}_{B1}}{\partial t} = 0 \tag{3.25}$$

The overall material balance is obtained by adding equations (3.24) and (3.25) and recognizing that the total concentration c_{T1} is neither a function of time (constant pressure during the adsorption step), nor a function of z (due to negligible pressure drop in the bed)

$$c_{T1} \frac{\partial v_1}{\partial z} + \left(\frac{1-\varepsilon}{\varepsilon}\right)\frac{\partial \bar{q}_{A1}}{\partial t} + \left(\frac{1-\varepsilon}{\varepsilon}\right)\frac{\partial \bar{q}_{B1}}{\partial t} = 0 \tag{3.26}$$

Sorption kinetics are represented by the LDF expression for each of the two components

$$\frac{\partial \bar{q}_{A\,I}}{\partial t} = k_A \left(q^*_{A\,I} - \bar{q}_{A\,I} \right) \tag{3.27}$$

$$\frac{\partial \bar{q}_{B\,I}}{\partial t} = k_B \left(q^*_{B\,I} - \bar{q}_{B\,I} \right) \tag{3.28}$$

Adsorption equilibrium isotherm is linear

$$q^*_{A\,I} = K_A \, c_{A\,I} \tag{3.29}$$

$$q^*_{B\,I} = K_B \, c_{B\,I} \tag{3.30}$$

The boundary conditions are (Danckwert's boundary conditions)

$$-D_L \left. \frac{\partial c_{A\,I}}{\partial z} \right|_{z=0} = v_I \Big|_{z=0} \left[\, c_{A\,I} \Big|_{z=0^-} - c_{A\,I} \Big|_{z=0^+} \, \right] \tag{3.31}$$

$$\left. \frac{\partial c_{A\,I}}{\partial z} \right|_{z=L} = 0 \tag{3.32}$$

Similar boundary conditions apply to component B.

Boundary condition for velocity

$$v_I \Big|_{z=0} = v_{0\,H} \tag{3.33}$$

Bed 2 (Desorption)

$$-D_L \frac{\partial^2 c_{A2}}{\partial z^2} + \frac{\partial (v_2 c_{A2})}{\partial z} + \frac{\partial c_{A2}}{\partial t} + \left(\frac{1-\varepsilon}{\varepsilon}\right)\frac{\partial \bar{q}_{A2}}{\partial t} = 0 \tag{3.34}$$

$$-D_L \frac{\partial^2 c_{B2}}{\partial z^2} + \frac{\partial (v_2 c_{B2})}{\partial z} + \frac{\partial c_{B2}}{\partial t} + \left(\frac{1-\varepsilon}{\varepsilon}\right)\frac{\partial \bar{q}_{B2}}{\partial t} = 0 \tag{3.35}$$

The overall material balance is obtained by adding equations (3.34) and (3.35) and recognizing that the total concentration c_{T2} is neither a function of time (constant total pressure during desorption step), nor a function of z (due to negligible pressure drop in the bed)

$$c_{T2}\frac{\partial v_2}{\partial z} + \left(\frac{1-\varepsilon}{\varepsilon}\right)\frac{\partial \bar{q}_{A2}}{\partial t} + \left(\frac{1-\varepsilon}{\varepsilon}\right)\frac{\partial \bar{q}_{B2}}{\partial t} = 0 \tag{3.36}$$

Sorption kinetics are represented by LDF expression for each of the two components

$$\frac{\partial \bar{q}_{A2}}{\partial t} = k_A \left(q^*_{A2} - \bar{q}_{A2}\right) \tag{3.37}$$

$$\frac{\partial \bar{q}_{B2}}{\partial t} = k_B \left(q^*_{B2} - \bar{q}_{B2}\right) \tag{3.38}$$

Adsorption equilibrium isotherm is linear

$$q^*_{A2} = K_A c_{A2} \tag{3.39}$$

$$q^*_{B2} = K_B c_{B2} \tag{3.40}$$

The boundary conditions are (Danckwert's boundary conditions)

$$-D_L \left.\frac{\partial c_{A2}}{\partial z}\right|_{z=L} = v_2\big|_{z=L}\left[\, c_{A2}\big|_{z=L^+} - c_{A2}\big|_{z=L^-} \,\right] \tag{3.41}$$

$$\left.\frac{\partial c_{A2}}{\partial z}\right|_{z=0} = 0 \tag{3.42}$$

Similar boundary conditions apply to component B.

Boundary condition for velocity

$$v_2\big|_{z=L} = v_{PF} \tag{3.43}$$

where v_{PF} stands for the purge to feed velocity ratio.

The equations representing the mass transfer and fluid flow in the two beds in steps 3 and 4 are similar to those for steps 1 and 2 with the roles of bed 1 and bed 2 interchanged. These equations are not written here but are solved for steps 3 and 4 with the difference in the direction of flow accounted for appropriately.

The initial conditions are:

$$c_{A1}(z,t=0) = c_{Ao}\,, \qquad c_{B1}(z,t=0) = c_{Bo}$$

$$\bar{q}_{A1}(z,t=0) = \bar{q}_{B1}(z,t=0) = 0$$

$$c_{A2}(z,t=0) = c_{Ao}\,, \qquad c_{B2}(z,t=0) = c_{Bo}$$

$$\bar{q}_{A2}(z,t=0) = \bar{q}_{B2}(z,t=0) = 0 \tag{3.44}$$

The above set of differential equations is written in normalized form using the following dimensionless variables:

$$y_{ij} = \frac{c_{ij}}{c_{Tj}} \qquad x = \frac{z}{L} \qquad c_{Tj} = \frac{p_j}{RT} \qquad u_j = \frac{v_j}{v_{0H}}$$

$$\psi_{ij} = \frac{\bar{q}_{ij}}{q_{i\,Ref}} \qquad \tau = \frac{t\,v_{0H}}{L} \qquad \psi^{*}_{ij} = \frac{q^{*}_{ij}}{q_{i\,Ref}} \tag{3.45}$$

In the above normalization variables,

$$q_{i\,Ref} = \frac{K_i\,p_H}{RT} \tag{3.46}$$

That is, $q_{i\,Ref}$ represents the solid phase concentration of component i in equilibrium with a gas phase of pure i at high pressure. The normalized model equations are presented only for step I (bed 2) and step II (bed 1). Since the sum of the two mole fractions for the present binary system is unity, solving only for component A in the gas phase gives complete gas phase concentration profile because mole fraction of B is calculated by difference.

Step I:

Bed 2 (Blowdown)

$$-\frac{1}{Pe}\frac{\partial^2 y_2}{\partial x^2}+\frac{\partial (u_2 y_2)}{\partial x}+\frac{\partial y_2}{\partial \tau}+\frac{y_2}{p_2}\frac{\partial p_2}{\partial \tau}+\left(\frac{1-\varepsilon}{\varepsilon}\right)\frac{RTq_{A\,Ref}}{p_2}\frac{\partial \psi_{A2}}{\partial \tau}=0 \tag{3.47}$$

$$\frac{\partial u_2}{\partial x}+\frac{1}{p_2}\frac{\partial p_2}{\partial \tau}+\left(\frac{1-\varepsilon}{\varepsilon}\right)\frac{RT}{p_2}\left(q_{A\,Ref}\frac{\partial \psi_{A2}}{\partial \tau}+q_{B\,Ref}\frac{\partial \psi_{B2}}{\partial \tau}\right)=0 \tag{3.48}$$

$$\frac{\partial \psi_{A2}}{\partial \tau}=\frac{k_A v_{0H}}{L}\left(\psi^{*}_{A2}-\psi_{A2}\right) \tag{3.49}$$

$$\frac{\partial \psi_{B2}}{\partial \tau} = \frac{k_B v_{0H}}{L}\left(\psi^{\bullet}_{B2} - \psi_{B2}\right) \tag{3.50}$$

$$\psi^{\bullet}_{A2} = K_A \frac{p_2}{RTq_{A\,Ref}} y_2 \tag{3.51}$$

$$\psi^{\bullet}_{B2} = K_B \frac{p_2}{RTq_{B\,Ref}} \left(1 - y_2\right) \tag{3.52}$$

$$\left.\frac{\partial y_2}{\partial x}\right|_{x=1} = 0 \tag{3.53}$$

$$\left.\frac{\partial y_2}{\partial x}\right|_{x=0} = 0 \tag{3.54}$$

$$u_2\big|_{x=1} = 0 \tag{3.55}$$

Step II:

Bed 1 (Adsorption)

$$-\frac{1}{Pe}\frac{\partial^2 y_1}{\partial x^2} + \frac{\partial (u_1 y_1)}{\partial x} + \frac{\partial y_1}{\partial \tau} + \left(\frac{1-\varepsilon}{\varepsilon}\right)\frac{RTq_{A\,Ref}}{p_1}\frac{\partial \psi_{A1}}{\partial \tau} = 0 \tag{3.56}$$

$$\frac{\partial u_1}{\partial x} + \left(\frac{1-\varepsilon}{\varepsilon}\right)\frac{RT}{p_1}\left(q_{A\,Ref}\frac{\partial \psi_{A1}}{\partial \tau} + q_{B\,Ref}\frac{\partial \psi_{B1}}{\partial \tau}\right) = 0 \tag{3.57}$$

$$\frac{\partial \psi_{A1}}{\partial \tau} = \frac{k_A v_{0H}}{L}\left(\psi^{\bullet}_{A1} - \psi_{A1}\right) \tag{3.58}$$

$$\frac{\partial \psi_{B\,l}}{\partial \tau} = \frac{k_B v_{0H}}{L}\left(\psi^{\bullet}_{B\,l} - \psi_{B\,l}\right) \tag{3.59}$$

$$\psi^{\bullet}_{A\,l} = K_A \frac{p_l}{RTq_{A\,Ref}} y_l \tag{3.60}$$

$$\psi^{\bullet}_{B\,l} = K_B \frac{p_l}{RTq_{B\,Ref}} \left(1 - y_l\right) \tag{3.61}$$

$$\left.\frac{\partial y_l}{\partial x}\right|_{x=0} = u_l\big|_{x=0}\left[y_{Feed} - y_l\big|_{x=0^-}\right] \tag{3.62}$$

$$\left.\frac{\partial y_l}{\partial x}\right|_{x=1} = 0 \tag{3.63}$$

$$u_l\big|_{x=0} = 1 \tag{3.64}$$

Similar sets of equations are written for both the beds for all four steps. Partial differential equations are reduced to ordinary differential equations by the method of orthogonal collocation. The overall mass balance equation reduces to a set of algebraic simultaneous linear equations. Simultaneous ordinary differential equations are solved using the method of Hindmarsch-Gear with functional iteration (Hindmarsch and Gear, 1972 ; Press *et al.*, 1992). Gaussian elimination method is used to solve simultaneous algebraic equations. Five internal collocation points are used for solution of each column.

The parameter values used in this PSA simulations are listed in Tables 3.3 and Table 3.4. Determination of some parametric values has been discussed before the model

Table 3.3. Parametric values used in the simulations of equilibrium PSA system with Skarstrom cycle

Feed	60 % methane , 40 % nitrogen
Adsorbent	MAXSORB activated carbon
Temperature [K]	300
Bed length [cm]	51.0
Bed voidage [-]	0.480
Blowdown / Desorption pressure [atm]	1.0
Isotherm type	Linear
Equilibrium constant for CH_4 [-]	20.1855
Equilibrium constant for N_2 [-]	6.6867
LDF constant for CH_4 [s^{-1}]	2.947
LDF constant for N_2 [s^{-1}]	8.255
Axial Dispersion coefficient [cm^2/s]	0.335
Initial conditions	Clean solid phase and all nitrogen in gas phase in both beds at respective pressures

Table 3.4. Velocity, cycle time, and other parameters input to PSA simulations

Parameter / Run number	Run 2	Run 3	Run 4	Run 5	Run 6	Run 7	Run 8
p_H [atm]	4.08	4.06	4.06	4.06	4.06	4.06	4.06
Total cycle time [s]	200	150	400	500	300	540	540
Pressurization / Blowdown time [s]	20	30	28	35	30	27	27
Adsorption / Desorption time [s]	80	45	172	215	270	243	243
Feed velocity, v_{0H} [cm / s]	0.84	0.79	0.85	0.7	0.8	1.0	0.8
Raffinate velocity [cm / s]	0.23	0.19	0.30	0.26	0.27	0.28	0.21

equations are listed. One of the most important parameter in the PSA simulations is the purge to feed velocity ratio. In the present PSA experiments the purge velocity is not directly measured. Rather a mass balance is developed on the point where raffinate and purge streams split. The measured raffinate velocity is provided to the program. The velocity at the outlet of the high-pressure bed is calculated as a solution of the overall mass balance equation. Hence the purge velocity is computed by a simple mass balance. Note that the mole fraction of methane in the raffinate, in the outlet stream of adsorption bed, and in the purge stream is the same as the purge stream at the desorption pressure.

3.5 RESULTS AND DISCUSSIONS (PSA MODELING)

The model equations are solved for PSA runs for which feed velocity during the adsorption step is measured. A summary of results at cyclic steady state is given in Table 3.5 where a comparison with experimental results has also been made. It is seen that a good match between experimental and model results is obtained for the present equilibrium-driven PSA system. For these PSA simulations cyclic steady state is achieved in 4 to 5 cycles. The gas phase concentration profiles in the two beds at the end of a cycle at cyclic steady state are shown in Figure 3.14 for run 2.

As mentioned in section 3.4 the model predictions at the cyclic steady state, for the present equilibrium PSA system with linear isotherms, are independent of the initial conditions. This is illustrated in Figure 3.15 where approach to the cyclic steady state is

Table 3.5. Summary of PSA simulation results (at the end of a cycle) at cyclic steady state

Run number	**Extract CH_4 purity**		**Raffinate CH_4 purity**		**Extract velocity**	
	MODEL %	EXPT %	MODEL %	EXPT %	MODEL [cm/s]	EXPT [cm/s]
2	74.68	70.60	23.82	24.25	2.348	2.238
3	77.61	69.9	25.43	23.00	2.402	2.376
4	70.52	71.50	22.10	18.00	1.897	1.95
5	65.44	69.05	19.48	17.52	1.914	2.009
6	66.49	66.50	22.58	20.80	1.669	1.75
7	69.95	70.00	25.98	18.00	1.715	1.869
8	59.80	61.00	18.52	8.00	2.360	2.371

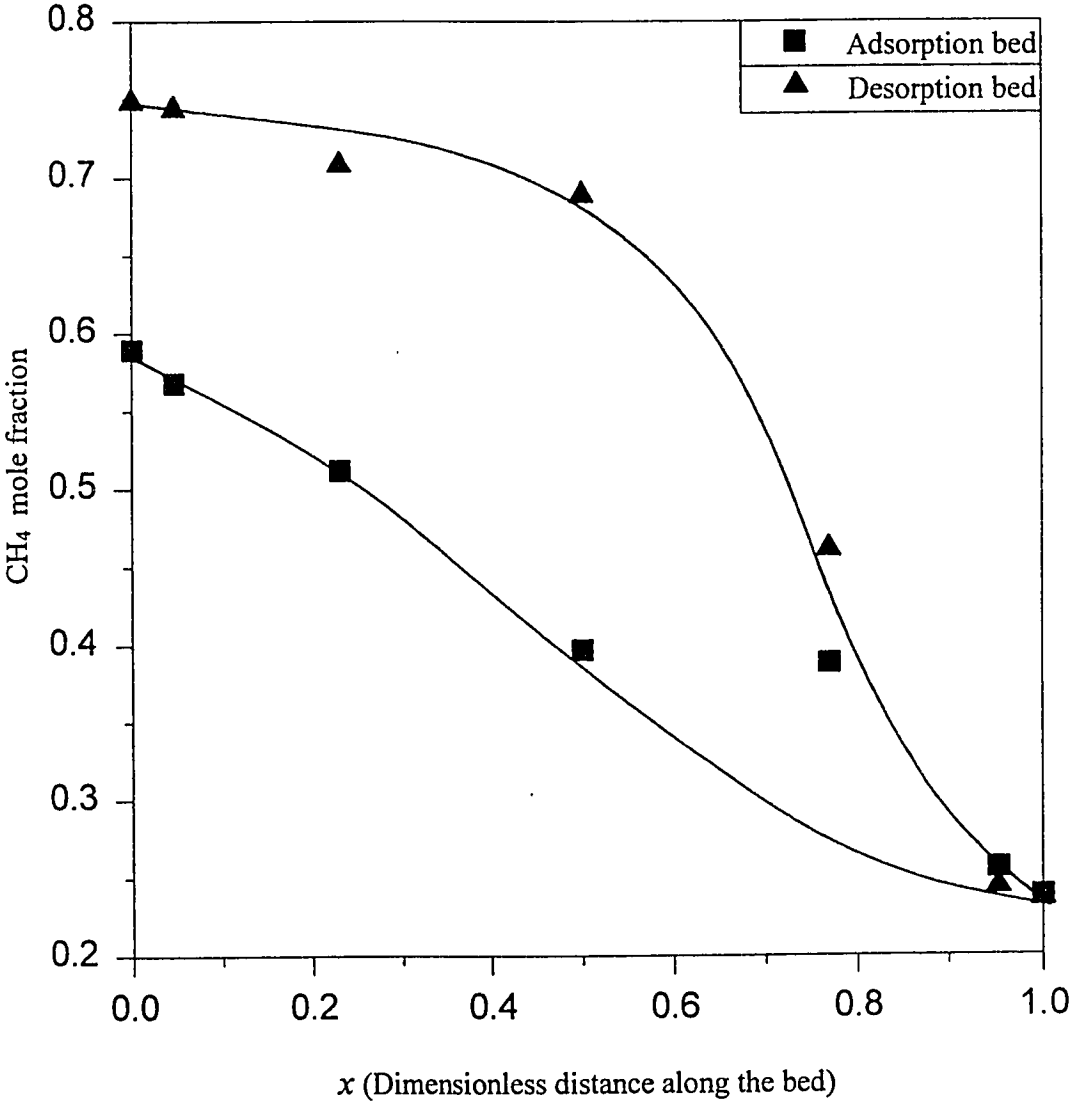

Figure 3.14. Gas phase concentration profiles in the beds at the end of cycle at cyclic steady state (Run 2)

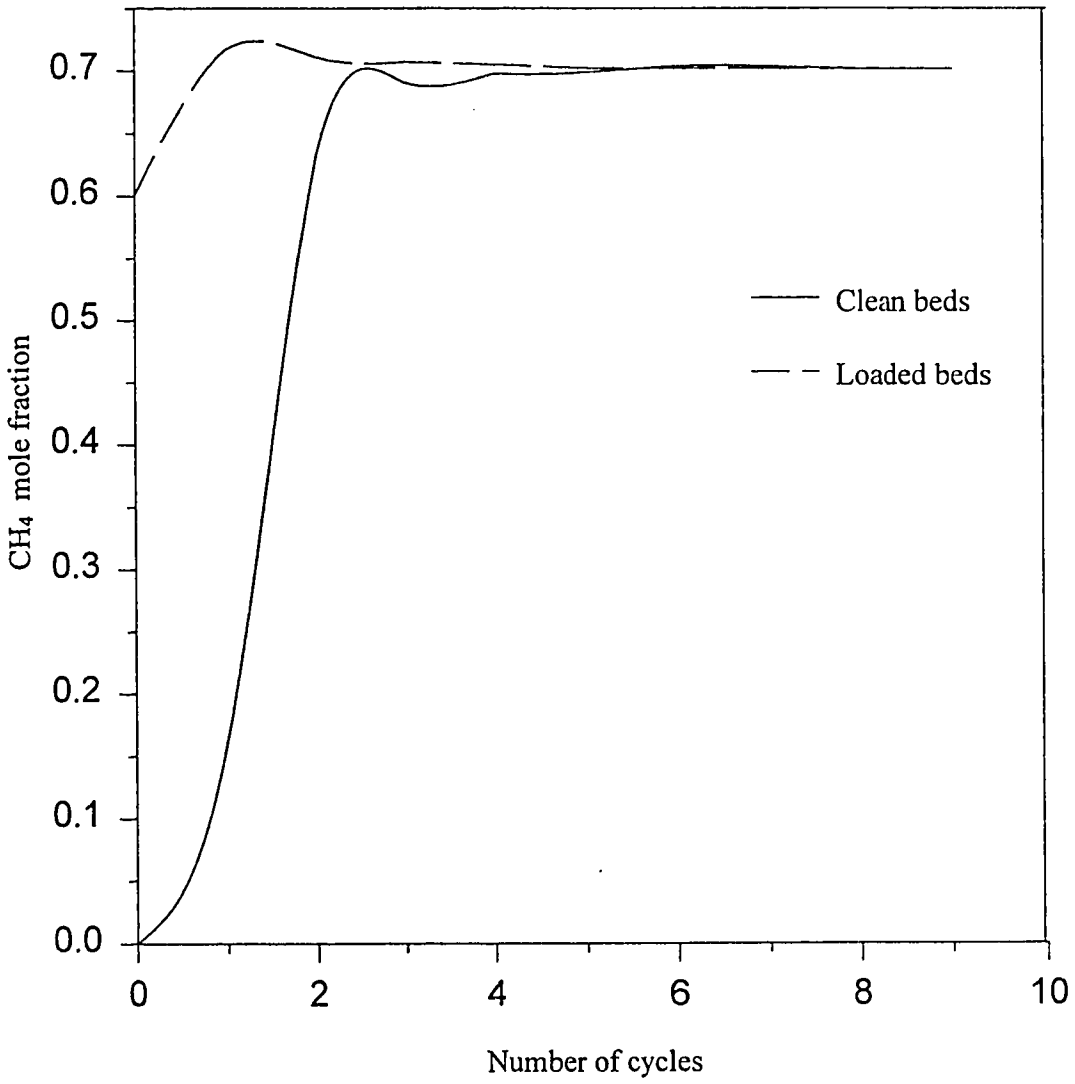

Figure 3.15. Theoretical approach to cyclic steady state with different initial conditions (Run 4)

shown starting from two different sets of initial conditions for run 4. The solid curve represents the approach to the cyclic steady state starting from pure nitrogen in the gas phase at low pressure and a solid phase free of any sorbates for both beds. The dashed curve represents the initial conditions of solid phase in equilibrium with 60/40 methane/nitrogen feed at respective pressure of each bed. In fact several sets of initial conditions are used and all are observed to lead to the same cyclic steady state which matches fairly well with the experimental results. Hence it is clear that the initial conditions do not have any effect on final cyclic steady state achieved by the present system. However, the approach to the cyclic steady state obviously changes with varying initial conditions.

Assumption 2 in section 3.4 states that the mass transfer equations between gas and solid phase are solved for all four steps (pressurization, adsorption, blowdown, and desorption) for the PSA simulation of the present methane / nitrogen / MAXSORB system. Otherwise the model predictions are not reliable. This is investigated for one of the PSA runs. Results are shown in Figure 3.16 where the dashed curve represents the model predictions when solid phase is assumed frozen during pressurization and blowdown steps. The calculation of gas phase concentration profiles has been discussed in section 3.4. Note that when equations for all the steps are solved the prediction of methane mole fraction in the raffinate coincides with the experimental value. Hence it is established that it is necessary to take into account the mass transfer during pressurization and blowdown steps if an equilibrium-driven PSA system is to be realistically modeled.

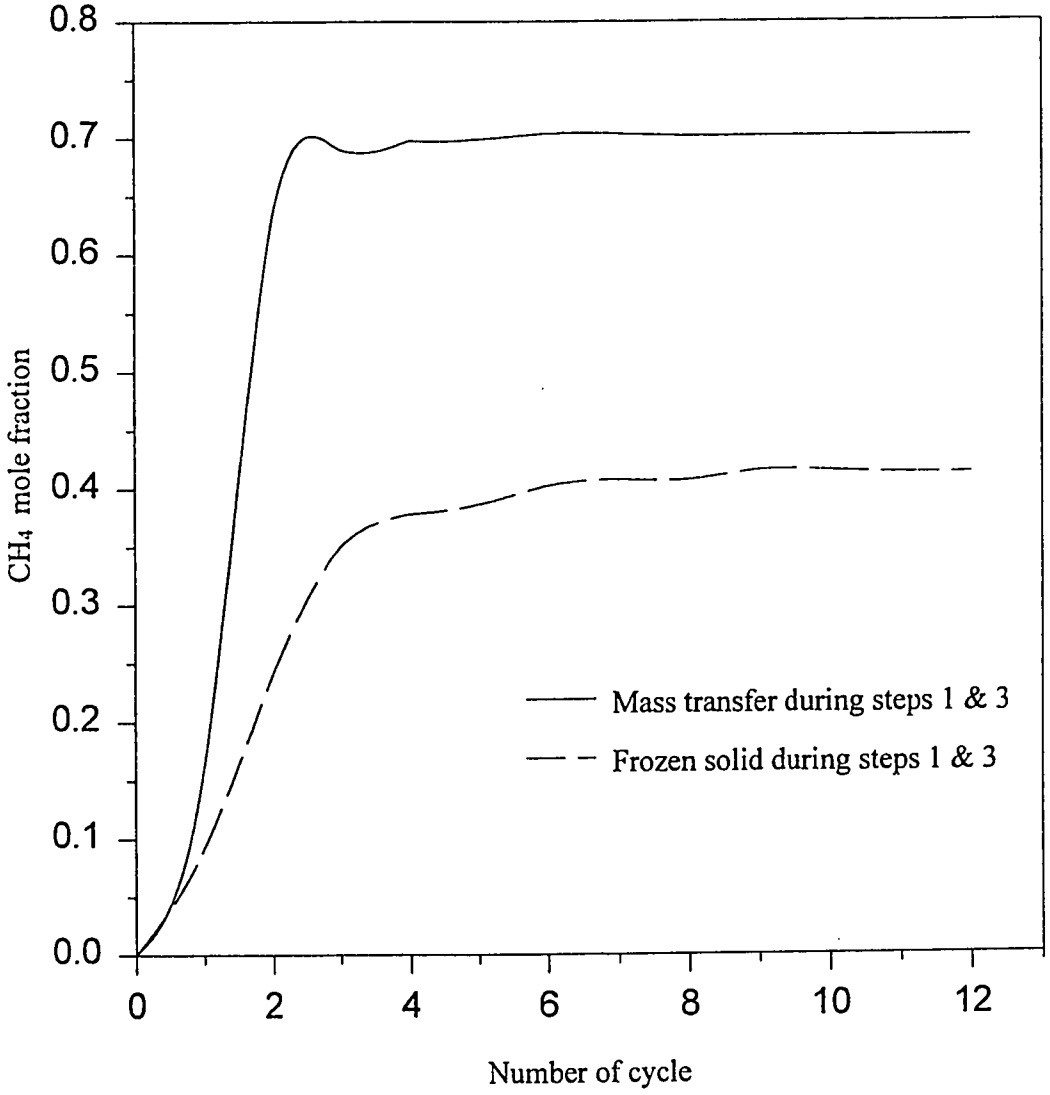

Figure 3.16. Theoretical approach to cyclic steady state with frozen solid phase during pressurization and blowdown steps (Run 4)
Experimental methane mole fraction = 0.715

3.6 CONCLUSION

This effort to separate methane and nitrogen on the Skarstrom PSA cycle does not give a significant improvement over the previous work in this direction mentioned in Chapter 1. However runs 1 to 17 should not be considered as an effort to optimize the CH_4 / N_2 / MAXSORB system. That is, further improvement in the extract methane purity is possible. This can be achieved by fixing all but one of the parameter values to find a local optimum. Similar local optima can be obtained by varying each parameter one by one. The overall optimal separation is a proper combination of these local optima. Nevertheless the present work justifies the option of an equilibrium PSA separation of methane and nitrogen over a methane selective adsorbent. A good separation behavior is shown by the present system as far as the effects of varying different operational parameters are concerned.

The recovery of methane in the bottom-product as in Table 3.1 may represent a higher value than the true recovery. Any difference can be attributed to problems in measuring the blowdown gas flowrate as this flowrate lies outside the range of the flow meter. A carefully extrapolated value is used for recovery calculations in Table 3.1. It is expected that the true methane recovery in the bottom-product may be 4 to 5% below the value reported in Table 3.1. Since the primary objectives of the present work is to obtain a rich extract or bottom product, low nitrogen purity and recovery in the raffinate product

as in Table 3.1 is not a matter of concern. However, the modified cycle gives better purity and recovery of both components.

Due to near absence of diffusional resistances the PSA system is seen to be very sensitive to any changes in the column pressure. This precludes keeping a proper track of actual conditions in the columns. These final conditions serve as the initial conditions for the next run. Furthermore the cyclic steady state is achieved quickly and, as evident from Figure 3.15, precisely the same cyclic steady state is reached regardless of the initial conditions. It is apparent that an inaccurate knowledge of initial conditions for a PSA run has no serious influence on any conclusions drawn once the cyclic steady state is reached.

A significant gain in the quality of the products is achieved when the methane / nitrogen / MAXSORB pressure swing adsorption system is run on a modified cycle with cocurrent depressurization. This illustrates that a cycle scheme more complex than the Skarstrom cycle is required if the objective of obtaining better products is to be fulfilled. Moreover it is established that an equilibrium PSA process can be a feasible route for separation of methane - nitrogen mixtures to upgrade the quality of natural gas with a high nitrogen content. This marks the general conclusion of the present separation attempt. It should be noted that the primary objective of experimental runs 1N through 6N is not to seek for the best bottom product. Rather, it is attempted to demonstrate that a richer bottom product is possible with the modified cycle. Even better methane purity can be achieved if the cycle time, pressure ratio, and the feed flowrate are varied to seek for an optimum. Upon inspection of Table 3.2 it is found that although methane purity in the

bottom-product is above 85%, methane recovery is still high enough to make the separation an attractive one. The overall separation performance is seen to tend towards furnishing two purified products; a nitrogen-rich top product and a methane-rich bottom product. The recoveries of nitrogen and methane in their respective streams are moderate and high respectively.

Generally, a good agreement is found in the predicted and experimentally observed behavior of the PSA system. The small differences arise from some of the model assumptions (isothermality, negligible frictional pressure drop, *etc.*) and from imperfections in the experimental setup and procedures (such as constant pressure and feed flowrate during adsorption step, time lags, any backflows, *etc.*). The LDF expression represents the adsorption kinetics adequately for an equilibrium system. This is because contrary to the kinetic PSA separations, the LDF constant is not a function of cycle time for this equilibrium separation process. It should be noted that the equilibrium and kinetic parameters used in the present simulations are obtained from independent experiments. Other input values to the simulation program such as bed length, porosity, feed velocity, *etc.* are measured system parameters. Hence the PSA simulations for the present system can be regarded as predictive modeling as no parameters are adjusted to obtain a match between the theoretical and experimental data. The modified cycle can also be simulated with the same modeling approach using the appropriate boundary conditions for the cocurrent depressurization step. This is, however, not done as a part of this research thesis owing to the limitations of time and scope.

Nomenclature

c	gas phase concentration of sorbent [mole cm^{-3}]
$\bar{c}$	instantaneous mole fraction of a component in top and bottom products [-]
c_T	total gas phase concentration of sorbent [mole cm^{-3}]
D_L	axial dispersion coefficient [cm^2 s^{-1}]
K	dimensionless Henry's law constant [-]
k	overall effective mass transfer coefficient used in the linear driving force expression [s^{-1}]
L	length of a PSA bed [cm]
p	pressure [atm]
p_H	absorption pressure [atm]
p_L	desorption pressure [atm]
p_{CD}	pressure at the end of cocurrent depressurization step [atm]
Pe	Peclet number $= v\,L\,/D_L$ [-]
q_{iRef}	reference sorbate concentration of component i defined by equation (3.46) [mole cm^{-3}]
$\bar{q}$	sorbate concentration averaged over a particle [mole cm^{-3}]
q^*	sorbate concentration in equilibrium with gas phase [mole cm^{-3}]
Q	flow rate of gases in top and bottom products averaged over a full PSA cycle at cyclic steady state [cm^3 STP s^{-1}]
$\bar{Q}$	instantaneous flow rate of gases [cm^3 STP s^{-1}]

R	gas constant [cm^3 atm $mole^{-1}$ K^{-1}]
t	time [s]
T	absolute temperature [K]
u	interstitial velocity through a PSA column [-]
v	interstitial velocity through a PSA column [cm s^{-1}]
v_{OH}	feed velocity during adsorption step [cm s^{-1}]
x	axial distance along the length of a PSA column [-]
y_{ij}	mole fraction of component i in bed [-]
z	axial distance along the length of a PSA column [cm]

Greek symbols

ε	porosity of a PSA column [-]
ψ	sorbate concentration of a component [-]
ψ^*	sorbate concentration of component in equilibrium with the gas phase [-]
τ	dimensionless time [-]

Subscripts

A	methane
B	nitrogen
T	total
i	component A or B
j	bed 1 or 2

References

Cen, P. L. and R. T. Yang, Separation of Binary Gas Mixture into Two High-Purity Products by a New Pressure Swing Adsorption Cycle, *Sep. Sci. Technol.*, 21, 845-864, 1986 a.

Cen, P. L. and R. T. Yang, Bulk Separation by Pressure Swing Adsorption, *Ind. Eng. Chem. Fundam.*, 25, 758-767, 1986 b.

Farooq, S., D. M. Ruthven, and H. A. Boniface, Numerical Simulation of a Pressure Swing Adsorption Oxygen Unit, *Chem. Eng. Sci.*, 44, 2809-2816, 1989.

Farooq, S. and D. M. Ruthven, A Comparison of Linear Driving Force and Pore Diffusion Models for a Pressure Swing Adsorption Bulk Separation Process, *Chem. Eng. Sci.*, 45, 107-115, 1990.

Hassan, M. M., N. S. Raghavan, D. M. Ruthven and H. A. Boniface, Pressure Swing Adsorption Part II : Experimental Study of a Nonlinear Trace Component Isothermal System, *AIChE J.*, 31, 2008-2016, 1985.

Hassan, M. M., N. S. Raghavan and D. M. Ruthven, Numerical Simulation of a Pressure Swing Adsorption System— A Comparative Study of Finite Difference and Collocation Methods, *Can. J. Chem. Eng.*, 65, 512-516, 1987.

Hindmarsch, A. C. and C. W. Gear, *Ordinary Differential Equations System Solver*, Lawrence Livermore Laboratory Report UCID 30001. Rev. 2, 1972.

Press, H. W., S. A. Teukolsky, W. T. Vetterling and B. P. Flannery, *Numerical Recipes in FORTRAN : The Art of Scientific Computing*, Cambridge University Press, 2nd ed., 1992.

Ruthven, D. M, Farooq, S., and K. S. Knaebel, *Pressure Swing Adsorption*, VCH Publishers, New York, 1994.

Suh, S-S. and P. C. Wankat, Combined Cocurrent-Countercurrent Blowdown Cycle in Pressure Swing Adsorption, *AIChE J.*, 35, 523-526, 1989.

Yang, R. T. and S. J. Doong, Gas Separation by Pressure Swing Adsorption : A Pore-Diffusion Model for Bulk Separation, *AIChE J.*, 31, 1829-1842, 1985.c

CHAPTER 4

MODIFICATION OF THE LDF EQUATION FOR CONCENTRATION DEPENDENT DIFFUSIVITY

In this chapter a modified form of the Glueckauf linear driving force (LDF) equation is presented. The new equation is based on the concentration dependent diffusivity and uses the gradient of chemical potential as the driving force for diffusional mass transport. Extension of this single component equation to binary diffusion is also presented. The purpose of deriving the new equations for the binary diffusion is to use them in place of pore diffusion equations based on concentration dependent diffusivity in a kinetic pressure swing adsorption model so as to accelerate and simplify the numerical modeling of the PSA process.

4.1 THEORETICAL FORMULATION

The diffusion equation for the case of unidirectional micropore diffusion processes, where the heat transfer limitations are absent and the adsorbent particles can be approximated as spherical, reduces to

$$\frac{\partial q}{\partial t} = \frac{1}{r^2}\frac{\partial}{\partial r}\left(D_c\, r^2 \frac{\partial q}{\partial r} \right) \tag{4.1}$$

If the step change in the concentration is small, D_c can be considered independent of concentration and equation (4.1) is written as

$$\frac{\partial q}{\partial t} = \frac{D_c}{r^2}\frac{\partial}{\partial r}\left(r^2\frac{\partial q}{\partial r}\right) \tag{4.2}$$

For a step change in sorbate concentration at the surface of the spherical particle equation (4.2) is subject to the following initial and boundary conditions

$$q(r,0) = q_0'$$

$$q(r_c,t) = q_0$$

$$\frac{\partial q}{\partial r}(0,t) = 0 \tag{4.3}$$

An analytical solution of the above distributed parameter system is possible and the resulting solution is

$$\frac{\bar{q} - q_0'}{q_0 - q_0'} = \frac{m_t}{m_\infty} = 1 - \frac{6}{\pi^2}\sum_{n=1}^{\infty}\frac{1}{n^2}\exp\left(\frac{-n^2\pi^2 D_c t}{r_c^2}\right) \tag{4.4}$$

Glueckauf and Coates (1947) suggested the following lumped parameter system to represent the diffusional process

$$\frac{\partial \bar{q}}{\partial t} = k(q^* - \bar{q}) \tag{4.5}$$

which subject to the initial condition in equation (4.3) can be solved to give

$$\frac{m_t}{m_\infty} = 1 - exp\left(-kt\right) \tag{4.6}$$

By a comparison of equations (4.4) and (4.6) Glueckauf and Coates proposed the following equation for the equivalent overall mass transfer coefficient valid for 90% of the uptake

$$k = 15\frac{D_c}{r_c^2} \tag{4.7}$$

where the constant 15 applies to spherical geometry. For other coordinate systems the constant has different values that can be easily derived.

However if the step change in the sorbate concentration is large and the isotherm is nonlinear over the concentration change, D_c is a strong function of the sorbate concentration and cannot be taken out of the differentiation in equation (4.1). Under these conditions, if the gradient of chemical potential is used as the driving force for diffusion (Kärger and Ruthven, 1992) and the isotherm nonlinearity can be represented by the Langmuir model, the following expression for the concentration dependent diffusivity can be derived (Garg and Ruthven, 1972)

$$D_c = D_0\frac{\partial\, ln\, p}{\partial\, ln\, q} = \frac{D_0}{1-\theta} \tag{4.8}$$

D_0 is the limiting diffusivity as $q \rightarrow 0$ and can be taken to be independent of concentration q ; θ is a measure of step size of the sorbate concentration. Then equation (4.1) is written as

$$\frac{\partial q}{\partial t} = \frac{D_0}{r^2}\frac{\partial}{\partial r}\left(\frac{r^2}{1-\theta}\frac{\partial q}{\partial r}\right) \tag{4.9}$$

Numerical solution to this equation has been given by Garg and Ruthven (1972) who have compared the solutions to equations (4.4) and (4.9) using an average diffusivity and have plotted the effective diffusivity D_c in (4.2) as a function of isotherm nonlinearity θ.

In the present work the following form of the constant in the LDF equation (4.5) is proposed

$$k = \frac{15 D_0}{(1-\bar{\theta})\, r_c^2} \tag{4.10}$$

where $\bar{\theta}$ is some average concentration representing the effective diffusivity. The basis of the proposed equation (4.10) is the analogy between (4.2) and (4.5). That is, the right hand side of (4.2) is a product of a transport property D_c and a concentration gradient term $\nabla^2 q$ (spherical coordinate system) and the right hand side of (4.5) is also a product of a transport property k and a concentration gradient term $(q^* - \bar{q})$. The expression for k given by (4.7) can be interpreted to be a result of this analogy. Based on the same reasoning the expression for the LDF constant k in equation (4.10) can be interpreted to be a result of the analogy between equations (4.9) and (4.5). The sorbate concentration θ is lumped in the transport property as an average concentration, $\bar{\theta}$ which is a function of curvature of the isotherm in the sorbate concentration change. This average concentration $\bar{\theta}$ can be determined, in principle, by comparing the numerical solutions of equations

(4.9) and (4.6) using k from equation (4.10). Here, an equation of the following form is suggested to account for the dependence of θ on the initial and final concentrations of the sorbate.

$$\overline{\theta} = \omega\theta_i + (1-\omega)\theta_f \tag{4.11}$$

where ω is a weighting factor having a value between 0 and 1.

Extension of the proposed modification in the Glueckauf LDF equation to multicomponent diffusion is also possible. For a binary system the extension is as follows. Based on the binary Langmuir isotherm the following distributed parameter model equations can be derived for the variable diffusivity (Round *et al.*., 1966)

$$\frac{\partial q_A}{\partial t} = \frac{D_{A0}}{r^2}\frac{\partial}{\partial r}\left[\frac{r^2}{1-\theta_A-\theta_B}\left\{(1-\theta_B)\frac{\partial q_A}{\partial r}+\theta_A\frac{\partial q_B}{\partial r}\right\}\right] \tag{4.12}$$

$$\frac{\partial q_B}{\partial t} = \frac{D_{B0}}{r^2}\frac{\partial}{\partial r}\left[\frac{r^2}{1-\theta_A-\theta_B}\left\{(1-\theta_A)\frac{\partial q_B}{\partial r}+\theta_B\frac{\partial q_A}{\partial r}\right\}\right] \tag{4.13}$$

Using the analogy between the distributed and the lumped parameter systems as outlined above the modified LDF approximation is extended to binary uptake

$$\frac{\partial \bar{q}_A}{\partial t} = \frac{15 D_{A0}}{r_c^2\left(1-\bar{\theta}_A-\bar{\theta}_B\right)}\left[(1-\bar{\theta}_B)\left(q_A^* - \bar{q}_A\right)+\bar{\theta}_A\left(q_B^* - \bar{q}_B\right)\right] \tag{4.14}$$

$$\frac{\partial \bar{q}_B}{\partial t} = \frac{15 D_{B0}}{r_c^2\left(1-\bar{\theta}_A-\bar{\theta}_B\right)}\left[(1-\bar{\theta}_A)\left(q_B^* - \bar{q}_B\right)+\bar{\theta}_B\left(q_A^* - \bar{q}_A\right)\right] \tag{4.15}$$

In the above equations the step size of each sorbate is taken into account as given by the following equations:

$$\bar{\theta}_A = \omega_A \theta_{A\,i} + (1-\omega_A)\,\theta_{A\,f}$$

$$\bar{\theta}_B = \omega_B \theta_{B\,i} + (1-\omega_B)\,\theta_{B\,f} \qquad (4.16)$$

4.2 COMPARISON OF LUMPED AND DISTRIBUTED PARAMETER MODELS

The next step is to solve the proposed modified LDF approximate equations and compare the results with the complete solution given by the distributed parameter equations. Since $\bar{\theta}$ in the new equations is a function of sorbate step size, different step sizes are used for comparison of both single and binary models with the respective distributed parameter model solutions. The dimensionless form of equations for the single component case, *i.e.*, equation (4.9), the new LDF equation, and the Glueckauf LDF equation with k given by (4.7), is given below

$$\frac{\partial Q}{\partial \tau} = \frac{1}{R^2}\frac{\partial}{\partial R}\left[\frac{R^2}{1-\lambda_1-(\lambda_2-\lambda_1)Q}\frac{\partial Q}{\partial R}\right] \qquad (4.17)$$

$$\frac{\partial \bar{Q}}{\partial \tau} = \frac{15}{1-\bar{\theta}}(1-\bar{Q}) \qquad (4.18)$$

$$\frac{\partial \bar{Q}}{\partial \tau} = 15\left(1-\bar{Q}\right) \tag{4.19}$$

Equation (4.17) is subject to the following initial and boundary conditions

$$Q\left(R,0\right)=0$$

$$Q\left(1,\tau\right)=1$$

$$\frac{\partial Q}{\partial R}\left(0,\tau\right)=0 \tag{4.20}$$

Equations (4.18) and (4.19) have an initial condition of $\bar{Q}$ equal to zero.

Each of the three models is solved using parametric values listed in Table 4.1 for the single component cases of adsorption and desorption. Note that the solution is obtained for both small and large step sizes with finite and zero initial concentrations for each step size. Equation (4.7) is solved using the method of orthogonal collocation with Jacobi polynomials as the trial solution. 10 internal collocation points are used for the sorbent particle and the resulting simultaneous ordinary differential equations are solved using IMSL subroutines. A value of 0.35 for ω is used to calculate $\bar{\theta}$ from equation (4.11). The value of ω is determined by a comparison of the theoretical plots of the mean diffusivity $\bar{D}$ as a function of the sorbate step size, as given by Garg and Ruthven (1972), versus θ for adsorption and desorption. Various values of ω are used in an attempt to fit these plots and a value of 0.35 is found to be most suitable for both adsorption and desorption. The value of 0.35 is not changed for any of the single or binary diffusion cases discussed here. The results of solution of distributed parameter model (4.17), the

Table 4.1. Parameter values used for comparison of different models for single component uptake

Case number and description	λ_1	λ_2
Case 1 (Small step size, Zero initial concentration)	0	0.1
Case 2 (Large step size, Zero initial concentration)	0	0.75
Case 3 (Small step size, Finite initial concentration)	0.1	0.15
Case 4 (Large step size, Finite initial concentration)	0.1	0.8
Case 5 (Small step size, Desorption)	0.2	0.1
Case 6 (Large step size, Desorption)	0.9	0.0

proposed LDF equation (4.18), and the Glueckauf LDF expression (4.19) are shown in Figures 4.1 to 4.6. From these results, it is concluded that the modified LDF expression proposed in the present thesis conforms to the complete solution much better than the Glueckauf LDF. When the sorbate step size is large the concentration dependence of diffusivity is more pronounced. Under these conditions the proposed LDF shows an excellent agreement with the distributed parameter model for both adsorption and desorption. Note that the base value of $\omega = 0.35$ is not adjusted to match the two models for any of these cases. A better match of the new LDF with the complete solution can be achieved if ω is adjusted. But with no fitted parameter the proposed LDF gives a satisfactory solution. The results of all three approaches nearly coincide for a small step size. Using the new LDF approximation instead of the Glueckauf equation is recommended as a safer approach. A general feature of the uptake predictions by the LDF equation is also seen to be present in the predictions by the new LDF equation with variable diffusivity. That is, the predicted initial uptake by both the new and Glueckauf's models is slower than that predicted by the distributed parameter model solution. Nevertheless, all three models converge to the same equilibrium value at long dimensionless time. However, the new LDF equation generally predicts a better uptake rate than the simple Glueckauf LDF expression.

Table 4.2 summarizes the parametric values used for the solution of the binary uptake equations. Note that different cases of codiffusion and counterdiffusion are solved with small and large concentration steps for each of the slow and fast diffusing

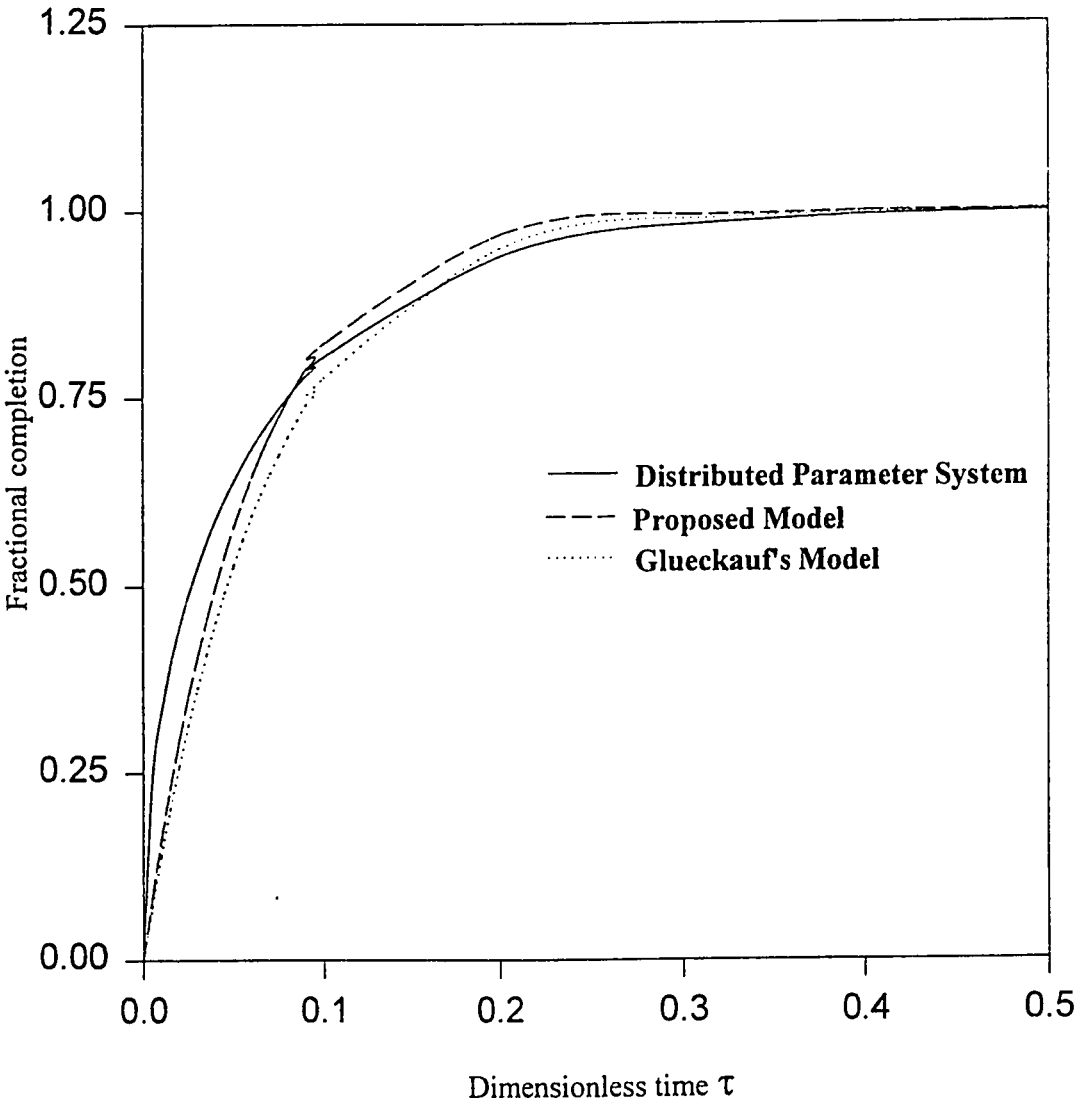

Figure 4.1. Comparison of three models for single component uptake. Case 1

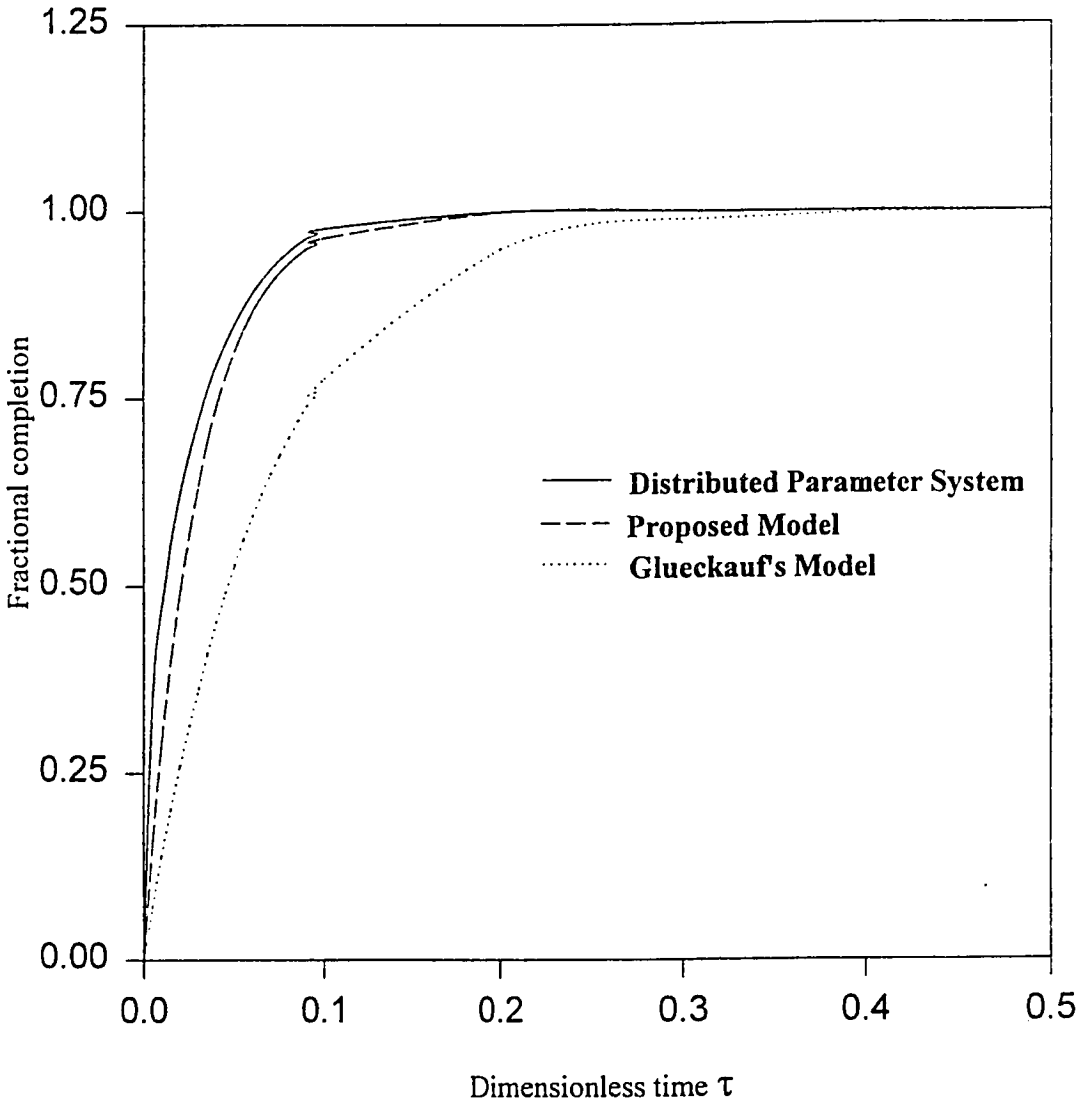

Figure 4.2. Comparison of three models for single component uptake. Case 2

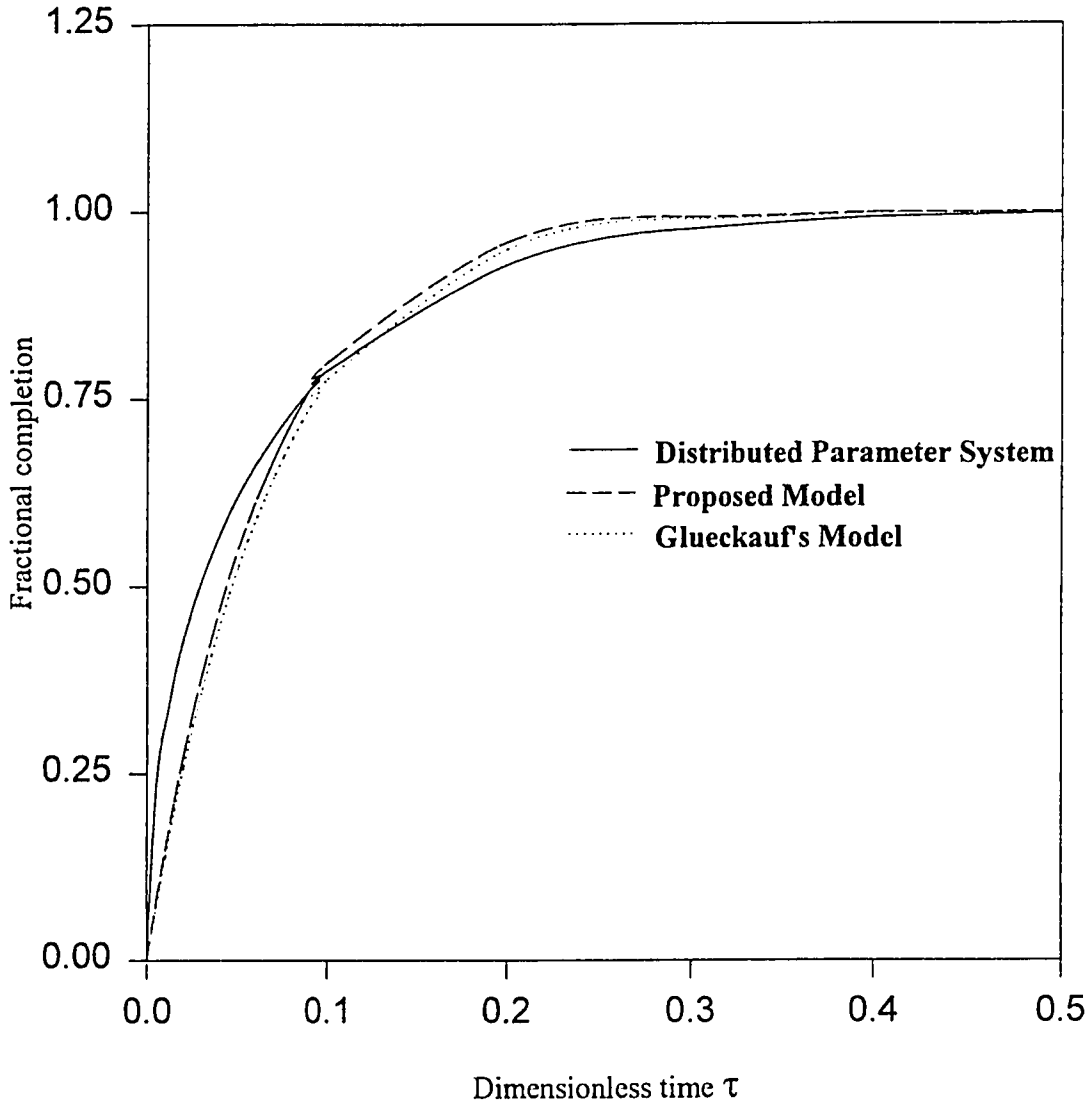

Figure 4.3. Comparison of three models for single component uptake. Case 3

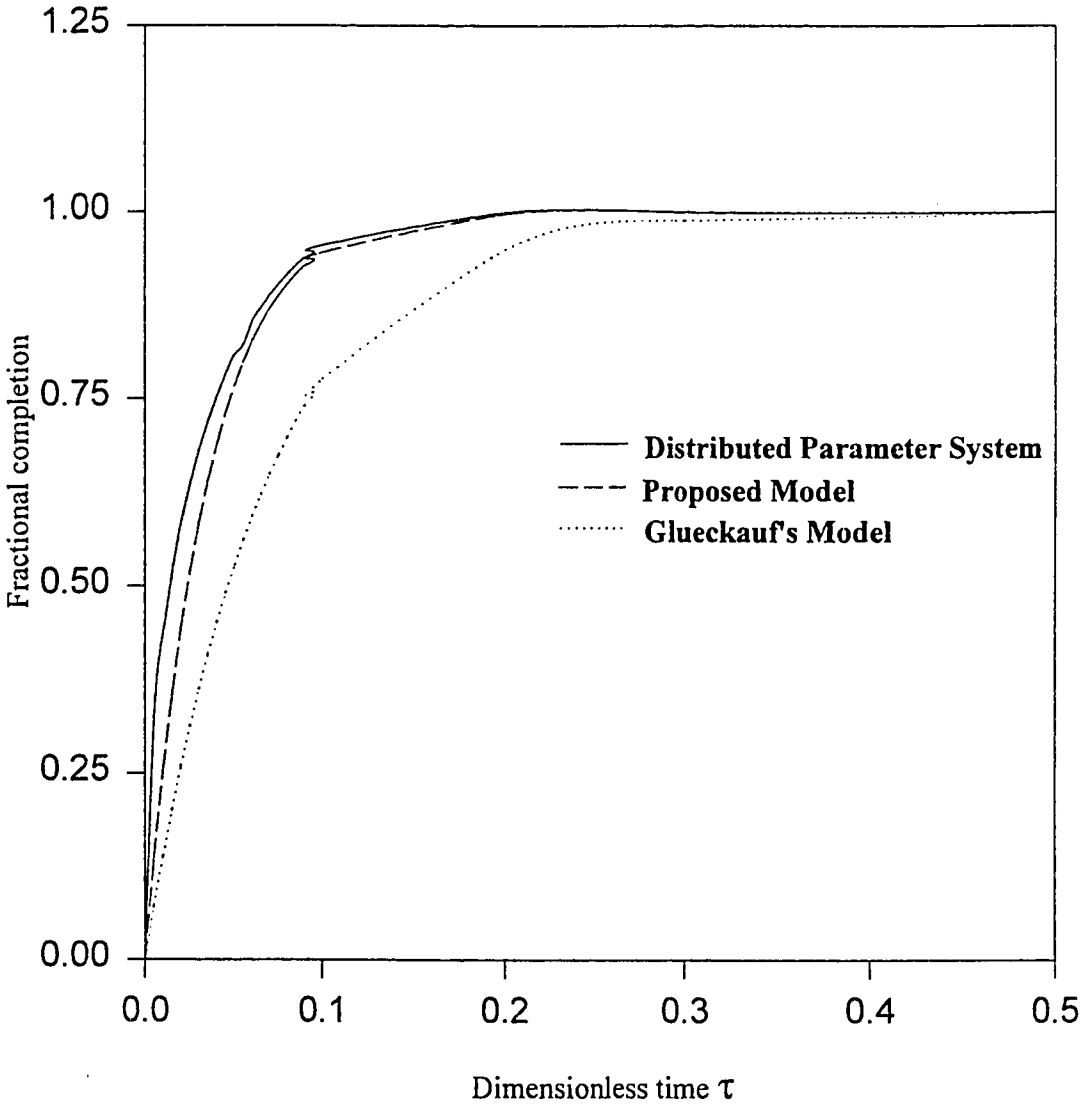

Figure 4.4. Comparison of three models for single component uptake. Case 4

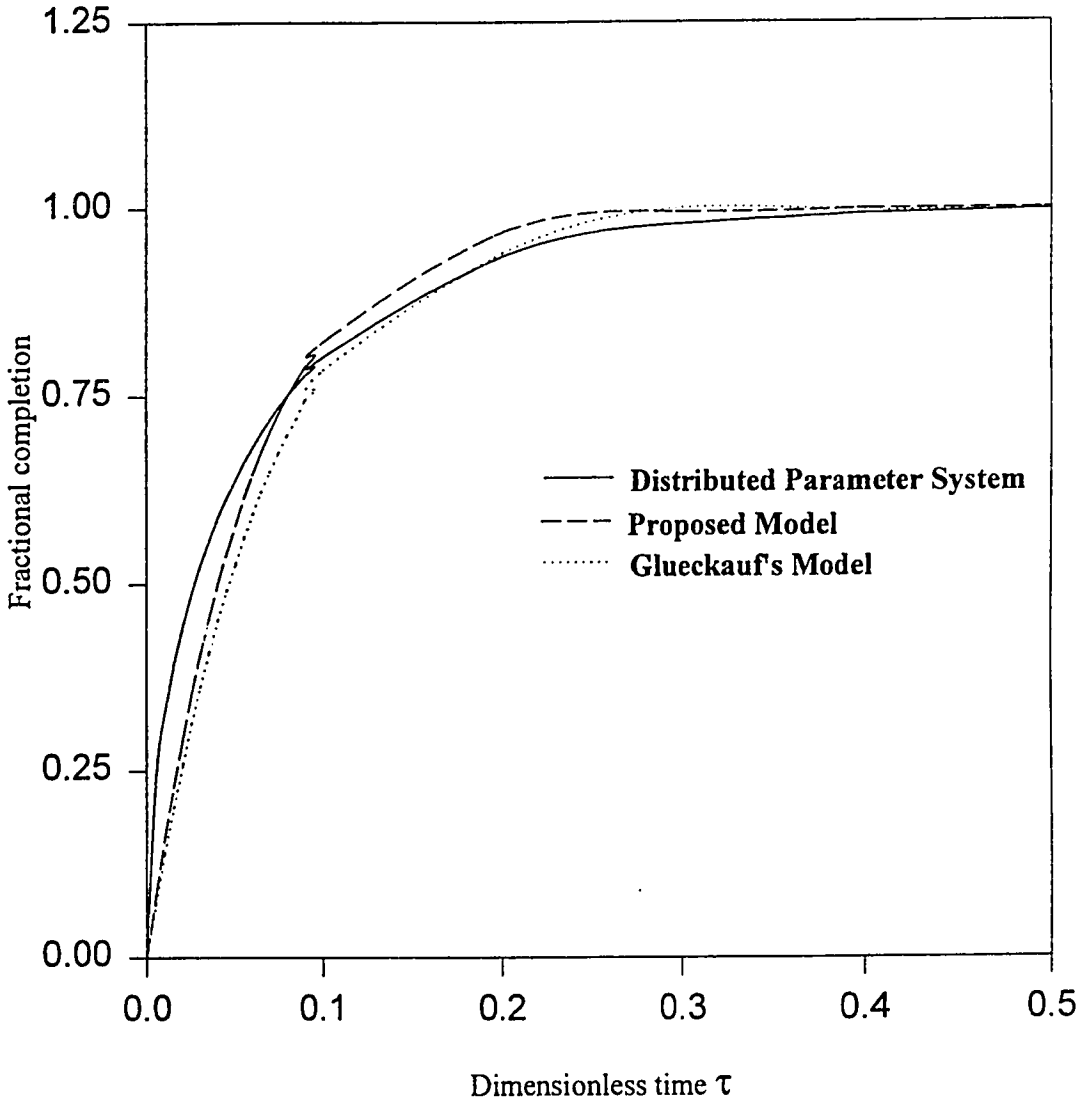

Figure 4.5. Comparison of three models for single component uptake. Case 5

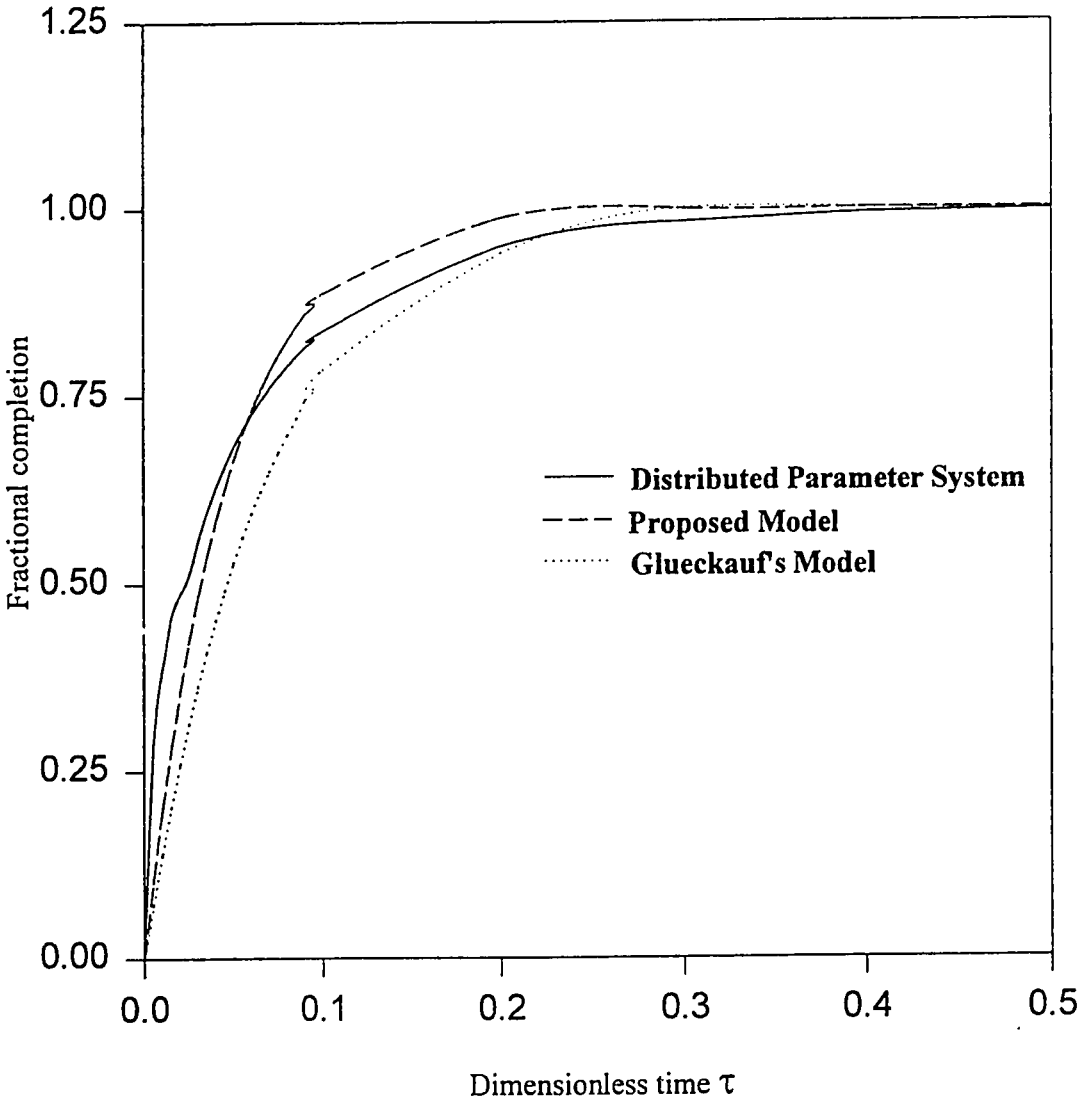

Figure 4.6. Comparison of three models for single component uptake. Case 6

Table 4.2. Parameter values used for comparison of distributed and lumped parameter models for binary uptake

Case number	Mode	λ_{A1}	λ_{A2}	λ_{B1}	λ_{B2}	D_{A0}/D_{B0}
Cases 7, 8, 9	Codiffusion	0	0.8	0	0.1	5, 15, 50
Cases 10, 11 ,12	Codiffusion	0	0.1	0	0.8	5, 15, 50
Case 13	Codiffusion	0.2	0.8	0.1	0.15	5
Case 14	Codiffusion	0.1	0.2	0.2	0.75	5
Cases 15, 16, 17	Counterdiffusion	0	0.8	0.8	0	5, 15, 50
Case 18	Counterdiffusion	0.8	0	0	0.8	5
Cases 19, 20, 21	Counterdiffusion	0.4	0.2	0.1	0.15	5, 15, 50
Case 22	Counterdiffusion	0.8	0.2	0.15	0.75	5

A = Fast diffusing species
B = Slow diffusing species

components. Moreover, the ratio of diffusivities D_{Ao} / D_{Bo} is varied for two cases of each of codiffusion and counterdiffusion. Note that the current analysis is limited to three different values of the limited diffusivity ratio The normalized form of the equations is as follows:

Distributed parameter system (coupled partial differential equations)

$$\frac{\partial Q_A}{\partial \tau} = \frac{1}{R^2}\frac{\partial}{\partial R}\left[\frac{R^2}{\rho}\left\{(1-\rho_B)\frac{\partial Q_A}{\partial R}+\xi\ \rho_A\frac{\partial Q_B}{\partial R}\right\}\right] \tag{4.21}$$

$$\frac{\partial Q_B}{\partial \tau} = \frac{\delta}{R^2}\frac{\partial}{\partial R}\left[\frac{R^2}{\rho}\left\{(1-\rho_A)\frac{\partial Q_B}{\partial R}+\beta\ \rho_A\frac{\partial Q_A}{\partial R}\right\}\right] \tag{4.22}$$

where

$$\rho = 1-\lambda_{A1}-(\lambda_{A2}-\lambda_{A1})Q_A - (\lambda_{B2}-\lambda_{B1})Q_B$$

$$\rho_A = \lambda_{A1} + (\lambda_{A2}-\lambda_{A1})Q_A$$

$$\rho_B = \lambda_{B1} + (\lambda_{B2}-\lambda_{B1})Q_B \tag{4.23}$$

For a step change in concentration at the surface the above equations are subject to

$$Q_A(R,0) = Q_B(R,0) = 0$$

$$Q_A(1,\tau) = Q_B(1,\tau) = 1$$

$$\frac{\partial Q_A}{\partial R}(0,\tau) = \frac{\partial Q_B}{\partial R}(0,\tau) = 0 \tag{4.24}$$

The partial differential equations (4.21) and (4.22) are reduced to ordinary differential equations by the method of orthogonal collocation using 10 collocation points. Note that the dimensionless time τ appearing in equations (4.21) and (4.22) is based on D_{A0}.

The proposed binary LDF equations have the following normalized form:

$$\frac{\partial \bar{Q}_A}{\partial \tau} = \frac{15}{1-\bar{\theta}_A-\bar{\theta}_B}\left[(1-\bar{\theta}_B)(1-\bar{Q}_A)+\bar{\theta}_A \xi\,(1-\bar{Q}_B)\right] \tag{4.25}$$

$$\frac{\partial \bar{Q}_B}{\partial \tau} = \frac{15\delta}{1-\bar{\theta}_A-\bar{\theta}_B}\left[(1-\bar{\theta}_A)(1-\bar{Q}_B)+\bar{\theta}_B \beta\,(1-\bar{Q}_A)\right] \tag{4.26}$$

These equations are solved subject to the initial conditions given in equation (4.24). Note that there is no analog of Glueckauf's LDF for a binary system. From Table 4.2 it is seen that the distributed and lumped parameter models are compared for binary systems using all combinations of parametric values; that is, cases 7 to 14 correspond to codiffusion and cases 15 to 22 to counterdiffusion. Step sizes of different magnitudes are used for each of the slow and fast diffusing components. Different ratios of diffusion speeds for the two components are used for some representative cases of both codiffusion and counterdiffusion. Results of cases 7 to 22 are shown in Figures 4.7 to 4.22.

The results of binary diffusion cases indicate that the new binary LDF equations show a fair to good accord with the complete solution based on partial differential equations. Cases 7, 8, and 9 represent codiffusion with zero initial concentration. The fast diffusing species A receives a large concentration step and the slow species B undergoes a small step change in concentration. Three different limiting diffusivity ratios are used for the comparison of the distributed and lumped parameter model solutions. From the results shown in Figures 4.7 to 4.9 it is clear that for such sorbate concentration step

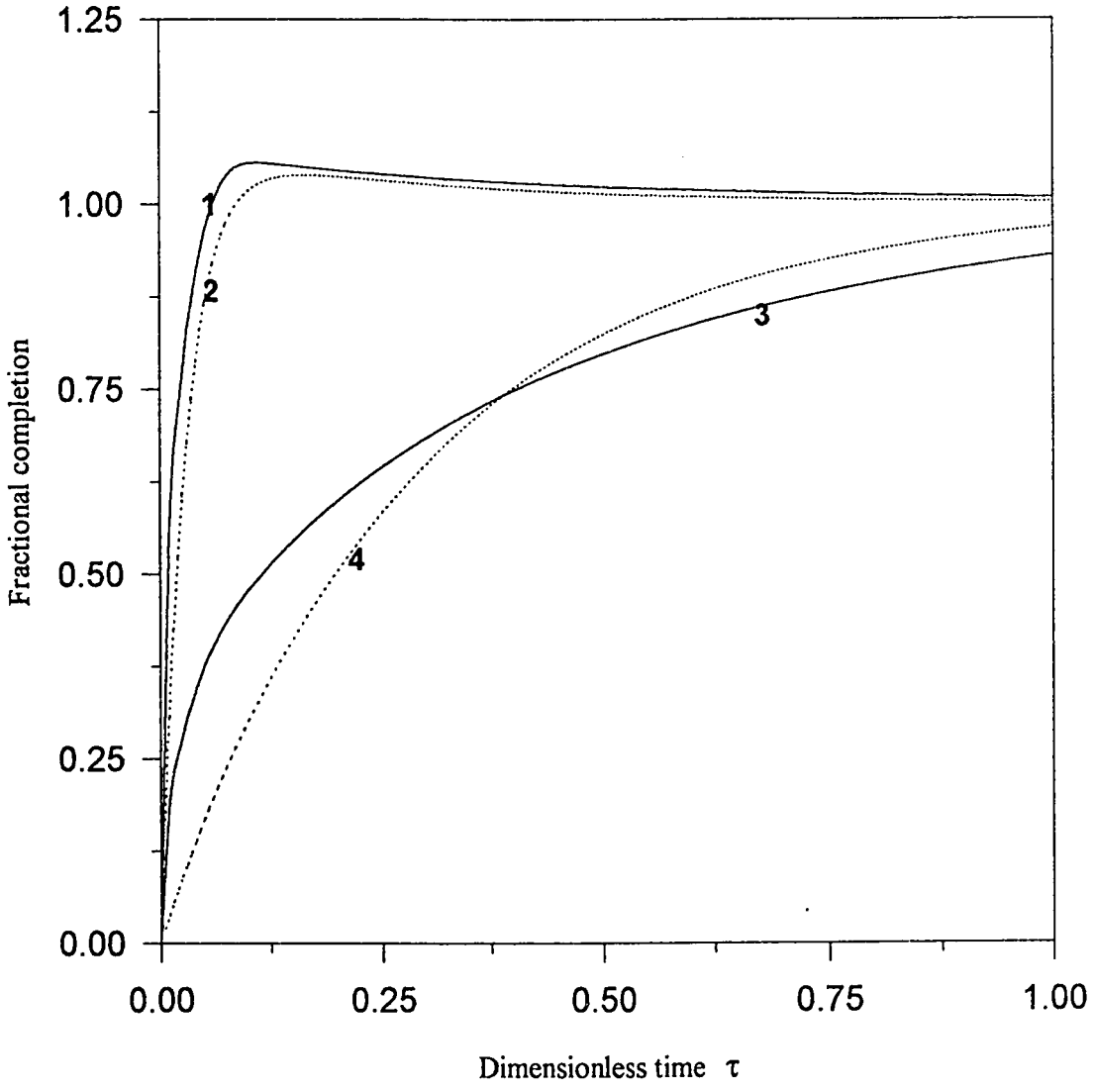

Figure 4.7. Comparison of the new binary LDF equation with the detailed model for binary diffusion. Case 7. (1 and 3 detailed model, 2 and 4 new LDF model; species A plots 1 and 2, species B plots 3 and 4)

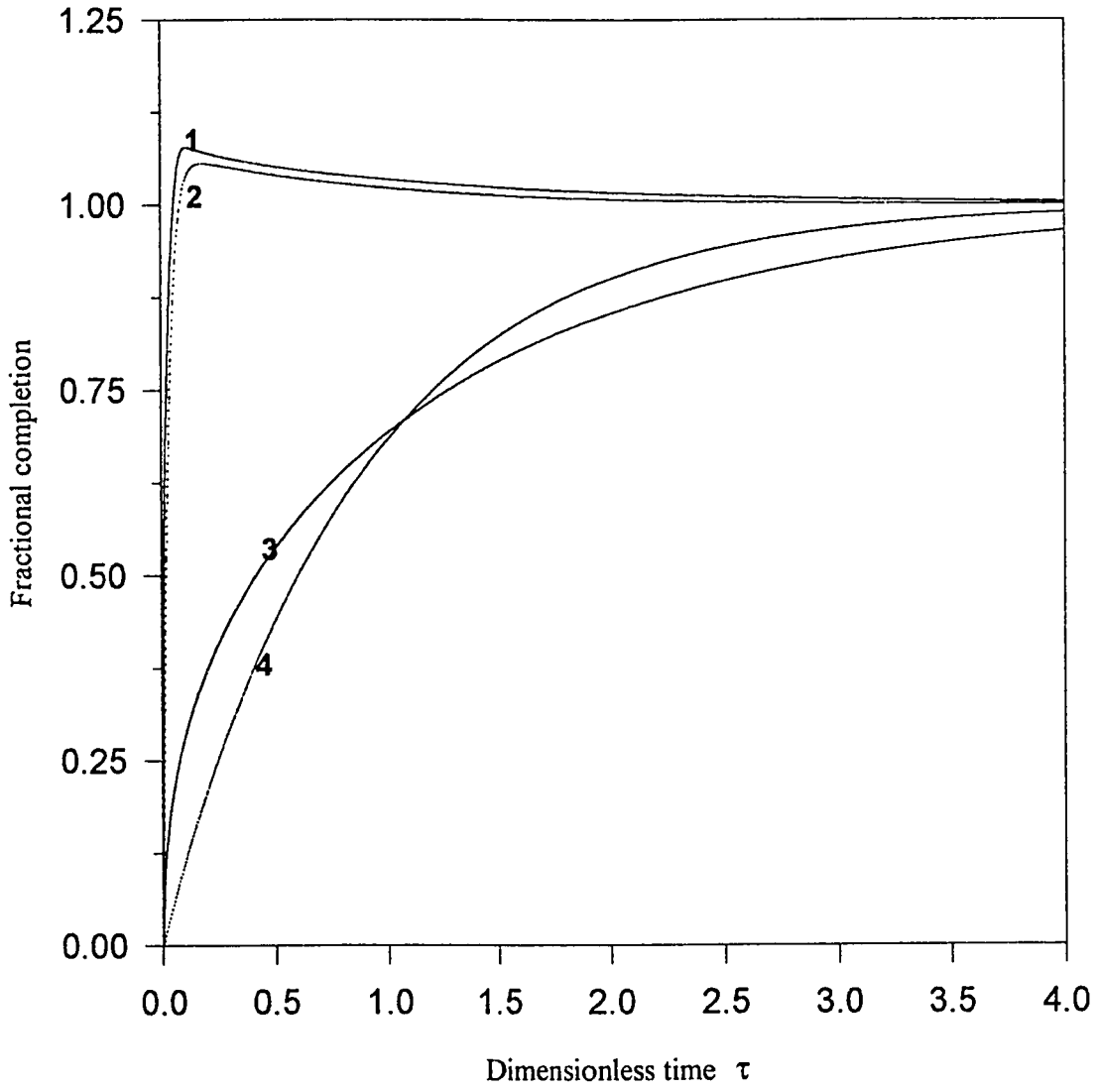

Figure 4.8. Comparison of the new binary LDF equation with the detailed model for binary diffusion. Case 8. (1 and 3 detailed model, 2 and 4 new LDF model; species A plots 1 and 2, species B plots 3 and 4)

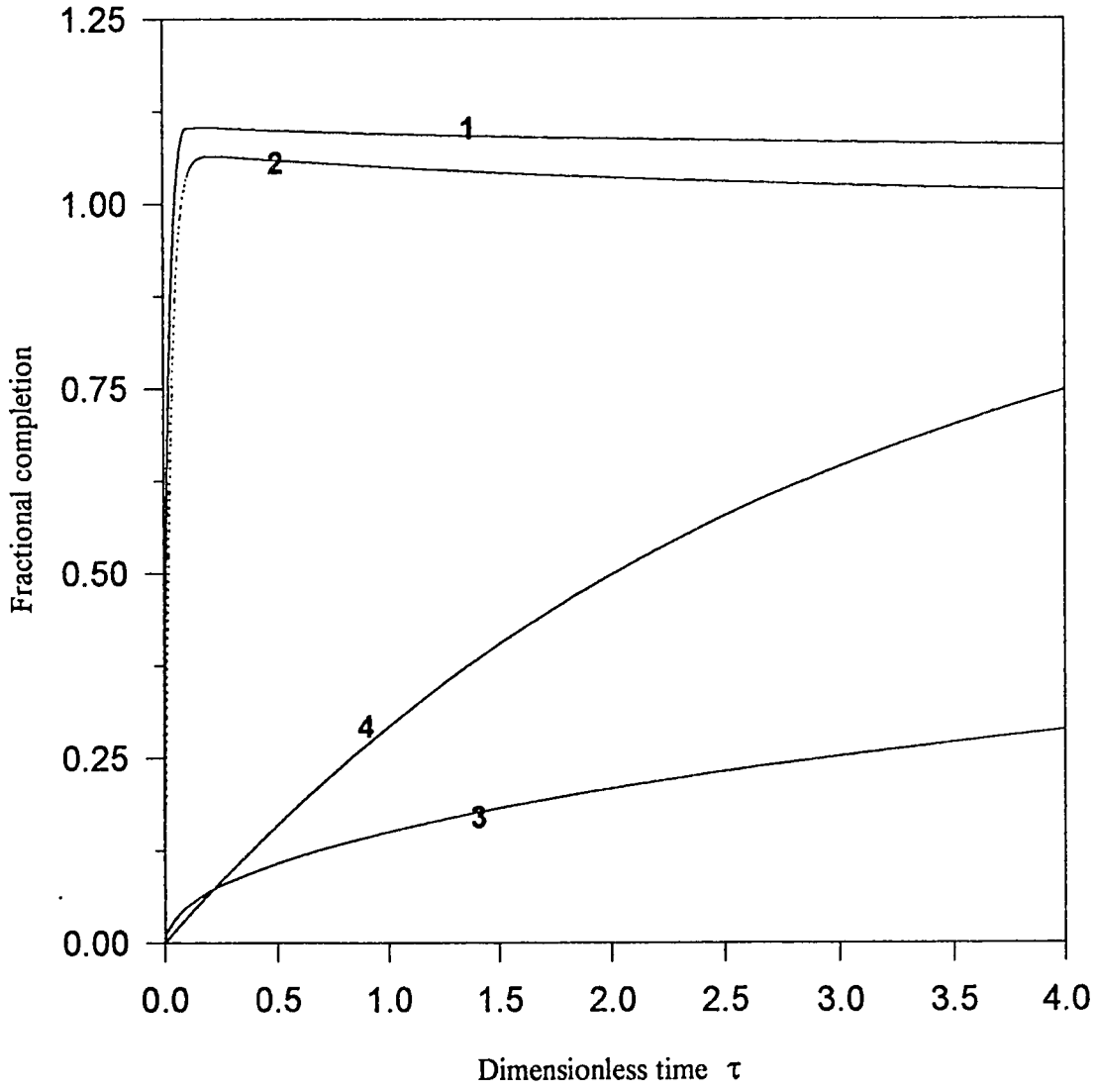

Figure 4.9. Comparison of the new binary LDF equation with the detailed model for binary diffusion. Case 9. (1 and 3 detailed model, 2 and 4 new LDF model; species A plots 1 and 2, species B plots 3 and 4)

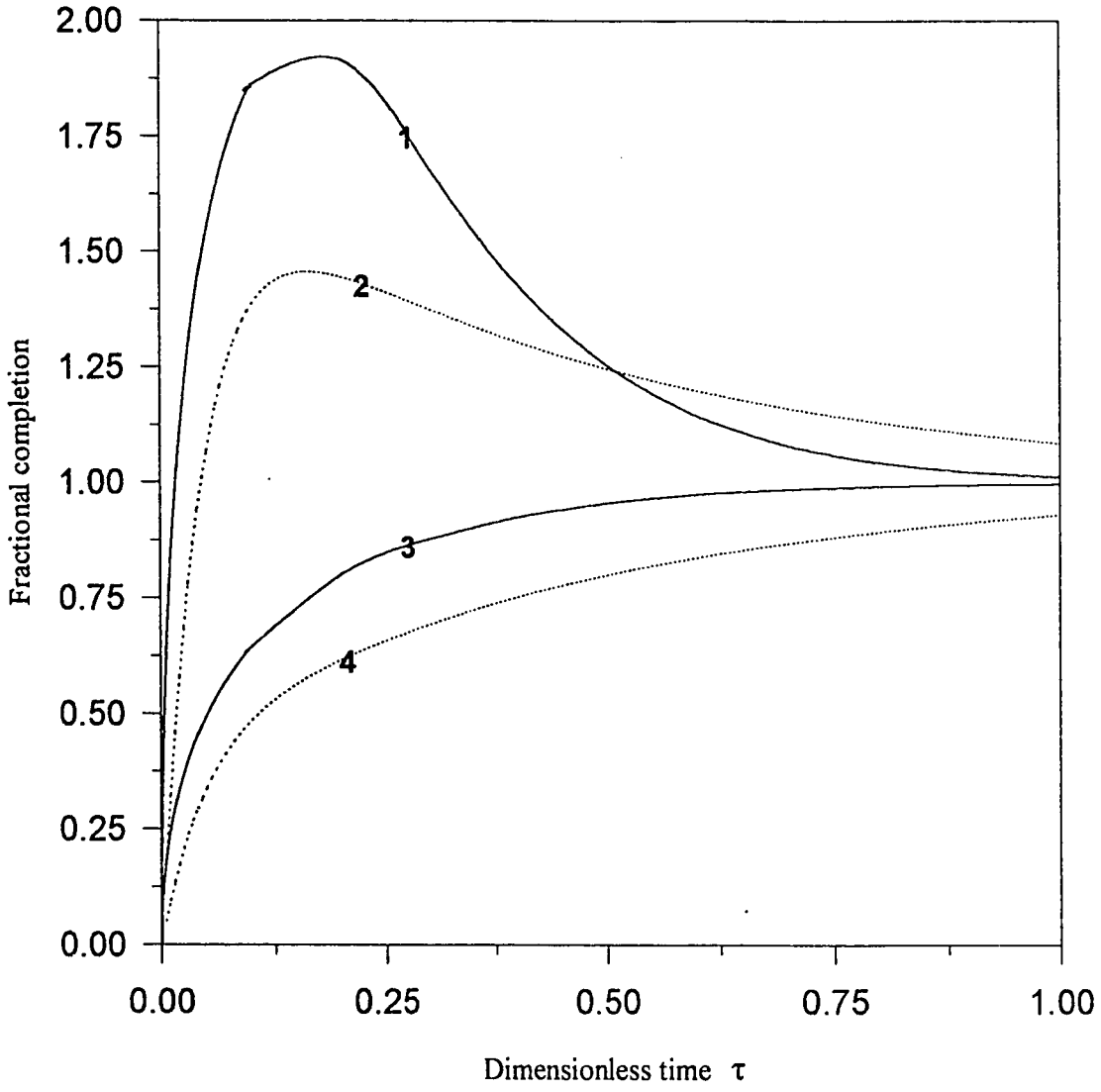

Figure 4.10. Comparison of the new binary LDF equation with the detailed model for binary diffusion. Case 10. (1 and 3 detailed model, 2 and 4 new LDF model; species A plots 1 and 2, species B plots 3 and 4)

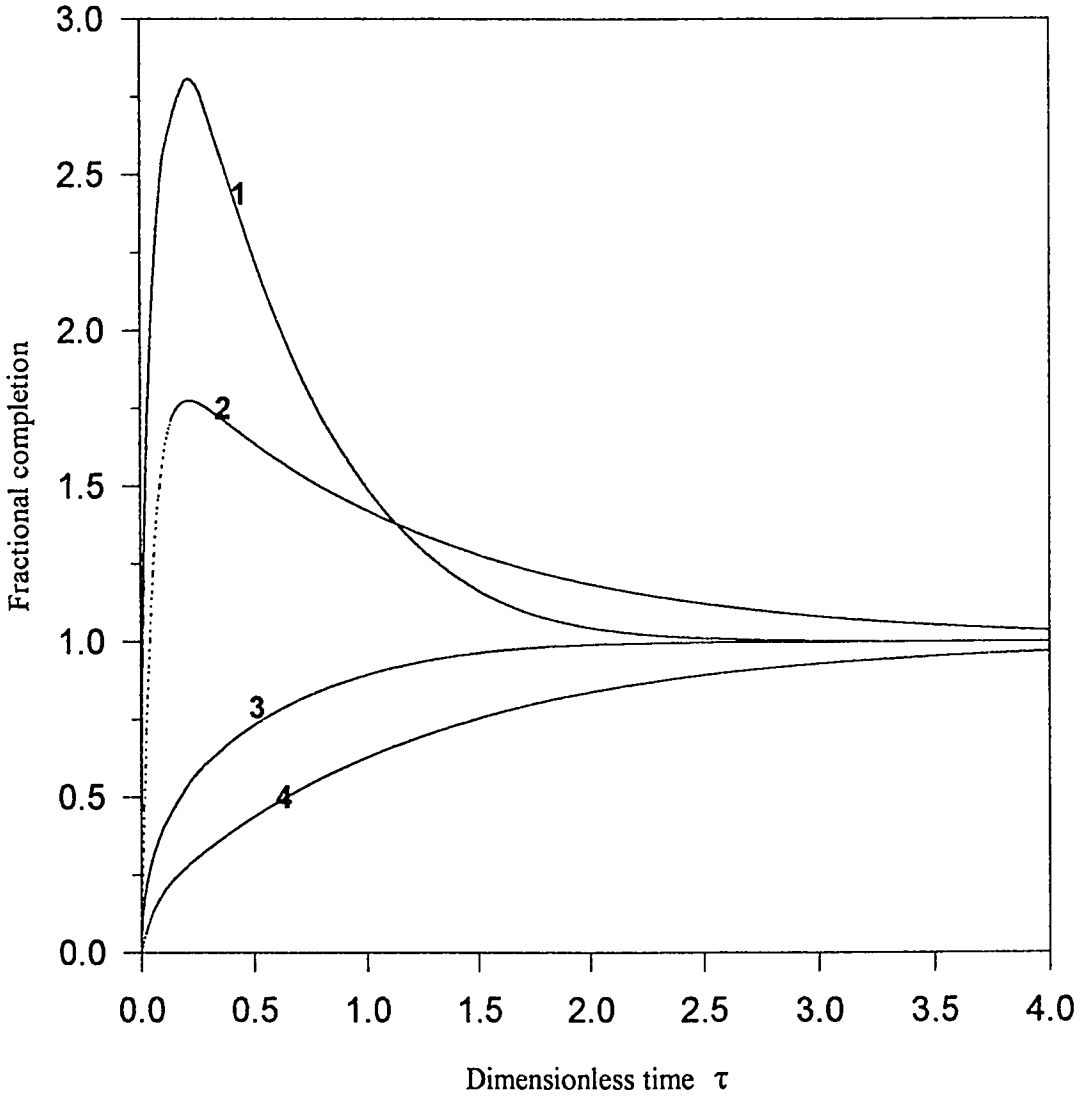

Figure 4.11. Comparison of the new binary LDF equation with the detailed model for binary diffusion. Case 11. (1 and 3 detailed model, 2 and 4 new LDF model; species A plots 1 and 2, species B plots 3 and 4)

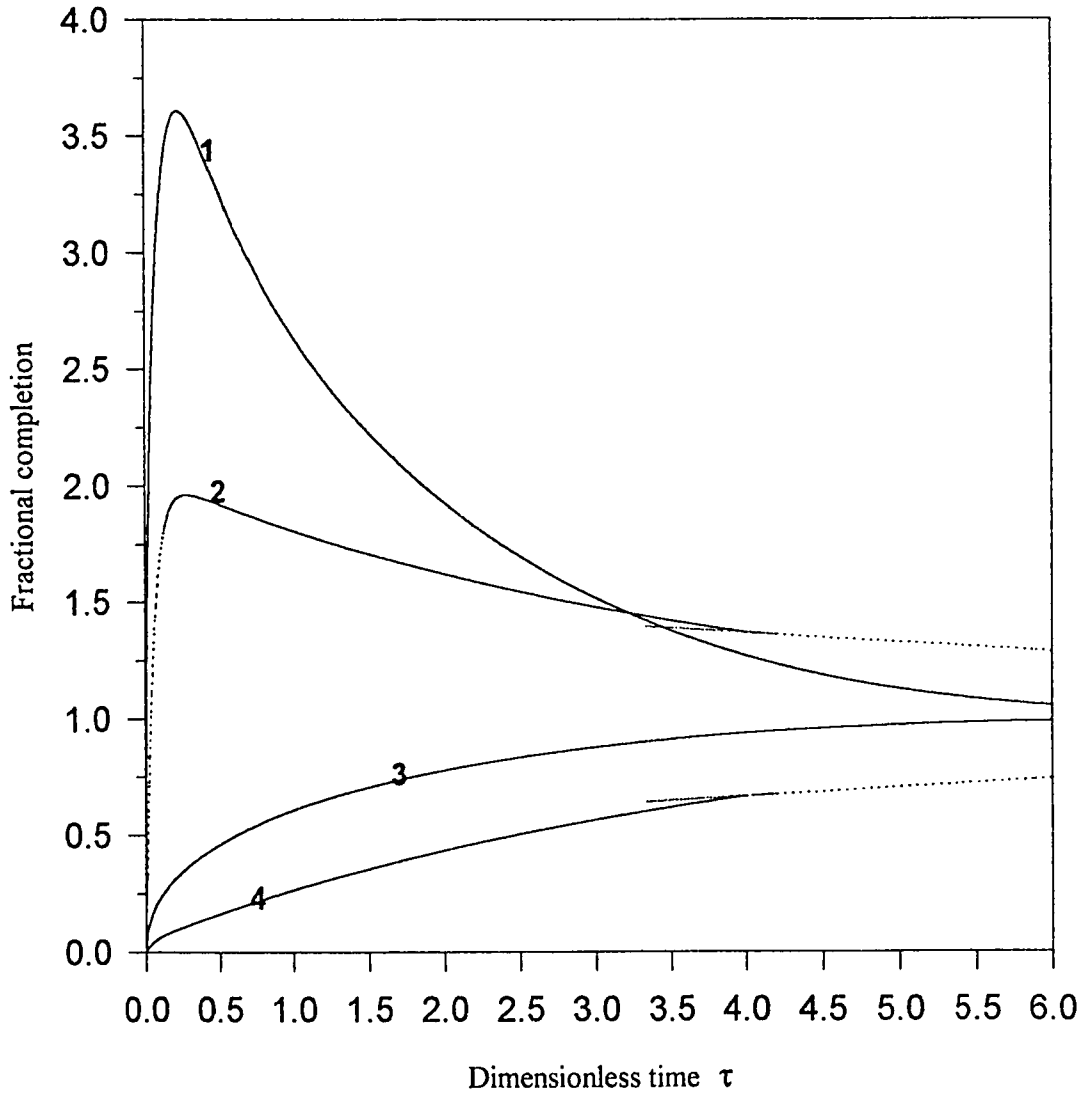

Figure 4.12. Comparison of the new binary LDF equation with the detailed model for binary diffusion. Case 12. (1 and 3 detailed model, 2 and 4 new LDF model; species A plots 1 and 2, species B plots 3 and 4)

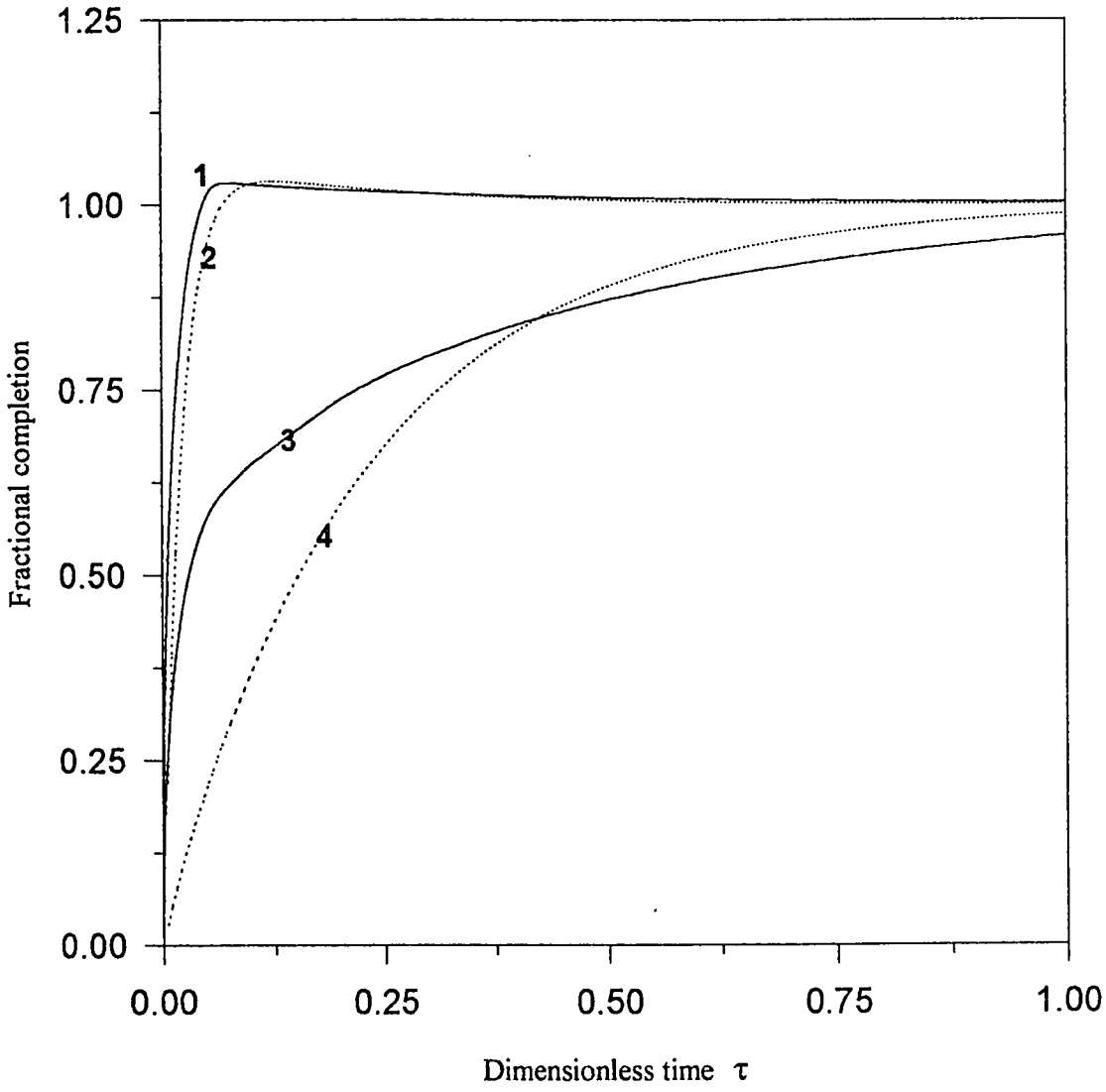

Figure 4.13. Comparison of the new binary LDF equation with the detailed model for binary diffusion. Case 13. (1 and 3 detailed model, 2 and 4 new LDF model; species A plots 1 and 2, species B plots 3 and 4)

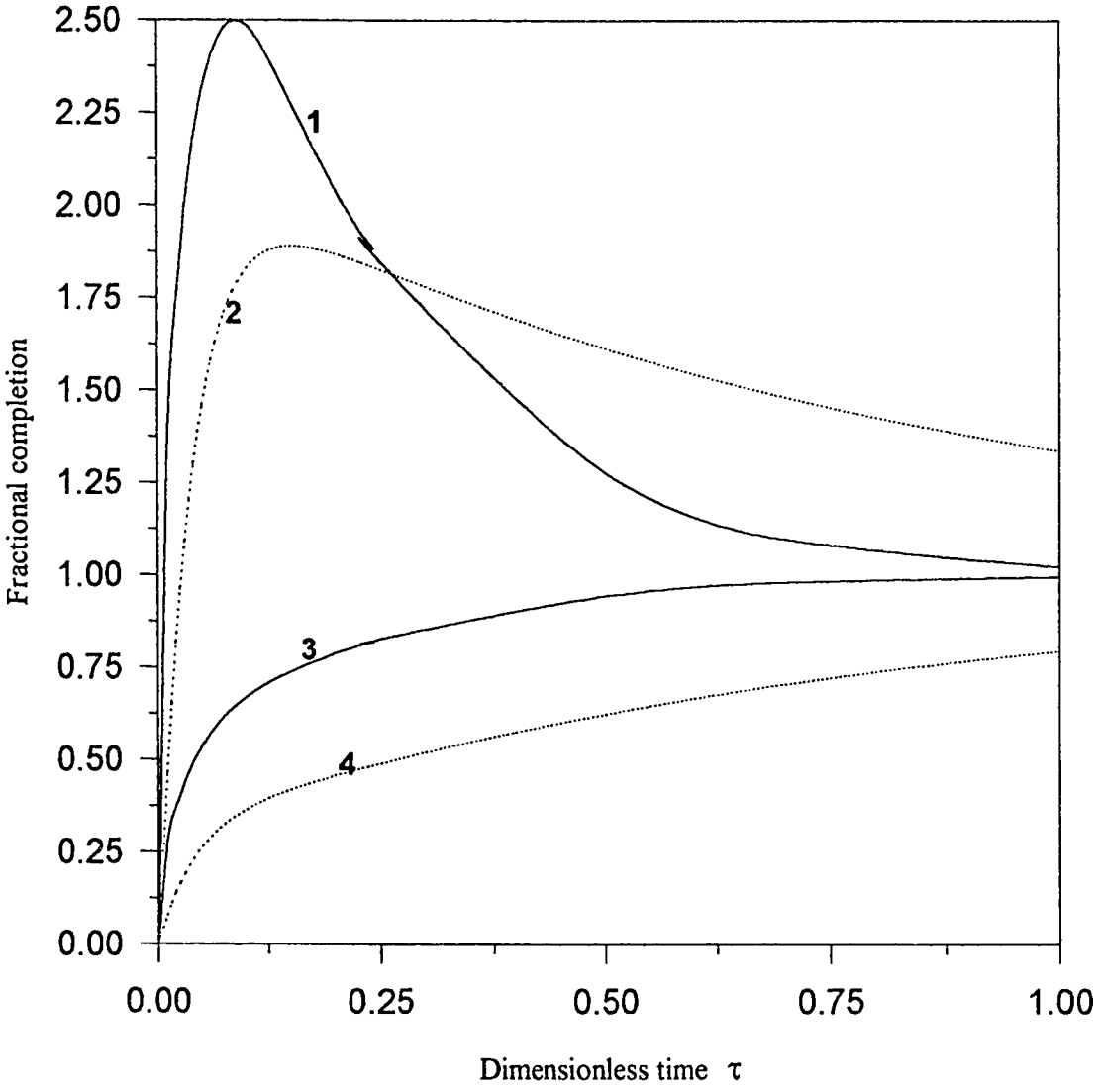

Figure 4.14. Comparison of the new binary LDF equation with the detailed model for binary diffusion. Case 14. (1 and 3 detailed model, 2 and 4 new LDF model; species A plots 1 and 2, species B plots 3 and 4)

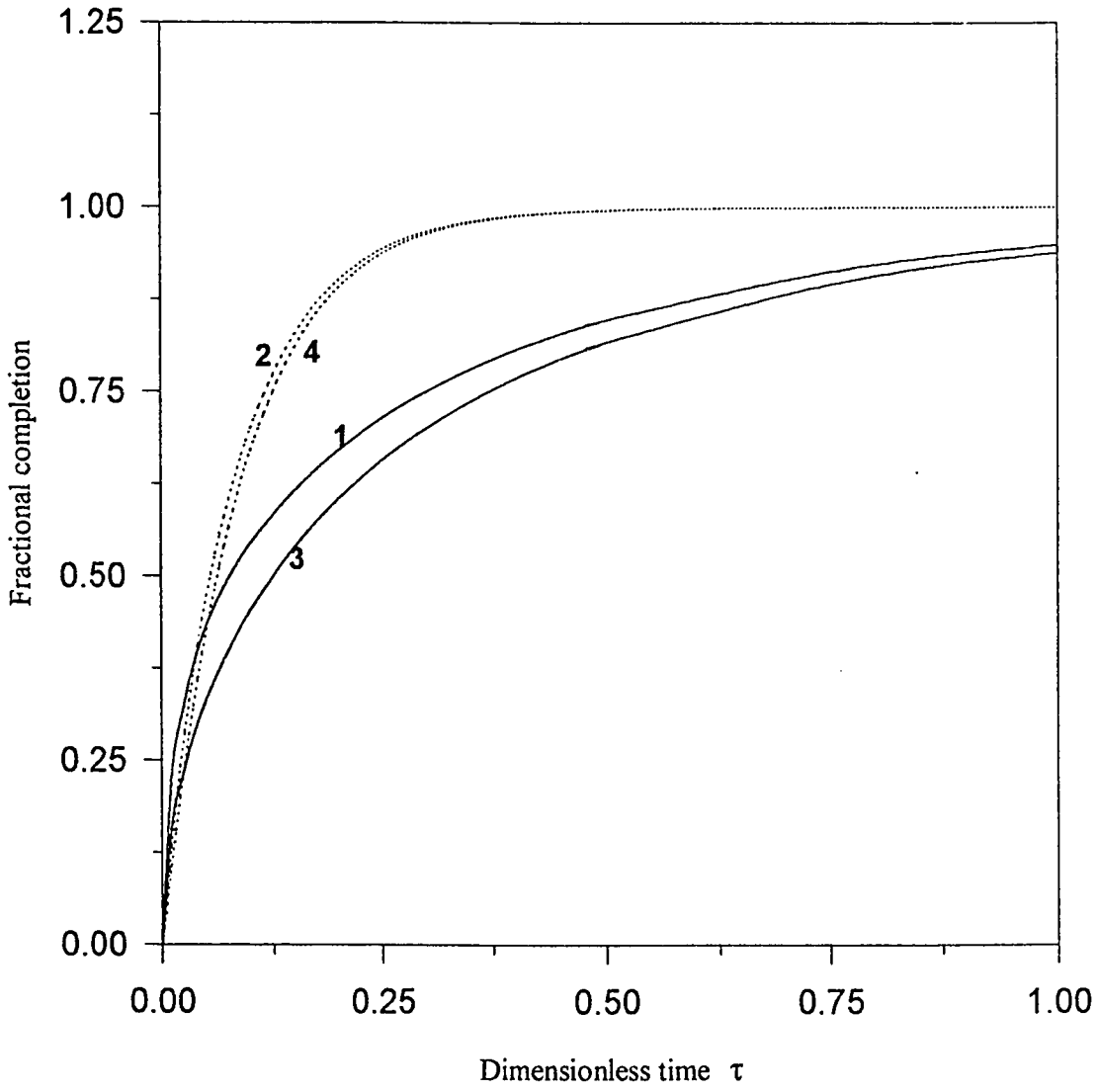

Figure 4.15. Comparison of the new binary LDF equation with the detailed model for binary diffusion. Case 15. (1 and 3 detailed model, 2 and 4 new LDF model; species A plots 1 and 2, species B plots 3 and 4)

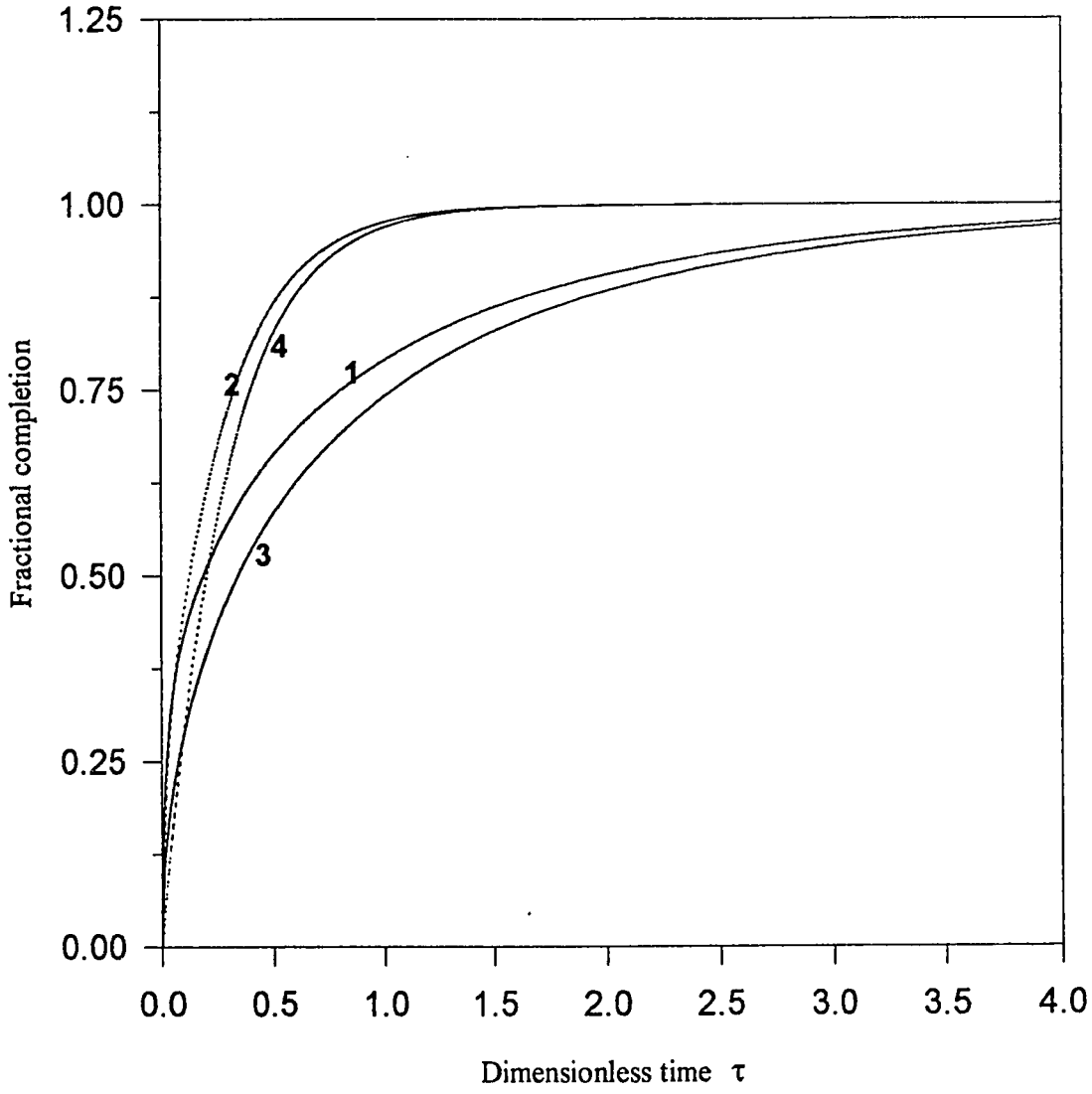

Figure 4.16. Comparison of the new binary LDF equation with the detailed model for binary diffusion. Case 16. (1 and 3 detailed model, 2 and 4 new LDF model; species A plots 1 and 2, species B plots 3 and 4)

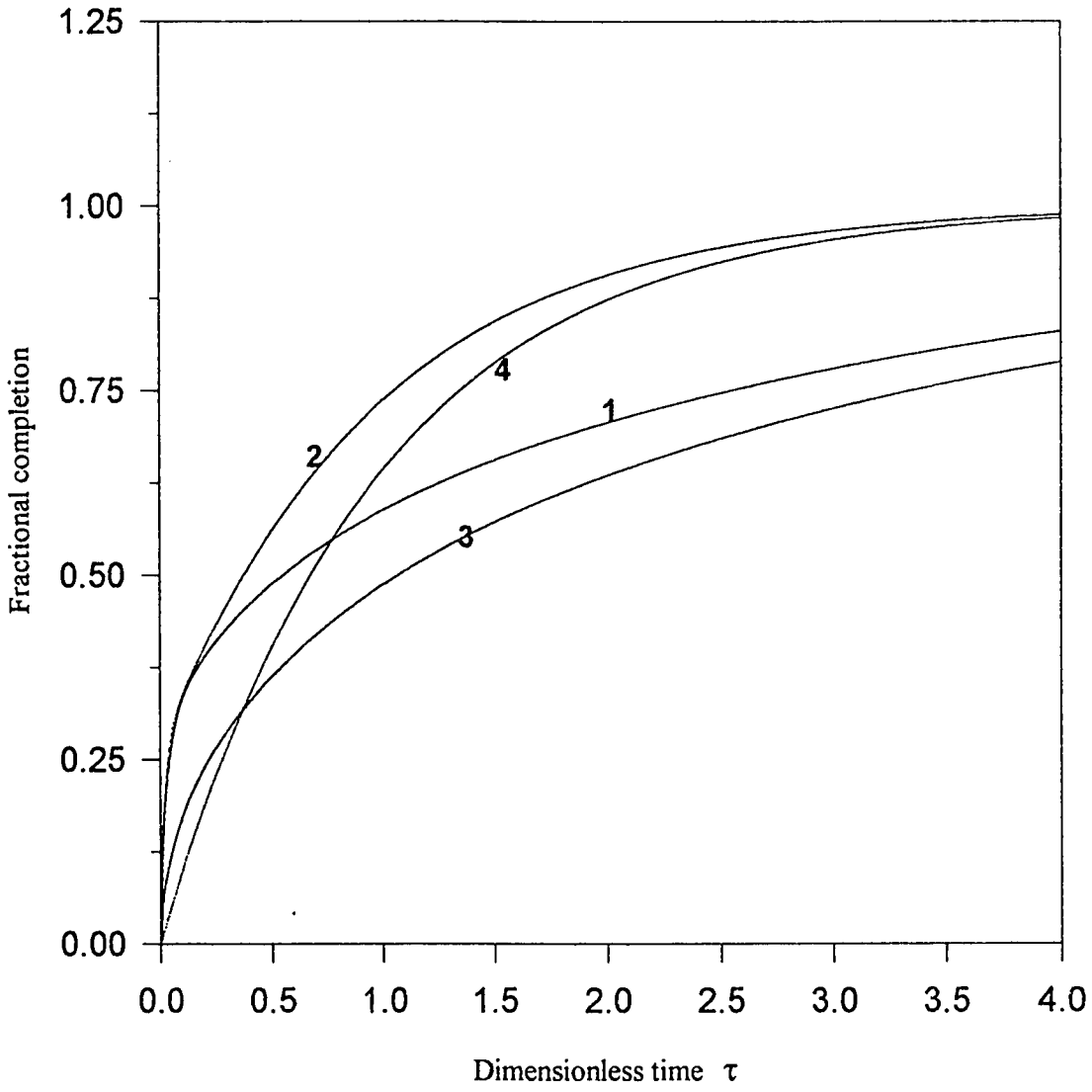

Figure 4.17. Comparison of the new binary LDF equation with the detailed model for binary diffusion. Case 17. (1 and 3 detailed model, 2 and 4 new LDF model; species A plots 1 and 2, species B plots 3 and 4)

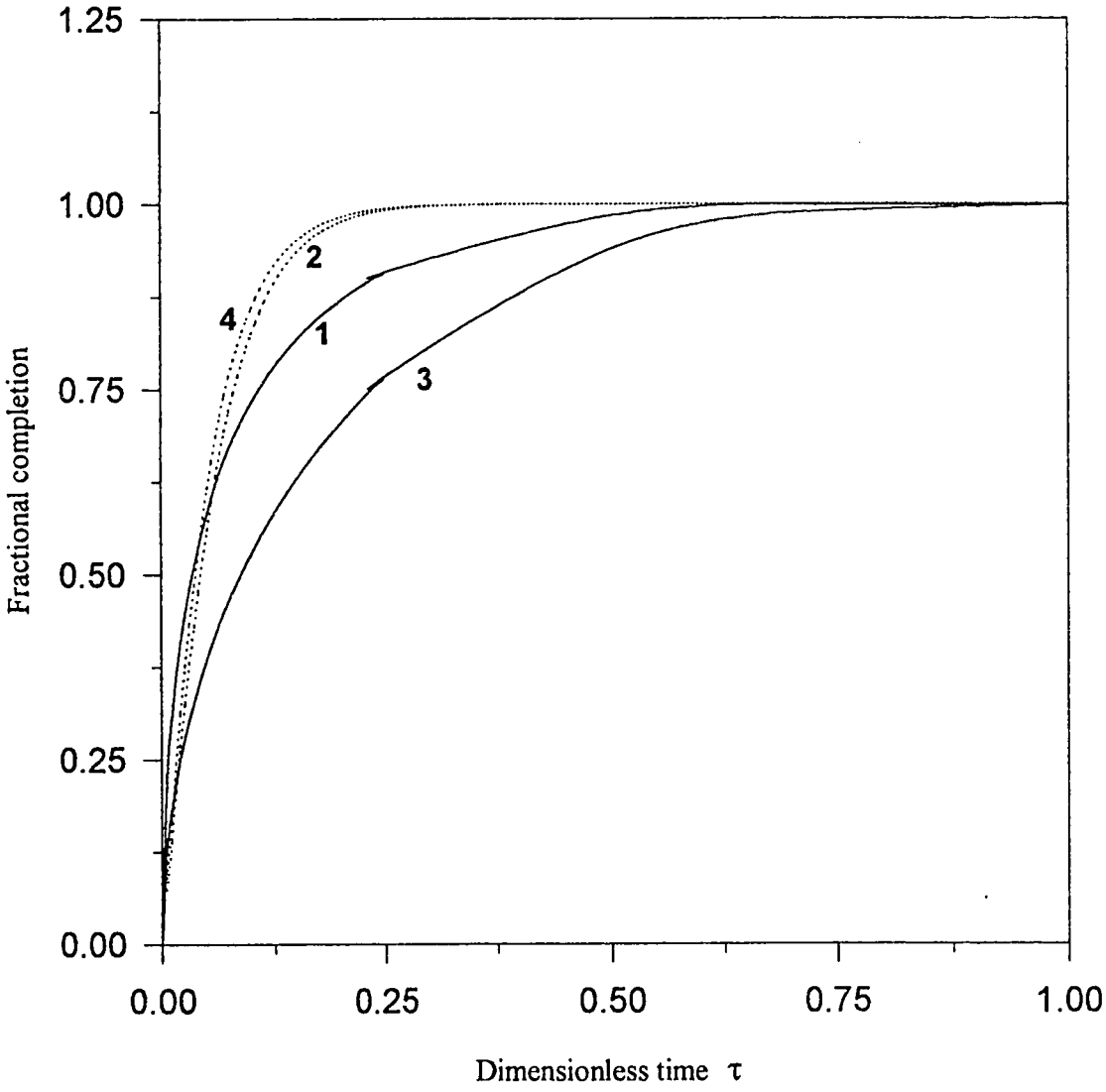

Figure 4.18. Comparison of the new binary LDF equation with the detailed model for binary diffusion. Case 18. (1 and 3 detailed model, 2 and 4 new LDF model; species A plots 1 and 2, species B plots 3 and 4)

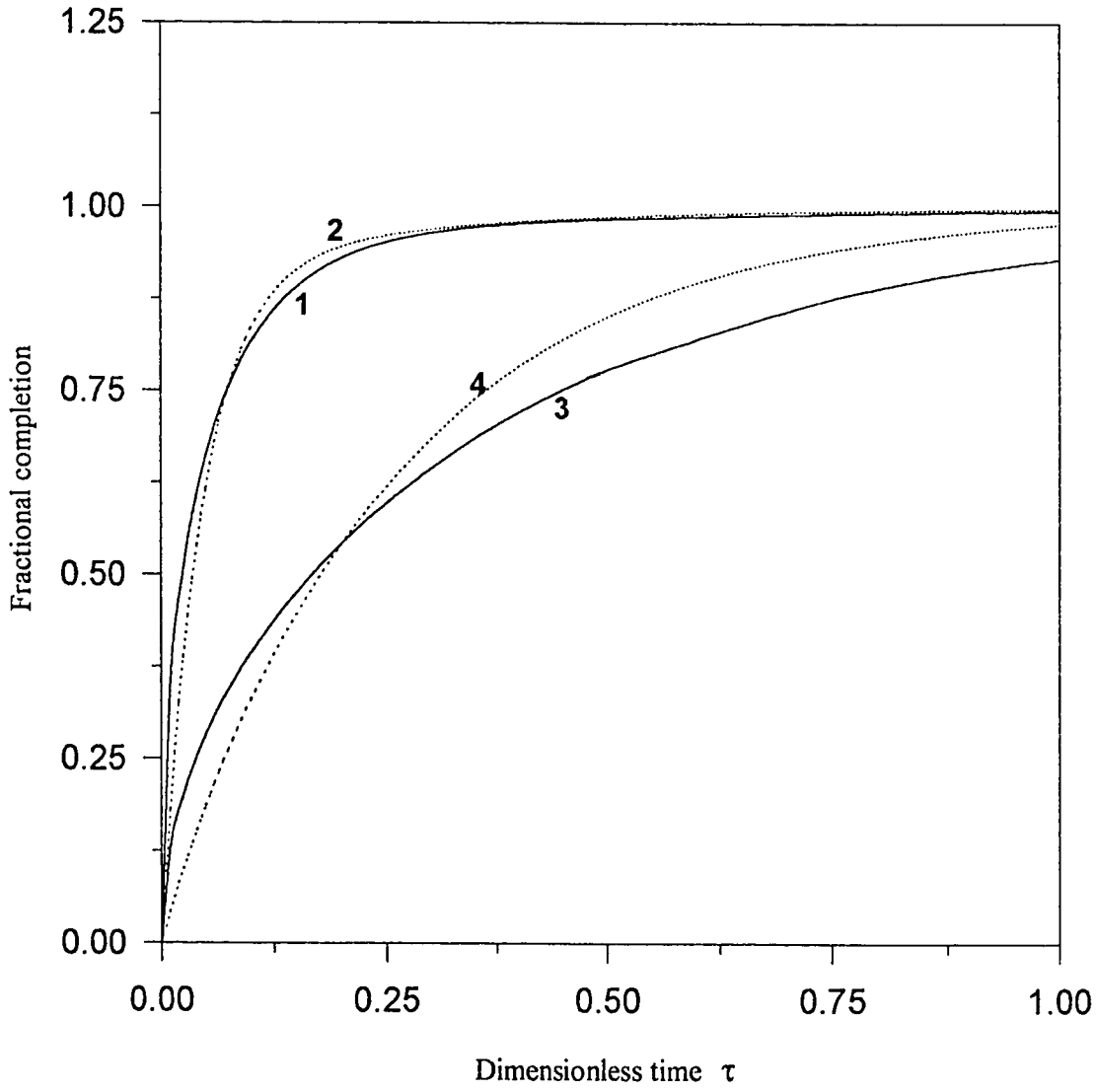

Figure 4.19. Comparison of the new binary LDF equation with the detailed model for binary diffusion. Case 19. (1 and 3 detailed model, 2 and 4 new LDF model; species A plots 1 and 2, species B plots 3 and 4)

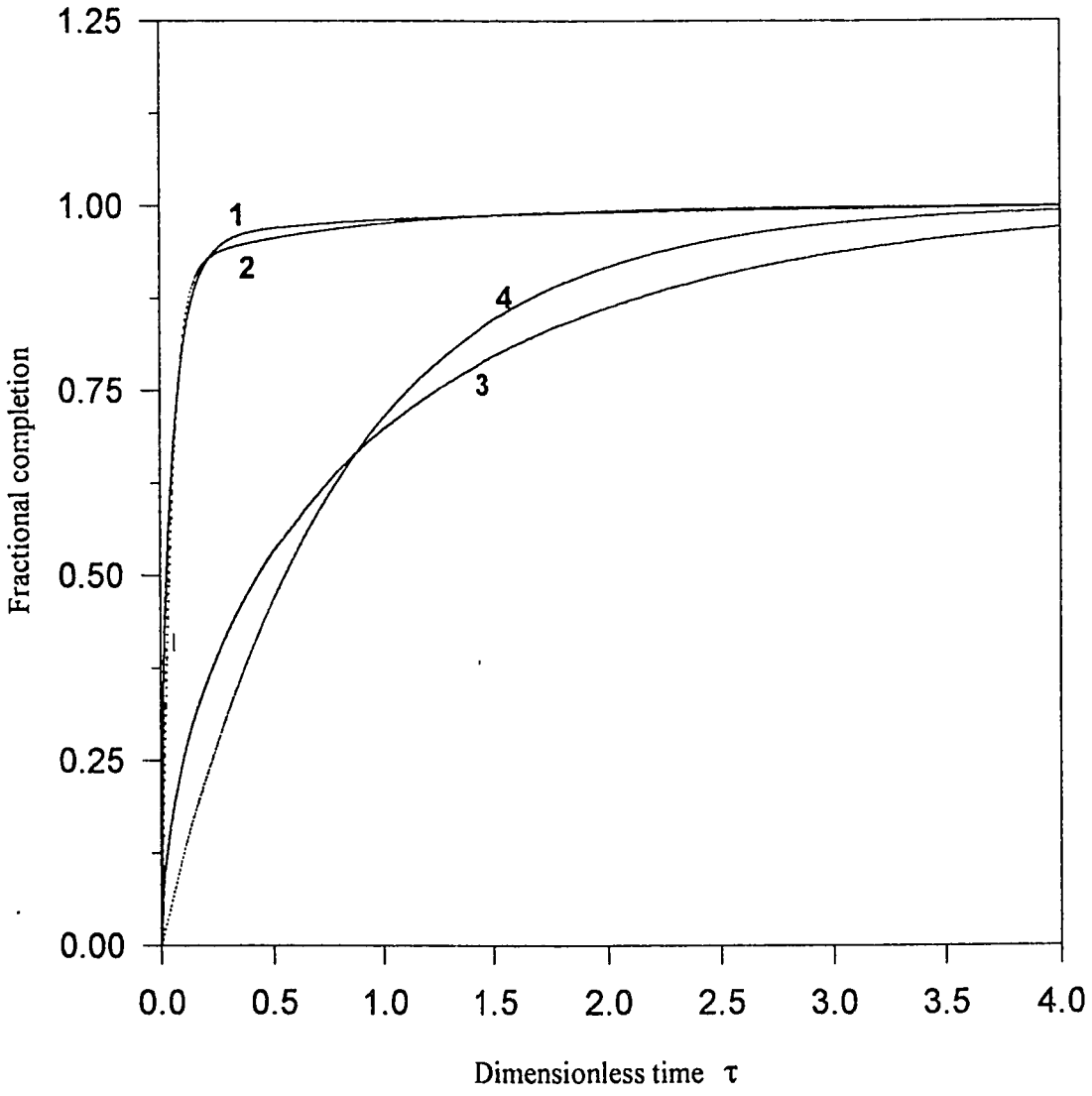

Figure 4.20. Comparison of the new binary LDF equation with the detailed model for binary diffusion. Case 20. (1 and 3 detailed model, 2 and 4 new LDF model; species A plots 1 and 2, species B plots 3 and 4)

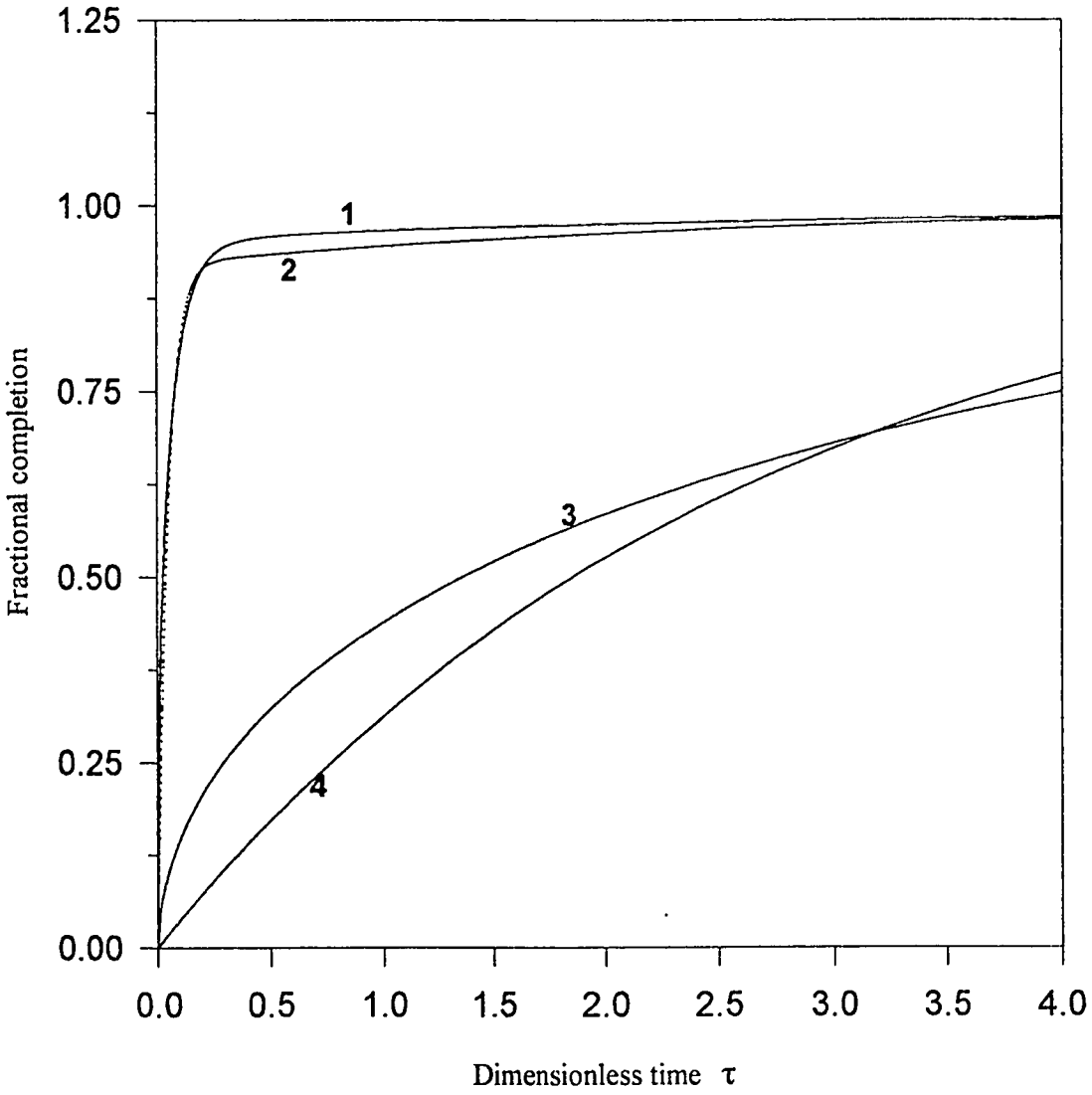

Figure 4.21. Comparison of the new binary LDF equation with the detailed model for binary diffusion. Case 21. (1 and 3 detailed model, 2 and 4 new LDF model; species A plots 1 and 2, species B plots 3 and 4)

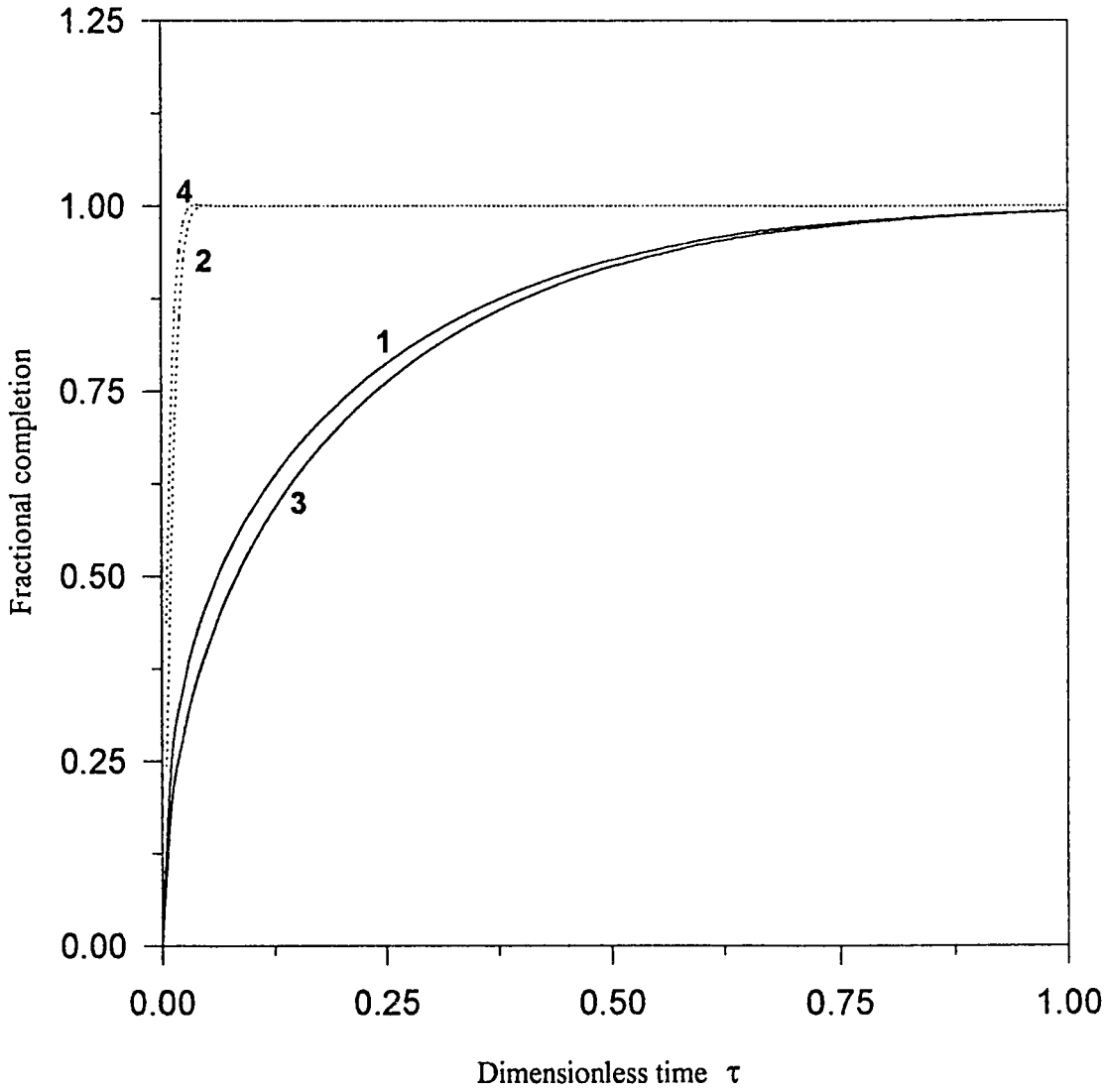

Figure 4.22. Comparison of the new binary LDF equation with the detailed model for binary diffusion. Case 22. (1 and 3 detailed model, 2 and 4 new LDF model; species A plots 1 and 2, species B plots 3 and 4)

changes the predictions of the proposed binary LDF equations, for different ratio of diffusion speeds of the two components, are in good agreement with the full partial differential equation solution especially for the faster species A. However, except for case 9, in the short time range the uptake predicted by the new model is slower than that obtained from the distributed parameter solution. For cases 10, 11, and 12 where the fast component is given a small step change in the concentration and the slower component is given a large step, the phenomenon of rollup is observed for the rapidly diffusing species. From Figures 4.10 to 4.12 it is seen that for the present value of parameter ω a lower rollup is predicted by the new model equations. The uptake rate prediction by the new LDF equation agrees fairly well with the distributed parameter model solution. Cases 13 and 14 correspond to the above two categories with nonzero initial concentrations and the prediction of the uptake rate is fair, although, once again, the predicted speed of attainment of equilibrium by the binary LDF is initially lower than that predicted by the comprehensive model.

Similar combinations of small and large concentration step for the two diffusing species are solved for cases of counterdiffusion. For cases 15, 16, and 17 both the species undergo a large concentration step change and the slow diffusing B is desorbing while the fast diffusing A is adsorbing. Here, except for very short times, the new LDF equations overpredict the uptake speed; at longer times, the predictions of the lumped and distributed parameter models match (see Figures 4.15 to 4.17). The reason for the overprediction of the uptake speed is that the term $1-\bar{\theta}_A-\bar{\theta}_B$ is small. This gives rise to a

Table 4.3. Summary of conclusions from the results of binary uptake cases using the new binary LDF equations (Figures 4.7 to 4.22)

Cases	Mode	Figures	Conclusions
7, 8, 9	CODIFFUSION	4.7, 4.8, 4.9	Good agreement for both components
10, 11, 12	CODIFFUSION	4.10, 4.11, 4.12	Good agreement for both components. Lower rollup predicted by the new model equations
13	CODIFFUSION	4.13	Good agreement for both components
14	CODIFFUSION	4.14	Fair agreement
15, 16, 17	COUNTERDIFFUSION	4.15, 4.16, 4.17	Fair agreement Rapid desorption predicted for fast diffusing component
18	COUNTERDIFFUSION	4.18	Fair agreement
19, 20, 21	COUNTERDIFFUSION	4.19, 4.20, 4.21	Good agreement
22	COUNTERDIFFUSION	4.22	Fair agreement

steep uptake curve which, for the present value of ω_A and ω_B , is even steeper than the uptake speed predicted by the distributed parameter model. For case 18 where the faster diffusing species is desorbing in counterdiffusion, the uptake rate prediction by the variable diffusivity LDF equation is in fair accord with the distributed parameter model. Cases 19 to 21 are for finite initial and final concentrations of the two diffusing species. As can be seen in figures 4.19 to 4.21 reliable predictions of the uptake rate are made by the new model. Case 22 is same as case 18 in principle with nonzero initial and final concentrations. The new LDF equations are seen to overpredict the approach towards equilibrium for the same reason as given for Figure 4.18. A summary of the conclusions form the results of the proposed binary LDF model relative to the distributed parameter model is given as Table 4.3.

The proposed LDF model equations are consistent with the physical picture of binary diffusion in a sphere. According to equation (4.8) there is an increase in diffusivity as the sorbate concentration increases. The same general trend of increase in diffusivity also applies to binary uptake where the diffusivity of a component increases with rising concentration of either of the two components. The present model equations incorporate this as the denominator term, $1 - \Sigma\bar{\theta}_i$, of the right hand side of equations (4.10), (4.14), and (4.15) is lower than unity for finite concentration of the sorbates. As evident from Figures 4.1 to 4.6 this gives rise to a faster uptake predicted by the new LDF equation than the Glueckauf LDF expression. A similar enhancement in attainment of equilibrium is manifested by binary diffusion cases. Since the equations (4.14) and (4.15) are coupled,

the uptake of either of the two components is influenced by the presence of the other. This is clear, for example, from the cases where the rollup of the rapidly diffusing species is predicted by the new binary LDF equations.

4.3 CONCLUSION

As a general conclusion it can be stated that the new LDF equation is promising especially for single component. For the cases of binary codiffusion and counterdiffusion the results of the new approximate model show a fair to good match with the full partial differential equation solution. Moreover, an adequate qualitative prediction of the phenomenon of rollup is made by the new LDF equations. However, the predictions of the new model are not good for one of the two components in some cases of counterdiffusion where the step change in sorbate surface concentration is large. This may be improved if value of parameter ω is adjusted to match the distributed parameter solution. But contrary to the distributed parameter system the solution of the new LDF takes much lower computer time. Savings in computer time are specially significant for mathematical modeling of pressure swing adsorption processes. It is expected that the binary LDF model, despite its slight quantitative deficiency, will give reasonable results when incorporated in the PSA model of a kinetically controlled process such as air separation on carbon molecular sieves or zeolite RS-10 (Farooq *et al.*, 1991, 1992). Presently the best approach to model such a process is to use the complete pore diffusion model with concentration dependent diffusivity for *a priori* predictions of the kinetic PSA

process. If Glueckauf's LDF model is to be used a plot of the parameter Ω versus cycle time is required. Such a plot is prepared by matching both the pore diffusion model and the Glueckauf's LDF model for the particular separation. Hence a tremendous computational effort is involved in each case. It would be desirable to combine the capability of predictions of a variable diffusivity pore diffusion model and computational ease of the LDF model. The proposed binary LDF model can be used to achieve this end if a standard procedure of calculating the values of parameter ω is devised using the concept of effective micropore diffusivity.

Nomenclature

D_c	intercrystalline diffusivity [$cm^2\ s^{-1}$]
D_o	limiting intercrystalline diffusivity as $q \rightarrow 0$ [$cm^2\ s^{-1}$]
m_t	moles of sorbate adsorbed/desorbed at time t [mole]
m_∞	moles of sorbate adsorbed/desorbed as $t \rightarrow \infty$ [mole]
m_t / m_∞	fractional approach to equilibrium [-]
p	sorbate partial pressure [atm]
q	sorbate concentration [mole cm^{-3}]
q^*	sorbate concentration in equilibrium with gas phase [mole cm^{-3}]
q_o'	initial sorbate concentration in a particle [mole cm^{-3}]
q_o	sorbate concentration at the surface of the particle [mole cm^{-3}]
Q_i	dimensionless sorbate concentration of component i defined as $\frac{q_i - q_{io}'}{q_{io} - q_{io}'}$
r	radial distance coordinate along the sorbate particle [cm]
r_c	particle radius [cm]
R	radial distance coordinate along the sorbent particle, r/r_c [-]
t	time [sec]

Greek symbols

β	$1/\xi$

δ	ratio of limiting diffusivities for two components in binary diffusion D_{Bo}/D_{Ao}
λ_1	dimensionless initial sorbate concentration, (q_o/q_{sat}) [-]
λ_2	dimensionless final sorbate concentration, (q_o/q_{sat}) [-]
θ	(q/q_{sat}) for a component [-]
$\overline{\theta}$	average concentration of a component— a function of initial and final concentration as defined by equations (4.11) and (4.16) [-]
θ_i	initial concentration of the sorbate [-]
θ_f	final concentration of sorbate [-]
τ	dimensionless time [-]
ω	weighting factor as in (4.11)
ξ	$\dfrac{(q_{B\infty}-q_{Bo})}{(q_{A\infty}-q_{Ao})}$

Subscripts

A	faster diffusing species
B	slower diffusing species

References

Farooq,S. and D. M. Ruthven, Numerical Simulation of a Kinetically Controlled Pressure Swing Adsorption Bulk Separation Process Based on a Diffusion Model, *Chem. Eng. Sci.*, 46, 2213-2229, 1991.

Farooq, S., M. N. Rathor and K. Hidajat, A Predictive Model for a Kinetically Controlled Pressure Swing Adsorption Separation Process, *Chem. Eng. Sci.*, 48, 4129-4141, 1993.

Garg, D. R. and D. M. Ruthven, The Effect of Concentration Dependence of Diffusivity on Zeolitic Sorption Curves, *Chem. Eng. Sci.*, 27, 417-423, 1972.

Glueckauf, E. and J. I. Coates, Theory of Chromatography. IV. The Influence of Incomplete Equilibrium on the Front Boundary of Chromatograms and on the Effectiveness of Separation, *J. Chem. Soc.*, 1315, 1947.

Kärger, J. and D. M. Ruthven, *Diffusion in Zeolites and Other Microporous* Solids, John Wiley & Sons, New York, 1992.

Round, G. F., H. W. Habgood and R. Newton, Numerical Analysis of Surface Diffusion in Binary Adsorbed Film, *Sep. Sci.*, 1, 219-244, 1966.

CHAPTER 5

SIMULATION OF A PRESSURE SWING ADSORPTION REACTOR PROCESS

In this chapter modeling simulation of a two-bed, four-step pressure swing adsorption reactor (PSAR) is presented. The results are compared to a simple tubular reactor operating under the same conditions.

5.1 REACTION SYSTEM

For the present simulation study a two-bed PSAR process is chosen with ethane dehydrogenation reaction to ethylene.

$$C_2H_6 \underset{k_2}{\overset{k_1}{\longleftrightarrow}} C_2H_4 + H_2$$

The reaction takes place on Cadmium supported 4A zeolite which adsorbs ethylene more strongly. Hydrogen actually has a little adsorption affinity on the catalyst / zeolite used here but for simulation purposes is assumed to be not adsorbed. Since there is an increase in the number of moles as a result of the forward reaction, low pressure in the reactor favors the production of the desired ethylene product. On the other hand, high pressure is favorable for the adsorption of ethylene obtained as a product in the low pressure desorption step. The adsorption pressure is taken to be 1.5 atm and the desorption

pressure is taken to be 1 atm. The pressurization step is not needed due to the limited value of the high-pressure in comparison to the low pressure. In the blowdown steps purging of the low pressure bed is continued. Figure 5.1 shows the cycle steps considered in modeling the present PSAR system.

The objective of choosing this reaction scheme is not to seek a new reactor for ethane dehydrogenation reaction. Rather the purpose is to demonstrate how a PSAR compares to a conventional tubular reactor. The choice of the reaction system is arbitrary

5.2 MATHEMATICAL MODELING

The modeling approach used for PSAR simulation is basically the same as used in chapter 3 to model a pressure swing adsorption bulk gas separation process. The only major difference in PSAR simulation is that an additional term to account for disappearance or production of a species by the chemical reaction is incorporated in the component material balance equation for that species. The model assumptions of chapter 3 are valid here except for the following changes:

(1) There is no pressurization step and the blowdown step is of a very short duration because of a low adsorption pressure. Therefore modeling only two steps, namely adsorption and desorption, is sufficient. In the blowdown step the solid phase is assumed to be frozen and the gas phase mole fractions do not change but the pressure reduces to the low pressure of 1 atm.

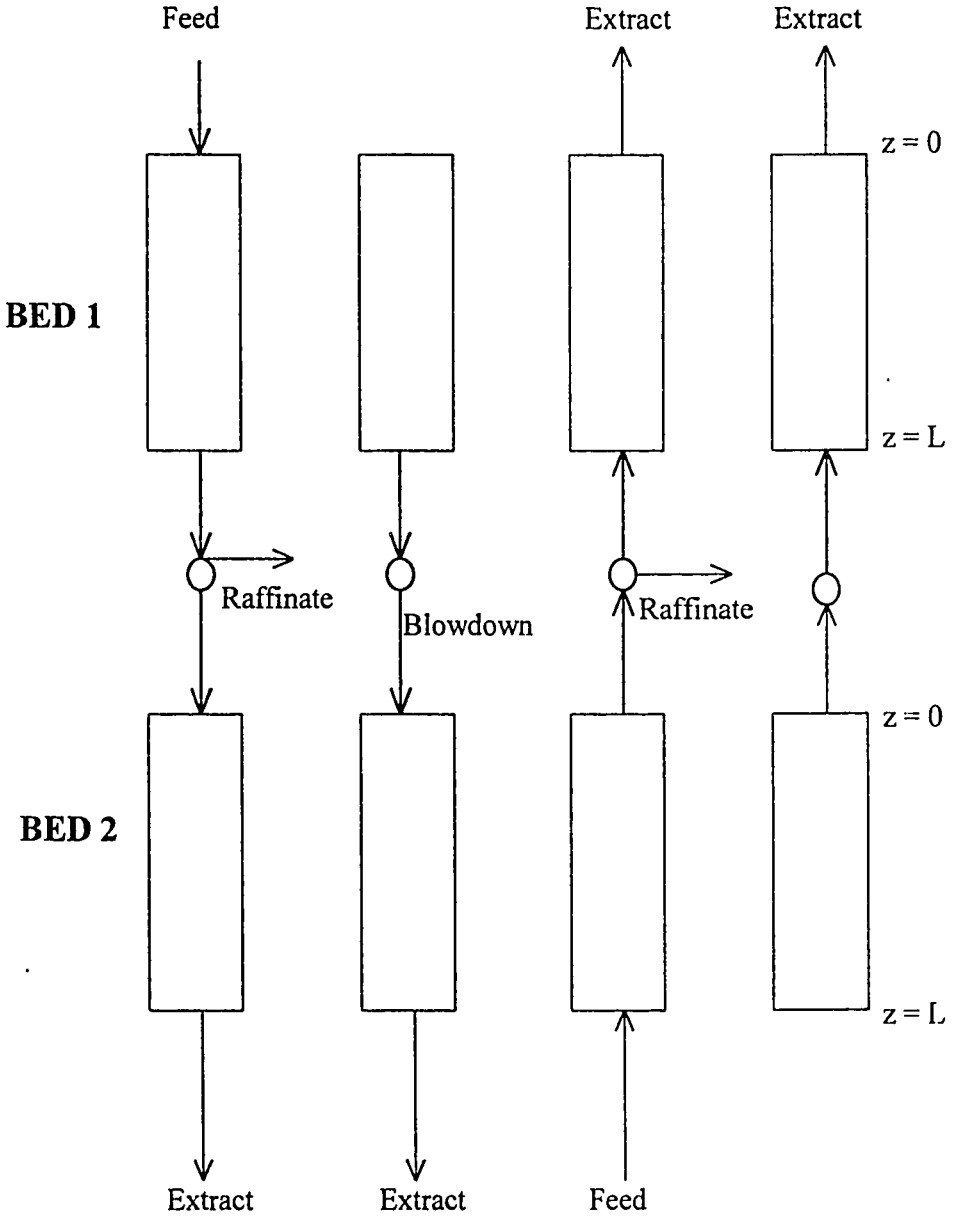

Figure 5.1. Schematic of the cycle steps used for simulation of PSA reactor process

(2) The equilibrium isotherm for both the adsorbable components A and B is taken to represented by the binary Langmuir model.

(3) Component C, *i.e.*, hydrogen is assumed to be a nonadsorbable inert.

(4) The initial conditions for PSAR process simulation are taken to be a clean solid phase with only hydrogen in the gas phase.

(5) The chemical reaction is local equilibrated and the rate expression is:

$$-r_A = k_1 \left(c_A - K_e' \, c_B \, c_C \right) \tag{5.1}$$

(6) Feed flow rate and concentration of different components in the feed are constant. The feed is taken to be pure A at the higher operating pressure.

(7) The compressibility factor of the gas phase is independent of pressure and composition.

The following general equation represents the model equations of the present system for different steps:

$$-D_{Lj}\frac{\partial c_{ij}}{\partial z^2}+\sigma v_j\frac{\partial c_{ij}}{\partial z}+\sigma c_{ij}\frac{\partial v_j}{\partial z}+\frac{\partial c_{ij}}{\partial t}+\left(\frac{1-\varepsilon}{\varepsilon}\right)\frac{\partial \bar{q}_{pj}}{\partial t}+\gamma_i k_1\left(c_{Aj}-K_e' c_{Bj} c_{cj}\right)=0 \tag{5.2}$$

where

i = component A (ethane), B (ethylene) or C (hydrogen)

j = bed 1 or 2

p = component A or B. Note that component C is assumed to be not adsorbed.

σ = +1 if the flow is in positive z-direction.

σ = -1 if the flow is in the negative z-direction

γ_i = stoichiometric coefficient, positive for the reaction products and negative for the reactants, *i.e.*, for i =A, B, or C, γ=-1, +1, +1 respectively

Adding three such equations for components A, B and C, and using the assumption that the total concentration given by $c_{Aj} + c_{Bj} + c_{Cj} = c_{Tj}$ is a constant, yields the following equation :

$$\sigma c_{Tj} \frac{\partial v_j}{\partial z} + \left(\frac{1-\varepsilon}{\varepsilon}\right)\frac{\partial \bar{q}_{Aj}}{\partial t} + \left(\frac{1-\varepsilon}{\varepsilon}\right)\frac{\partial \bar{q}_{Bj}}{\partial t} + k_l\left(c_{Aj} - K_e' c_{Bj} c_{Cj}\right) = 0 \tag{5.3}$$

A linear driving force rate expression is used for adsorbate components,

$$\frac{\partial \bar{q}_{pj}}{\partial t} = k_p\left(q_{pj}^{*} - \bar{q}_{pj}\right) \tag{5.4}$$

A binary Langmuir isotherm model is used as the equilibrium relationship between solid and the fluid phase

$$\frac{q_{pj}^{*}}{q_{SAT}} = \frac{b_p c_{pj}}{1 + \sum b_p c_{pj}} \tag{5.5}$$

The above set of partial differential equations is subject to the Danckwerts boundary conditions.

$$-D_{Lj}\left.\frac{\partial c_{ij}}{\partial z}\right|_{z=0} = v_j\left(\left.c_{ij}\right|_{z=0^-} - \left.c_{ij}\right|_{z=0}\right)$$

$$\left.\frac{\partial c_{ij}}{\partial z}\right|_{z=L} = 0 \tag{5.6}$$

For the case when the flow is from z = L to z = 0 [as in step (II)], the appropriate form of Danckwerts' boundary conditions is

$$-D_{Lj}\left.\frac{\partial c_{ij}}{\partial z}\right|_{z=L} = v_j\left(c_{ij}\big|_{z=L^+} - c_{ij}\big|_{z=L}\right)$$

$$\left.\frac{\partial c_{ij}}{\partial z}\right|_{z=0} = 0 \tag{5.7}$$

The next step is to solve the model equations (5.2) to (5.7) using the dimensionless variables defined at the end of this chapter to normalize the equations. The fluid-phase concentrations are normalized as follows:

i) For the step (I) where bed 1 is at high-pressure and bed 2 is at low pressure

$$c_{A1} = y_{A1}\, c_{OH}$$

$$c_{B1} = y_{B1}\, c_{OH}$$

$$c_{A2} = y_{A2}\, c_{OL}$$

$$c_{B2} = y_{A2}\, c_{OL} \tag{5.8}$$

ii) For the step (II) where bed 1 is at low-pressure and bed 2 is at high pressure

$$c_{A1} = y_{A1}\, c_{OL}$$

$$c_{B1} = y_{B1}\, c_{OL}$$

$$c_{A2} = y_{A2}\, c_{OH}$$

$$c_{B2} = y_{B2}\, c_{OH} \tag{5.9}$$

The dimensionless form of the model equations is,

$$\frac{1}{Pe_m}\frac{\partial^2 y_{pj}}{\partial x^2}+\sigma u_m\frac{\partial y_{pj}}{\partial x}+\sigma y_{pj}\frac{\partial u_m}{\partial x}+\frac{\partial y_{pj}}{\partial \tau}+\left(\frac{1-\varepsilon}{\varepsilon}\right)\frac{\overline{q}_{pO}}{c_{Om}}$$
$$\frac{k_p L}{v_{Om}}\left[\frac{y_{pj}}{\frac{\lambda_p}{\beta_p}+\lambda_p y_{pj}+\lambda_p\frac{\beta_{p'}}{\beta_p}y_{p'j}}-\psi_{pj}\right]-\gamma\, Da\left[y_{Aj}-K_e\, y_{Bj}\left(1-y_{Aj}-y_{Bj}\right)\right]=0 \qquad (5.10)$$

where m=1 or 2 for high-pressure or low pressure bed respectively. When p = A, p′ = B and *vice versa*. Note that we have two such equations; one for each of component A and B. Since the identity

$$y_A+y_B+y_C=1.0 \qquad (5.11)$$

must be satisfied there is no need to solve a differential equation for transient concentration profile of component C which can be determined by difference.

$$\sigma\frac{\partial u_m}{\partial x}+\left(\frac{1-\varepsilon}{\varepsilon}\right)\frac{q_{AO}}{c_{Om}}\frac{k_A L}{v_{Om}}\left[\frac{y_{Aj}}{\frac{\lambda_A}{\beta_A}+\lambda_A y_{Aj}+\lambda_A\frac{\beta_B}{\beta_A}y_{Bj}}-\psi_{Aj}\right]+\left(\frac{1-\varepsilon}{\varepsilon}\right)\frac{\overline{q}_{BO}}{c_{Om}}$$
$$\frac{k_B L}{v_{Om}}\left[\frac{y_{Bj}}{\frac{\lambda_B}{\beta_B}+\lambda_B y_{Bj}+\lambda_B\frac{\beta_A}{\beta_B}y_{Aj}}-\psi_{Bj}\right]+Da\left[y_{Aj}-K_e\, y_{Bj}\left(1-y_{Aj}-y_{Bj}\right)\right]=0 \qquad (5.12)$$

$$\frac{\partial \psi_{Aj}}{\partial \tau} = \frac{k_A L}{v_{Om}} \left[\frac{y_{Aj}}{\frac{\lambda_A}{\beta_A} + \lambda_A y_{Aj} + \lambda_A \frac{\beta_B}{\beta_A} y_{Bj}} - \psi_{Aj} \right] \tag{5.13}$$

$$\frac{\partial \psi_{Bj}}{\partial \tau} = \frac{k_B L}{v_{Om}} \left[\frac{y_{Bj}}{\frac{\lambda_B}{\beta_B} + \lambda_B y_{Bj} + \lambda_B \frac{\beta_A}{\beta_B} y_{Aj}} - \psi_{Bj} \right] \tag{5.14}$$

The boundary conditions applicable to step (I) when the flow is in positive z-direction are:

$$-\frac{1}{Pe_m} \frac{\partial y_{pj}}{\partial x}\bigg|_{x=0} = u_m \left(y_{pj}\big|_{x=0^-} - y_{pj}\big|_{x=0} \right)$$

$$\frac{\partial y_{pj}}{\partial x}\bigg|_{x=1} = 0 \tag{5.15}$$

For step (II) when the flow is in negative z-direction

$$-\frac{1}{Pe_m} \frac{\partial y_{pj}}{\partial x}\bigg|_{x=1} = u_m \left(y_{pj}\big|_{x=1^+} - y_{pj}\big|_{x=1} \right)$$

$$\frac{\partial y_{pj}}{\partial x}\bigg|_{x=0} = 0 \tag{5.16}$$

The dimensionless equations for transient concentration profiles are solved employing the method of orthogonal collocation. The resulting ordinary differential equations and simultaneous algebraic linear equations are solved using standard IMSL subroutines. The solution procedure is the same as in chapter 3. Parametric values used

for solution are listed in Table 5.1. These are taken from the papers of Schweich and Villermaux (1982), Lu and Rodrigues (1994), Loughlin and Ruthven (1972), and Antonucci *et al.* (1978).

The same reaction system has also been modeled by Lu and Rodrigues (1994) as a single-bed, three-step process. They have ignored the diffusional mass transfer resistance and have taken the solid and gas phase to be at equilibrium. Moreover, arbitrary adsorption parameters are used for adsorption of ethane and ethylene. In the present work realistic values of the Langmuir isotherm parameters and mass transfer coefficients of ethane and ethylene on 4A zeolite are taken from published literature. However, the reaction rate constants used here are same as in the work of Lu and Rodrigues (1994) and the purpose is to compare the PSAR with a conventional tubular reactor. To model the tubular reactor same values of the reaction rate constants and other parameters are used. The model equations are also similar to the equations for a PSAR but the catalyst is assumed to have no adsorption capacity and the process takes place continuously in a single reactor at a pressure of 1.5 atm and at the reaction temperature.

5.3 DISCUSSION

A summary of results of the above PSAR simulation at cyclic steady state is given in Table 5.2. As mentioned before arbitrary values of reaction rate constant and reaction equilibrium constant are used as model parameters. Still some conclusions can be drawn

Table 5.1. Parametric values used in the simulations of PSAR

Feed	100 % A (ethane)
Catalyst / Adsorbent	Cd impregnated 4A zeolite
Temperature [K]	723.15
Bed length [cm]	100.0
Bed voidage [-]	0.40
Adsorption pressure [atm]	1.5
Blowdown / Desorption pressure [atm]	1.0
Reaction rate constant k_1 [s^{-1}]	2.50
Reaction equilibrium constant [cm^3 / mol]	1.5×10^4
Isotherm type	Binary Langmuir
Langmuir constant b for A [cm^3 / mol]	5×10^5
Langmuir constant b for B [cm^3 / mol]	9.88×10^5
Saturation adsorbed concn. [mol / cm^3]	6.0×10^{-4}
LDF constant for A [s^{-1}]	1.0×10^{-4}
LDF constant for B [s^{-1}]	1.5×10^{-4}
Feed velocity v_{0H} [cm / s]	29.23
Purge to feed ratio	1.2
Peclet number [-]	1000
Adsorption / desorption time [s]	45
Initial conditions	Clean solid phase and all hydrogen in gas phase in both beds at respective pressures

Table 5.2. Summary of results of PSAR simulation

Outlet mole fraction (High pressure bed)	A	0.087
	B	0.462
	C	0.450
Outlet mole fraction (Low pressure bed)	A	0.875
	B	0.062
	C	0.062
Outlet mole fraction (Tubular reactor)	A	0.145
	B	0.427
	C	0.428

A = ethane

B = ethylene

C = hydrogen

from the comparison of two different reactor schemes. The outlet concentration of the desired product of the reaction, *i.e.*, ethylene, from the adsorption step in a PSAR is somewhat higher than the outlet of a conventional packed bed reactor. This might lead to the deduction that a PSAR performs better than a packed bed reactor for the reaction scheme presently considered. However, two factors are crucial in deciding the better reactor configuration for a reaction like the one in consideration. First, some A is adsorbed in the solid phase in the PSAR scheme. This adsorbed A is recovered as the outlet stream of the desorption step as shown in Table 5.2. It means that, on an overall basis, some A is left unconverted and represents a loss in terms of the overall system performance. Secondly, the desorption product may be recycled back to the PSAR along with the feed in the adsorption step. This will minimize the loss of unconverted reactant A. Therefore, the relative performance of the two reactor systems, a PSAR and a conventional catalytic reactor, is subject to the way the outlet stream of the desorption step of the PSAR is handled. Nevertheless, there is some reaction enhancement due to removal of B from the reaction zone by adsorption.

It is evident that the adsorption of A is not favorable for the process efficiency. The PSAR reaction system is better suited to a reaction scheme where a maximum of the reactant is allowed to be present in the reaction zone and the desired product of the forward reaction is adsorbed in order to retard the undesired reverse reaction. When the adsorption of these two species is comparable or the adsorption of the reactant is significant, full advantage of a PSAR cannot be achieved. Based on these arguments it can be suggested that if the adsorption separation of the two species is based on kinetics

with a very favorable ratio of diffusion speeds, a PSAR scheme may give a better conversion. However, any conclusions about the comparison of the two reactors for a reaction scheme such as the one considered here can only be drawn if a detailed reaction mechanism is available with reliable reaction rate constants. The present comparison of a PSAR with a tubular reactor is limited to the case when the outlet of the low pressure bed, predominantly species A, is not recycled to the high pressure bed with the fresh feed which is pure A at the adsorption pressure.

Nomenclature

b Langmuir's constant [cm^3 $mole^{-1}$]

c fluid phase concentration of a species [mole cm^{-3}]

c_{OH} concentration of stream inlet to the high pressure bed [mole/cm^{-3}]

c_{OL} concentration of stream inlet to the low pressure bed [mole/cm^{-3}]

$Da = \dfrac{k_1 L}{v_{OH}}$ = Damkohler number for the reaction

D_L axial dispersion coefficient [cm^2 s^{-1}]

K'_e equilibrium constant for the chemical reaction [cm^3 $mole^{-1}$ s^{-1}]

k_1 chemical reaction rate constant [s^{-1}]

$K_e = K'_e c_{OH}$ = Dimensionless reaction equilibrium constant

k_p LDF constant for component p [s^{-1}]

L length of the packed bed [cm]

Pe_m Peclet number for axial dispersion [-]

$\overline{q}$ average sorbed concentration in a particle [mole cm^{-3}]

$-r$ rate of disappearance of a species by the chemical reaction [mole cm^{-3} s^{-1}]

t time [s]

$u_1 = \dfrac{v_1}{v_{OH}}$ = Dimensionless velocity in the high pressure (feed) bed

$u_2 = \dfrac{v_2}{v_{OL}}$ = Dimensionless velocity in the low-pressure (purge) bed

v interstitial velocity through the column [cm s^{-1}]

v_{OH} interstitial feed velocity [cm/s]

$x = \frac{z}{L}$ = Dimensionless distance along the column length

y mole fraction of a species

z axial distance along the column length [cm]

Greek symbols

$\beta_p = b_p c_{OH}$ = Dimensionless Langmuir constant of component p corresponding to high pressure bed

$\beta'_p = b_p c_{OL}$ = Dimensionless Langmuir constant of component p corresponding to low pressure bed

γ stoichiometric coefficient (+ for products; - for reactants)

ε bed voidage

$\lambda_p = \frac{q_p}{q_{SAT}}$ = equilibrium loading in high-pressure bed

$\lambda'_p = \frac{q_p}{q_{SAT}}$ = equilibrium loading in low-pressure bed

σ +1 or -1 depending on the flow direction

$\tau = \frac{t v_{OH}}{L}$ = Dimensionless time

$\psi_{pj} = \frac{\bar{q}_{pj}}{q_{pO}}$ = Dimensionless solid phase concentration of component p

Subscripts

A	ethane
B	ethylene
C	hydrogen
i	component A, B, or C
j	bed 1 or 2
m	1 for the high pressure bed, 2 for the low pressure bed
p	species A or B
SAT	saturation value

References

Antonucci, P., N. Giordano and J. C. J. Bart, Chemical Reactions in Chromatographic Columns, *J. Chromat.*, 150, 309-317, 1978.

Loughlin, K. F. and D. M. Ruthven, The Sorption and Diffusion of Ethane in Type A Zeolites, *Chem. Eng. Sci.*, 27, 1401-1408, 1972.

Lu, Z. P. and A. E. Rodrigues, Pressure Swing Adsorption Reactors: Simulation of a Three-Step One-Bed Process, *AIChE J.*, 40, 1118-1137, 1994.

Schweich, D. and J. Villermaux, Model for Catalytic Dehydrogenation of Cyclohexane in a Chromatographic Reactor: Comparison of Theory and Experience, *Ind. Eng. Chem. Fundam.*, 21, 47-51, 1982.

CHAPTER 6

CONCLUSIONS AND RECOMMENDATIONS

6.1 SUMMARY OF CONCLUSIONS

- Equilibrium isotherms of both methane and nitrogen on MAXSORB are measured by volumetric method at a temperature of 300 K. The isotherms are linear up to a pressure of 5 atm ; hence the need to measure mixed gas isotherm is eliminated.
- Due to rapid attainment of equilibrium, it is difficult to extract any reliable data on kinetic parameters of methane and nitrogen on MAXSORB activated carbon by the volumetric method. Hence the system dynamics are measured by pulse chromatography; that is, the moments methods is used to determine Henry's constant and kinetic parameters for each of the two gases. Henry's constant for both gases are in a good agreement with the values measured by the volumetric method.
- The results of binary breakthrough experiments match accurately with numerical solution of the mathematical model using pure gas equilibrium and rate parameters obtained from volumetric and chromatographic methods. The axial dispersion coefficient for methane-nitrogen system is calculated from an empirical correlation. The experimental and theoretical results are in agreement for the calculated value of axial dispersion coefficient.

- The PSA separation of methane and nitrogen on MAXSORB is equilibrium based with a separation factor of 3.0 in favor of methane. Hence the desired methane-rich product is obtained in the extract step.
- Although the separation factor of 3.0 is rather low, the present PSA separation is relatively easy because of nearly complete absence of mass transfer resistance. The predominant mechanism of concentration front broadening is the axial dispersion in the packed sorbent bed.
- An important feature of the present PSA separation is that the blowdown product contains methane of reasonably high purity and represents a large portion of the total flow. Hence the blowdown gas is recovered as a part of methane-rich product along with the extract product. This allows a high recovery of methane in blowdown and extract products. The mixed stream containing the blowdown and extract products called the bottom product in this work is the desirable final product.
- The maximum methane purity of the bottom product is about 79% using the Skarstrom cycle with a 60/40 mixture of methane/nitrogen as the feed cycle.
- In a conventional PSA process, the desired product is the raffinate which is obtained at approximately the pressure of the feed gas. In the present case the methane-rich product is obtained at a low pressure in the blowdown and purge steps. Hence, extra energy of recompression is required if this product is needed at the feed pressure.
- Incorporating a cocurrent depressurization step in the PSA cycle gives a dramatic improvement in the purity of methane in the bottom product. A mixed stream containing the cocurrent depressurization product and the raffinate product is called

the top product in this work. The recovery of nitrogen in the top product also shows an improvement when the cocurrent depressurization step is used.

- The present separation of a methane-nitrogen mixture with modified PSA cycle is performed only to demonstrate the influence of cocurrent depressurization step. It should not be construed that the highest methane purity obtainable is about 88% in a dual-bed process. Using different combinations of cycle time, adsorption pressure, purge to feed ratio *etc.*, it may be possible to achieve an improvement in methane purity of the bottom-product and nitrogen recovery in the top-product. Two pure products may be furnished by the modified cycle if a proper combination of operational parameters is used.
- The results of PSA mathematical model are in a fair accord with the present experimental data.
- It is necessary to model all four steps of this equilibrium based PSA separation.
- A modified form of the linear driving force (LDF) expression for the cases of variable diffusivity is proposed in this work. The single component equation manifests a significant improvement over the conventional Glueckauf's equation for the cases where the step size of sorbate concentration is large.
- The proposed LDF model is extended to a binary uptake case. The results of binary system match fairly well with the full distributed parameter model solution for different cases of codiffusion.
- A reasonable agreement is observed between the distributed and lumped parameter models for binary counterdiffusion.

- A preliminary effort to simulate a pressure swing adsorption reactor (PSAR) shows that an improvement in performance over a conventional packed bed reactor is possible with certain combinations of parametric values.

6.2 RECOMMENDATIONS FOR FURTHER WORK

- Although the adsorbent used in the present work gives a good separation behavior, the search for a better absorbent is recommended to continue to achieve a higher separation factor.
- A systematic optimization of the present experimental PSA separation of methane and nitrogen is recommended. This can be accomplished by varying the operating parameters (cycle time, cycle configuration, pressure ratio, purge to feed ratio) one by one to find a set of local optima. The global optima is dictated by these local values of optimum operating parameters. A mathematical model simulation may be used to save experimental effort and expense.
- Further improvement in the performance of PSA separation of methane / nitrogen mixture on MAXSORB activated carbon may be possible if other cycle schemes are used. It is recommended to use the rinse step to obtain purer methane in the bottom-product. Also, multiple bed scheme may be employed to enhance the efficiency of the PSA separation by using pressure equalization steps.

- The modified cycle with cocurrent depressurization step should be optimized to increase the purity of the products; *i.e.*,. a bottom-product containing high purity methane and a top-product containing high purity nitrogen.
- The modified cycle with cocurrent depressurization should be modeled using the same modeling approach as for the Skarstrom cycle.
- Garg and Ruthven (*Chem. Eng. Sci.*, 27, 417-423, 1972) have plotted effective mean diffusivity against the sorbate step size for the case of concentration dependent diffusivity for single component diffusion. It is recommended to use this effective diffusivity in the LDF equation. This will eliminate the parameter ($\omega = 0.35$) from the proposed LDF equation. Similar plots of effective diffusivity against the sorbate step size can be generated for cases of codiffusion and counterdiffusion of a binary system. Using effective diffusivity in the proposed binary LDF equation will eliminate the parameters ω_A and ω_B.
- The new LDF equations use concentration dependence of diffusivity from Langmuir and binary Langmuir isotherm models. In reality, a very few systems truly conform to such idealized isotherm models. Therefore, it is recommended to use the experimental isotherm data (i.e. local value of $\partial\ ln\ p/\partial\ ln\ q$) rather than an isotherm model to account for concentration dependence of diffusivity. The use of other common isotherm models is straightforward in deriving LDF equations with variable diffusivity.
- The proposed binary LDF equations are valid for a system with intracrystalline diffusion control. A majority of kinetic PSA systems have micropore and film

resistances. Hence, it is recommended to attempt a kinetic PSA model using the new LDF equations instead of the Glueckauf equations with variable Ω factor.

- A lumped parameter model for a ternary or a multicomponent system is expected to be computationally much more involved than that of a binary system. However, the new LDF equations can easily be extended to a ternary or a multicomponent system and the numerical solution is expected to be very quick. It is recommended to derive the new LDF model for a ternary system using some representative isotherm models.
- It is recommended to use a more realistic kinetic rate law in the present PSAR simulations. A diffusion mechanism modeled by Langmuir-Hinshelwood kinetics may limit the overall chemical reaction. Moreover, a nonisothermal model may be used and a parameter sensitivity analysis may be performed for the present simulations.
- An overall performance index such as reaction enhancement due to pressure swing adsorption or enhancement in yield and selectivity should be developed to judge the performance of a PSAR.
- It is recommended to use the present PSAR modeling approach for two different types of chemical reactions. First, a case where a high pressure favors the desired forward reaction may be used. This is expected to give an improved performance because high pressure favors the adsorption of products of the forward reaction. Secondly, a pure kinetic separation where one of the species is totally excluded from the molecular sieve, such as the separation of *n*- and *iso*-paraffins on 5A zeolite, should be studied in a PSAR.

APPENDIX

A) The following equations are obtained as calibration factors for the flow meters marked as FI-1, FI-2, and FIC with reference to Figure 3.1: (F = flow rate in cm^3 STP/s ; R = digital reading of the flow meter)

FI-1 :

$F = 0.272\ R + 1.461$ (for 60% methane-40% nitrogen)

8 measurements of flow rate are performed up to a flow of approximately 10 cm^3 STP/s.

$F = 0.222\ R + 1.093$ (for 100% methane)

7 measurements of flow rate are performed up to a flow of approximately 5 cm^3 STP/s.

FI-2 :

$F = 0.239\ R + 1.644$ (for 60% methane-40% nitrogen)

5 measurements of flow rate are performed up to a flow of approximately 10 cm^3 STP/s.

$F = 0.205\ R + 1.418$ (for 100% methane)

5 measurements of flow rate are performed up to a flow of approximately 5 cm^3 STP/s.

FIC :

$F = 12.660\ R + 5.495$ (for 60% methane-40% nitrogen)

6 measurements of flow rate are performed up to a flow of approximately 10 cm^3 STP/s.

$F = 12.793\ R + 4.998$ (for 100% methane)

11 measurements of flow rate are performed up to a flow of approximately 5 cm^3 STP/s.

Composition correction :

Based on a linear interpolation of methane percentage and the heat capacity of methane and nitrogen, the following equation is used for composition correction to the flow rate measured by the flow meters:

$$F_x = \frac{F_{60/40}\ (1.0 - 0.187\,x)}{0.8878}$$

where F_x = cm^3 STP/s of a gas of methane mole fraction = x

$F_{60/40}$ = cm3 STP/s of 60% methane-40% nitrogen mixture as given by the above calibration curve equations.

B) Calculations for a typical pressure swing adsorption experiment (Run 7) are made from the data read-off the chart recorder outputs presented on the next page. For the numerical integration as in equations 3.1 and 3.2 in the text, Simpson's rule is used. Results of calculations are as follows :

Cycle time = 540 seconds

Cycle configuration is 5 - 45 %

Pressurization / Blowdown time = 27 seconds

Adsorption / Desorption time = 243 seconds

Flow rate of FI-1 averaged over the whole cycle = 22.51 cm^3 STP/s

Flow rate of FI-2 averaged over the whole cycle = 4.24 cm^3 STP/s

Methane mole percent in extract + blowdown streams = 75.998 %

Methane mole percent in the raffinate stream = 13.67 %

Nitrogen mole percent in the raffinate stream = 86.33 %

Flow rate of the extract averaged over the time for desorption step = 12.11 cm^3 STP/s

Average flow rate of the blowdown stream = 99.62 cm^3 STP/s

Methane mole percent in the blowdown stream = 74.93 %

C) Experimental data for other runs is also attached.

D) Computer program for the solution of binary LDF model equations.

Run 7

Time (sec)	FI-1 reads	CH_4 botm.	Flow rate cm^3 STP/s		FI-2 reads	CH_4 raffnt.	Flow rate cm^3 STP/s
0	520.0	0.720	139.092		13.4	0.200	5.250
10	410.0	0.745	109.376		4.0	0.245	2.793
20	310.0	0.770	82.593		0.0	0.255	1.764
30	234.0	0.778	62.580		12.0	0.269	4.822
40	120.0	0.802	32.606		9.8	0.290	4.243
50	56.0	0.803	15.959		9.2	0.302	4.081
60	45.0	0.804	13.096		9.4	0.330	4.096
70	41.0	0.806	12.051		9.2	0.333	4.056
80	38.0	0.808	11.266		9.0	0.358	3.985
90	36.0	0.809	10.745		8.9	0.359	3.959
100	35.0	0.810	10.483		8.8	0.310	3.973
110	34.0	0.809	10.225		8.6	0.230	3.985
120	33.0	0.807	9.970		8.5	0.208	3.976
130	32.0	0.805	9.715		8.4	0.185	3.968
140	32.0	0.804	9.717		8.3	0.182	3.944
150	31.5	0.802	9.591		8.3	0.155	3.952
160	31.0	0.800	9.465		8.2	0.152	3.941
170	30.5	0.797	9.341		8.2	0.130	3.944
180	30.0	0.780	9.245		8.2	0.126	3.947
190	29.5	0.775	9.125		8.1	0.110	3.946
200	29.0	0.774	8.996		8.1	0.102	3.939
210	28.5	0.773	8.867		8.1	0.100	3.941
220	28.0	0.770	8.742		8.1	0.080	3.969
230	27.0	0.750	8.517		8.2	0.075	3.986
240	26.0	0.748	8.258		8.3	0.073	4.014
250	24.0	0.745	7.736		8.4	0.071	4.055
260	23.5	0.728	7.633		8.6	0.069	4.110
270	525.0	0.726	140.233		8.8	0.066	4.152
280	430.0	0.725	115.140		4.0	0.065	2.892
290	350.0	0.750	93.475		1.2	0.064	2.149
300	266.0	0.761	71.210		-0.7	0.063	1.644
310	160.0	0.770	43.311		13.0	0.064	5.282

320	64.0	0.785	18.110		10.8	0.070	4.693
330	48.0	0.786	13.931		10.8	0.097	4.655
340	44.0	0.788	12.881		10.7	0.140	4.591
350	41.5	0.790	12.224		10.5	0.210	4.491
360	39.0	0.790	11.572		10.5	0.234	4.470
370	38.0	0.788	11.316		10.5	0.170	4.526
380	37.0	0.788	11.055		10.5	0.100	4.574
390	36.5	0.787	10.927		10.5	0.080	4.591
400	36.0	0.785	10.801		10.5	0.075	4.609
410	35.0	0.784	10.543		10.5	0.060	4.622
420	34.0	0.781	10.288		10.6	0.052	4.642
430	33.5	0.763	10.198		10.7	0.048	4.672
440	33.0	0.762	10.069		10.7	0.047	4.687
450	32.0	0.760	9.811		10.8	0.046	4.714
460	30.5	0.738	9.462		11.0	0.047	4.753
470	30.0	0.738	9.330		11.2	0.048	4.805
480	29.0	0.739	9.065		11.4	0.049	4.871
490	28.5	0.737	8.937		11.8	0.049	4.978
500	28.0	0.725	8.828		12.4	0.065	5.122
510	27.0	0.715	8.582		12.8	0.073	5.220
520	26.0	0.715	8.317		13.2	0.090	5.309
530	26.0	0.712	8.322		13.7	0.135	5.395
540	26.0	0.710	8.326		14.0	0.165	5.429

Run 2

Time (sec)	FI-1 reads	CH_4 botm.	FI-2 reads	CH_4 raffnt.
0	610.0	0.702	10.500	0.210
10	485.0	0.689	4.600	0.145
20	330.0	0.690	1.200	0.133
30	220.0	0.690	9.700	0.125
40	110.0	0.690	8.500	0.124
50	42.0	0.692	8.200	0.123
60	35.0	0.694	7.950	0.160
70	32.0	0.695	7.850	0.200
80	30.0	0.698	6.750	0.300
90	28.0	0.700	7.800	0.360
100	560.0	0.701	7.900	0.340
110	415.0	0.703	3.150	0.270
120	345.0	0.686	0.650	0.219
130	238.0	0.684	10.800	0.190
140	128.0	0.687	9.800	0.151
150	50.0	0.700	9.400	0.147
160	39.0	0.701	9.350	0.143
170	35.0	0.703	9.500	0.180
180	30.0	0.703	9.650	0.245
190	30.0	0.704	10.100	0.265
200	30.0	0.705	10.600	0.240

Run 3

Time (sec)	Fl-1 reads	CH_4 botm.	Fl-2 reads	CH_4 raffnt.
0	605.0	0.700	8.4	0.209
10	450.0	0.700	2.4	0.250
20	320.0	0.679	0.0	0.210
30	210.0	0.679	18.0	0.173
40	100.0	0.680	7.3	0.160
50	42.0	0.683	6.7	0.152
60	35.0	0.690	6.4	0.164
70	31.0	0.692	6.4	0.205
80	500.0	0.694	3.0	0.290
90	409.0	0.679	0.7	0.300
100	290.0	0.666	-0.8	0.300
110	160.0	0.669	13.0	0.250
120	65.0	0.690	8.4	0.178
130	42.0	0.665	8.0	0.161
140	34.5	0.667	8.0	0.182
150	31.5	0.696	8.1	0.195

Run 4

Time (sec)	FI-1 reads	CH_4 botm.	FI-2 reads	CH_4 raffnt.
0	550.0	0.700	17.0	0.221
10	450.0	0.715	5.0	0.275
20	340.0	0.724	0.2	0.288
30	200.0	0.740	13.8	0.305
40	88.0	0.754	12.8	0.320
50	47.0	0.754	12.0	0.340
60	40.0	0.755	11.7	0.342
70	36.0	0.756	11.5	0.353
80	34.0	0.757	11.4	0.300
90	32.5	0.757	11.2	0.225
100	31.5	0.759	11.1	0.185
110	30.0	0.759	11.0	0.180
120	29.5	0.757	10.9	0.154
130	28.5	0.755	10.8	0.128
140	28.0	0.753	10.8	0.125
150	28.0	0.751	10.8	0.105
160	26.0	0.750	10.9	0.095
170	26.5	0.749	11.2	0.092
180	26.0	0.730	11.5	0.082
190	25.0	0.729	11.9	0.076
200	552.0	0.728	8.0	0.077
210	480.0	0.708	3.8	0.077
220	380.0	0.713	1.0	0.100
230	180.0	0.715	15.6	0.102
240	107.0	0.732	14.0	0.130
250	60.0	0.738	13.6	0.200
260	43.0	0.740	13.2	0.250
270	40.0	0.742	13.0	0.272
280	37.0	0.744	12.9	0.187
290	36.5	0.745	12.8	0.125
300	35.5	0.746	12.7	0.100
310	35.0	0.742	12.8	0.096
320	34.0	0.741	13.0	0.072
330	32.0	0.740	13.1	0.070
340	30.5	0.738	13.4	0.068
350	29.0	0.720	14.1	0.065
360	29.0	0.719	14.6	0.065
370	27.8	0.717	15.4	0.080
380	27.0	0.715	16.2	0.100
390	26.5	0.712	16.4	0.160
400	26.0	0.710	16.6	0.210

Run 5

Time (sec)	FI-1 reads	CH_4 botm.	FI-2 reads	CH_4 raffnt.
0	625.0	0.695	14.6	0.238
10	500.0	0.740	4.0	0.270
20	375.0	0.750	0.8	0.282
30	240.0	0.770	-0.8	0.285
40	98.0	0.770	14.0	0.285
50	55.0	0.775	10.3	0.320
60	44.0	0.778	10.1	0.347
70	38.0	0.778	9.8	0.350
80	37.0	0.778	9.7	0.340
90	34.5	0.780	9.6	0.280
100	33.5	0.782	9.4	0.230
110	32.0	0.780	9.3	0.190
120	31.0	0.780	9.2	0.173
130	30.5	0.780	9.1	0.162
140	30.0	0.776	9.1	0.140
150	29.5	0.775	9.0	0.134
160	29.0	0.775	9.0	0.120
170	29.0	0.770	8.9	0.109
180	28.5	0.770	8.9	0.105
190	28.0	0.750	8.9	0.083
200	28.0	0.749	8.9	0.081
210	27.5	0.740	9.0	0.080
220	27.0	0.726	9.1	0.078
230	26.0	0.727	9.2	0.078
240	25.0	0.723	9.4	0.073
250	24.0	0.725	9.8	0.071
260	450.0	0.723	4.0	0.070
270	354.0	0.740	1.2	0.070
280	245.0	0.750	-0.6	0.072
290	117.0	0.755	14.0	0.074
300	62.0	0.768	11.6	0.110
310	47.0	0.768	11.0	0.150

Run 5

320	41.5	0.768	10.9	0.230
330	40.0	0.768	10.8	0.255
340	38.0	0.769	10.8	0.200
350	37.5	0.768	10.8	0.110
360	36.0	0.766	10.8	0.100
370	35.5	0.765	10.8	0.088
380	34.5	0.762	10.8	0.070
390	34.0	0.760	10.8	0.061
400	33.0	0.742	10.8	0.060
410	32.5	0.730	11.0	0.058
420	32.0	0.736	11.1	0.056
430	31.0	0.735	11.3	0.055
440	30.0	0.733	11.5	0.055
450	29.5	0.715	11.9	0.055
460	28.0	0.712	12.4	0.070
470	27.5	0.710	13.0	0.083
480	27.0	0.710	13.4	0.118
490	26.5	0.690	13.9	0.160
500	26.0	0.690	14.1	0.235

Run 6

Time (sec)	FI-1 reads	CH_4 botm.	FI-2 reads	CH_4 raffnt.
0	500.0	0.720	15.7	0.290
10	400.0	0.750	4.5	0.320
20	300.0	0.768	-0.4	0.335
30	190.0	0.795	14.0	0.335
40	80.0	0.795	11.0	0.338
50	52.0	0.795	10.5	0.351
60	42.0	0.795	10.3	0.365
70	38.5	0.797	10.2	0.383
80	35.5	0.800	10.0	0.290
90	34.5	0.800	9.9	0.233
100	33.0	0.800	9.8	0.205
110	32.0	0.800	9.7	0.190
120	31.0	0.800	9.6	0.178
130	30.5	0.797	9.5	0.160
140	29.5	0.795	9.4	0.152
150	29.0	0.794	9.3	0.127
160	29.0	0.792	9.2	0.125
170	28.0	0.775	9.2	0.104
180	28.0	0.774	9.2	0.103
190	28.0	0.773	9.2	0.080
200	27.5	0.755	9.2	0.078
210	27.0	0.754	9.1	0.074
220	26.0	0.750	9.0	0.065
230	26.0	0.731	9.0	0.055
240	25.0	0.729	9.0	0.053
250	25.0	0.727	9.0	0.052
260	24.5	0.710	9.1	0.050
270	24.0	0.709	9.2	0.048
280	24.0	0.705	9.4	0.046
290	23.5	0.690	9.7	0.045
300	495.0	0.710	10.1	0.046
310	400.0	0.735	3.0	0.055

Run 6

320	310.0	0.742	0.6	0.068
330	208.0	0.762	-0.9	0.070
340	100.0	0.763	15.0	0.071
350	57.0	0.766	11.9	0.130
360	46.0	0.768	11.6	0.198
370	42.0	0.770	11.6	0.250
380	39.0	0.771	11.5	0.150
390	38.0	0.772	11.4	0.100
400	37.0	0.772	11.4	0.090
410	36.0	0.771	11.4	0.069
420	35.0	0.770	11.4	0.063
430	34.0	0.768	11.4	0.060
440	33.5	0.765	11.4	0.043
450	33.0	0.764	11.3	0.040
460	32.0	0.745	11.4	0.039
470	31.0	0.742	11.5	0.038
480	30.5	0.741	11.6	0.037
490	30.0	0.720	11.6	0.038
500	29.5	0.720	11.8	0.039
510	29.0	0.718	12.0	0.040
520	28.0	0.705	12.3	0.055
530	27.0	0.692	12.7	0.063
540	26.5	0.690	13.2	0.070
550	26.0	0.680	13.7	0.095
560	25.5	0.676	14.4	0.128
570	24.0	0.674	14.8	0.164
580	23.0	0.643	15.0	0.215
590	22.0	0.641	15.3	0.255
600	22.0	0.620	15.5	0.298

Run 8

Time (sec)	FI-1 reads	CH_4 botm.	FI-2 reads	CH_4 raffnt.
0	460.0	0.720	12.0	0.020
10	410.0	0.720	4.6	0.021
20	350.0	0.740	1.6	0.034
30	290.0	0.760	14.0	0.035
40	252.0	0.771	9.6	0.036
50	180.0	0.786	9.5	0.052
60	118.0	0.788	9.4	0.550
70	80.0	0.790	9.3	0.087
80	64.0	0.792	9.1	0.130
90	53.0	0.793	9.0	0.190
100	52.0	0.797	8.9	0.241
110	48.0	0.796	8.8	0.250
120	46.0	0.794	8.8	0.183
130	45.5	0.793	8.7	0.151
140	44.0	0.790	8.5	0.123
150	43.0	0.773	8.5	0.120
160	42.0	0.772	8.4	0.095
170	41.0	0.755	8.4	0.080
180	40.5	0.754	8.4	0.068
190	40.0	0.754	8.4	0.068
200	39.0	0.753	8.4	0.050
210	38.0	0.731	8.4	0.045
220	37.0	0.729	8.4	0.044
230	36.0	0.705	8.4	0.042
240	35.0	0.701	8.4	0.040
250	34.5	0.675	8.4	0.038
260	33.0	0.640	8.4	0.035
270	490.0	0.670	8.5	0.034
280	440.0	0.670	4.0	0.033
290	380.0	0.690	1.0	0.030
300	320.0	0.718	-0.2	0.029
310	264.0	0.720	13.0	0.027

320	196.0	0.744	10.8	0.025
330	131.0	0.748	10.4	0.024
340	92.0	0.750	10.2	0.023
350	70.0	0.752	10.2	0.022
360	60.0	0.753	10.2	0.021
370	56.0	0.755	10.2	0.024
380	52.0	0.758	10.2	0.080
390	50.0	0.757	10.2	0.064
400	49.0	0.755	10.2	0.031
410	48.0	0.753	10.2	0.029
420	46.0	0.730	10.2	0.027
430	45.5	0.726	10.2	0.026
440	44.0	0.710	10.3	0.025
450	43.0	0.703	10.3	0.023
460	42.0	0.695	10.4	0.020
470	40.0	0.680	10.4	0.018
480	39.0	0.650	10.4	0.018
490	38.0	0.647	10.5	0.015
500	36.0	0.618	10.6	0.014
510	35.0	0.603	10.8	0.015
520	34.0	0.595	11.3	0.016
530	32.0	0.568	11.6	0.018
540	30.0	0.565	12.4	0.021

Run 9

Time (sec)	FI-1 reads	CH_4 botm.	FI-2 reads	CH_4 raffnt.
0	550.0	0.750	25.9	0.450
10	400.0	0.750	4.8	0.451
20	240.0	0.765	-0.8	0.452
30	100.0	0.778	16.9	0.452
40	40.0	0.780	16.4	0.455
50	29.0	0.782	16.6	0.456
60	24.0	0.785	16.6	0.456
70	22.0	0.787	16.6	0.458
80	20.5	0.788	16.5	0.340
90	20.0	0.790	16.3	0.314
100	19.0	0.792	16.2	0.300
110	18.0	0.794	16.0	0.290
120	17.5	0.795	16.0	0.290
130	17.0	0.799	16.0	0.266
140	16.5	0.798	16.2	0.260
150	16.0	0.797	16.7	0.240
160	15.6	0.795	17.1	0.238
170	15.3	0.794	18.0	0.237
180	15.0	0.792	18.7	0.235
190	15.0	0.790	19.2	0.270
200	14.5	0.789	19.2	0.315
210	14.0	0.788	19.2	0.367
220	14.0	0.785	19.2	0.405
230	14.0	0.784	19.2	0.420
240	14.0	0.783	19.2	0.430
250	14.0	0.780	19.2	0.433
260	13.5	0.779	19.2	0.436
270	535.0	0.778	19.2	0.437
280	420.0	0.740	2.0	0.440
290	80.0	0.742	-0.6	0.441
300	120.0	0.760	25.8	0.443
310	40.0	0.766	21.6	0.445

Run 9

320	28.0	0.767	21.6	0.446
330	25.0	0.770	21.5	0.401
340	23.0	0.772	21.3	0.310
350	22.0	0.775	21.1	0.280
360	21.0	0.776	20.9	0.260
370	20.5	0.779	21.0	0.248
380	20.0	0.780	21.7	0.223
390	19.5	0.780	22.5	0.221
400	19.0	0.778	23.6	0.220
410	17.5	0.775	24.8	0.240
420	17.0	0.774	25.4	0.305
430	16.5	0.773	25.7	0.370
440	16.0	0.771	25.7	0.430
450	16.0	0.770	25.7	0.455
460	16.0	0.768	25.7	0.455
470	16.0	0.764	25.6	0.460
480	16.0	0.763	25.6	0.460
490	15.5	0.761	25.6	0.465
500	15.0	0.759	25.6	0.460
510	15.0	0.742	25.6	0.460
520	14.5	0.742	25.6	0.460
530	14.0	0.742	25.6	0.458
540	14.0	0.741	25.6	0.456

Run 10

Time (sec)	FI-1 reads	CH_4 botm.	FI-2 reads	CH_4 raffnt.
0	568.0	0.725	20.7	0.455
10	430.0	0.725	4.8	0.455
20	271.0	0.740	-0.4	0.456
30	121.5	0.745	13.4	0.454
40	40.0	0.745	13.0	0.453
50	26.5	0.746	13.0	0.453
60	22.5	0.747	12.8	0.453
70	20.5	0.750	12.7	0.452
80	19.9	0.751	12.5	0.450
90	18.0	0.751	12.3	0.343
100	17.0	0.753	12.2	0.305
110	16.5	0.753	12.3	0.278
120	16.0	0.753	12.4	0.252
130	15.5	0.753	12.7	0.240
140	15.0	0.751	13.3	0.225
150	15.0	0.751	13.8	0.224
160	14.0	0.747	14.3	0.222
170	13.5	0.746	14.7	0.223
180	13.0	0.745	15.0	0.279
190	12.5	0.744	15.0	0.325
200	12.0	0.742	15.1	0.370
210	465.0	0.739	15.1	0.396
220	330.0	0.726	4.4	0.423
230	280.0	0.713	-0.5	0.424
240	157.0	0.714	17.9	0.424
250	52.0	0.715	17.5	0.426
260	28.5	0.734	17.2	0.444
270	24.0	0.734	17.0	0.443
280	22.0	0.735	16.7	0.333
290	21.0	0.736	16.6	0.275
300	20.0	0.738	16.7	0.243
310	19.0	0.739	17.0	0.220
320	18.0	0.739	18.0	0.200
330	17.0	0.739	18.8	0.197
340	16.5	0.737	19.5	0.218
350	16.0	0.734	20.1	0.273
360	16.0	0.732	20.3	0.335
370	15.0	0.732	20.5	0.380
380	14.5	0.731	20.6	0.410
390	14.5	0.729	20.6	0.430
400	14.0	0.727	20.6	0.445
410	14.0	0.725	20.6	0.447
420	14.0	0.724	20.6	0.448

Run 11

Time (sec)	FI-1 reads	CH_4 botm.	FI-2 reads	CH_4 raffint.
0	610.0	0.700	16.2	0.365
10	480.0	0.700	4.0	0.390
20	252.0	0.750	-1.2	0.392
30	104.0	0.790	17.6	0.392
40	52.0	0.796	10.3	0.395
50	40.0	0.798	9.8	0.397
60	37.0	0.800	9.6	0.414
70	36.0	0.802	9.5	0.414
80	34.0	0.804	9.3	0.441
90	33.0	0.806	9.2	0.442
100	32.5	0.808	9.0	0.410
110	32.0	0.809	8.8	0.315
120	32.0	0.804	8.7	0.282
130	31.5	0.802	8.5	0.286
140	31.5	0.795	8.3	0.251
150	31.0	0.800	8.3	0.228
160	31.0	0.798	8.2	0.210
170	30.0	0.780	8.1	0.198
180	30.0	0.779	8.0	0.170
190	29.5	0.778	7.9	0.155
200	29.0	0.758	7.9	0.145
210	29.0	0.759	7.8	0.120
220	28.2	0.759	7.8	0.118
230	28.0	0.738	7.9	0.094
240	28.0	0.738	7.9	0.092
250	27.5	0.737	8.0	0.090
260	26.5	0.715	8.3	0.072
270	26.0	0.713	8.6	0.071
280	25.0	0.694	9.0	0.070
290	24.0	0.687	10.0	0.069
300	23.0	0.676	10.3	0.069
310	450.0	0.730	6.0	0.070
320	280.0	0.745	-0.4	0.089
330	152.0	0.756	-1.7	0.090
340	72.0	0.779	17.0	0.092
350	44.0	0.781	12.8	0.140
360	41.0	0.782	12.5	0.200
370	39.0	0.785	12.2	0.283
380	37.5	0.787	11.8	0.368
390	36.5	0.786	11.7	0.300
400	36.5	0.787	11.6	0.220
410	36.0	0.787	11.4	0.168
420	35.5	0.786	11.3	0.136
430	35.0	0.784	11.3	0.120
440	34.0	0.767	11.3	0.102
450	34.0	0.764	11.4	0.078

Run 11

460	33.5	0.762	11.4	0.075
470	32.5	0.770	11.6	0.073
480	32.0	0.742	11.8	0.072
490	32.0	0.742	11.9	0.070
500	31.0	0.725	12.3	0.068
510	30.5	0.720	12.6	0.068
520	29.5	0.719	13.0	0.060
530	28.5	0.708	13.8	0.092
540	28.0	0.696	14.3	0.110
550	27.0	0.696	14.7	0.126
560	26.0	0.685	15.3	0.180
570	25.5	0.673	12.6	0.220
580	34.5	0.672	15.8	0.270
590	24.0	0.650	16.1	0.318
600	24.0	0.643	16.3	0.353

Run 12

Time (sec)	FI-1 reads	CH_4 botm.	FI-2 reads	CH_4 raffint.
0	550.0	0.700	14.6	0.310
10	427.0	0.720	3.0	0.344
20	264.0	0.775	-0.4	0.363
30	122.0	0.800	-1.6	0.366
40	60.0	0.810	10.5	0.367
50	49.0	0.811	8.7	0.398
60	45.0	0.813	8.5	0.401
70	43.0	0.815	8.3	0.429
80	42.5	0.817	8.1	0.452
90	42.0	0.817	7.9	0.460
100	41.5	0.817	7.7	0.380
110	40.5	0.815	7.5	0.319
120	40.5	0.814	7.4	0.295
130	40.0	0.812	7.3	0.262
140	39.5	0.810	7.1	0.241
150	39.0	0.809	7.0	0.230
160	38.0	0.782	6.9	0.200
170	37.0	0.781	6.8	0.174
180	37.5	0.780	6.8	0.150
190	37.0	0.765	6.7	0.145
200	36.5	0.757	6.7	0.120
210	37.0	0.754	6.6	0.105
220	36.0	0.733	6.6	0.093
230	35.5	0.726	6.6	0.090
240	35.0	0.705	6.6	0.069
250	33.5	0.685	6.6	0.065
260	33.0	0.678	6.7	0.064
270	32.5	0.656	6.7	0.061
280	31.0	0.655	6.8	0.060
290	29.0	0.623	7.0	0.058
300	546.0	0.700	7.4	0.056
310	430.0	0.700	3.0	0.054

Run 12

320	305.0	0.740	0.0	0.052
330	166.0	0.772	-1.5	0.050
340	76.0	0.798	14.0	0.490
350	54.5	0.799	10.8	0.048
360	50.0	0.801	10.4	0.085
370	48.0	0.802	10.1	0.190
380	46.0	0.802	9.9	0.320
390	45.5	0.802	9.8	0.242
400	45.0	0.800	9.7	0.150
410	44.0	0.798	9.7	0.127
420	43.5	0.796	9.7	0.087
430	43.0	0.795	9.7	0.066
440	42.0	0.773	9.7	0.059
450	41.5	0.770	9.7	0.058
460	41.5	0.769	9.7	0.039
470	40.5	0.750	9.8	0.038
480	40.0	0.747	9.8	0.037
490	39.5	0.732	9.9	0.038
500	39.0	0.719	10.1	0.039
510	38.0	0.716	10.2	0.040
520	37.0	0.691	10.4	0.042
530	35.0	0.685	10.7	0.055
540	34.0	0.663	11.1	0.068
550	32.5	0.661	11.7	0.069
560	30.5	0.638	12.5	0.099
570	30.0	0.618	13.0	0.125
580	29.0	0.610	13.5	0.168
590	27.0	0.582	14.0	0.230
600	26.5	0.579	14.3	0.284

Run 13

Time (sec)	FI-1 reads	CH_4 botm.	FI-2 reads	CH_4 raffnt.
0	575.0	0.720	6.0	0.030
10	500.0	0.760	2.0	0.055
20	382.0	0.726	0.0	0.056
30	258.0	0.727	10.0	0.057
40	140.0	0.728	5.2	0.080
50	58.0	0.740	4.9	0.085
60	38.0	0.743	4.8	0.113
70	34.0	0.745	4.7	0.130
80	29.0	0.747	4.6	0.170
90	27.0	0.748	4.5	0.180
100	25.0	0.750	4.5	0.183
110	24.0	0.750	4.4	0.150
120	22.5	0.750	4.4	0.135
130	22.5	0.750	4.4	0.108
140	22.0	0.750	4.3	0.082
150	21.0	0.750	435.0	0.081
160	20.0	0.745	4.4	0.079
170	19.8	0.743	4.4	0.064
180	19.0	0.742	4.2	0.057
190	19.0	0.741	4.2	0.055
200	18.5	0.740	4.2	0.054
210	18.5	0.738	4.3	0.050
220	18.0	0.735	4.3	0.050
230	18.0	0.732	4.2	0.048
240	18.0	0.716	4.2	0.460
250	17.5	0.711	4.2	0.450
260	17.0	0.710	4.2	0.042
270	575.0	0.710	4.2	0.040
280	500.0	0.753	1.6	0.039
290	382.0	0.720	0.0	0.037
300	258.0	0.719	14.0	0.035
310	170.0	0.719	5.7	0.035

Run 13

320	84.0	0.720	5.7	0.035
330	45.0	0.741	5.3	0.036
340	37.0	0.741	5.1	0.038
350	32.5	0.741	5.1	0.042
360	30.0	0.742	5.1	0.061
370	29.0	0.742	5.1	0.090
380	27.0	0.741	5.1	0.108
390	26.0	0.741	5.1	0.056
400	25.5	0.740	5.1	0.038
410	25.0	0.738	5.1	0.032
420	24.0	0.736	5.1	0.030
430	23.5	0.735	5.1	0.028
440	22.0	0.732	5.1	0.027
450	22.5	0.730	5.2	0.025
460	21.5	0.722	5.2	0.023
470	21.0	0.710	5.2	0.023
480	21.0	0.710	5.3	0.023
490	20.5	0.709	5.3	0.025
500	20.5	0.708	5.4	0.026
510	20.0	0.705	5.4	0.028
520	19.5	0.703	5.5	0.030
530	19.0	0.702	5.9	0.032
540	18.5	0.700	6.1	0.035

Run 14

Time (sec)	FI-1 reads	CH_4 botm.	FI-2 reads	CH_4 raffnt.
0	578.0	0.748	4.2	0.010
10	480.0	0.748	1.2	0.010
20	390.0	0.748	-0.2	0.010
30	288.0	0.747	9.4	0.010
40	200.0	0.748	3.2	0.010
50	92.0	0.749	3.1	0.010
60	58.0	0.750	3.1	0.010
70	50.0	0.752	3.1	0.010
80	46.0	0.753	3.1	0.010
90	42.0	0.754	3.1	0.010
100	40.0	0.752	3.1	0.010
110	38.0	0.739	3.1	0.010
120	37.0	0.731	3.1	0.010
130	35.5	0.729	3.1	0.010
140	35.0	0.720	3.1	0.010
150	33.5	0.709	3.1	0.010
160	32.0	0.708	3.1	0.010
170	31.5	0.688	3.1	0.010
180	31.0	0.686	3.1	0.010
190	30.0	0.670	3.1	0.010
200	29.5	0.659	3.1	0.010
210	29.0	0.640	3.1	0.010
220	28.5	0.633	3.1	0.010
230	28.0	0.613	3.1	0.010
240	27.0	0.610	3.1	0.010
250	26.0	0.587	3.1	0.010
260	25.0	0.585	3.1	0.010
270	568.0	0.750	3.1	0.010
280	480.0	0.750	1.1	0.005
290	400.0	0.730	-0.2	0.005
300	305.0	0.728	12.5	0.005
310	252.0	0.728	4.3	0.005

Run 14

320	130.0	0.728	4.1	0.005
330	70.0	0.728	4.1	0.005
340	54.0	0.729	4.1	0.005
350	49.0	0.730	4.1	0.005
360	45.5	0.714	4.2	0.005
370	43.0	0.714	4.2	0.005
380	41.5	0.694	4.2	0.005
390	39.5	0.689	4.2	0.005
400	38.5	0.686	4.2	0.005
410	37.5	0.666	4.2	0.005
420	36.0	0.645	4.2	0.005
430	35.0	0.636	3.1	0.005
440	34.0	0.620	2.7	0.005
450	32.5	0.608	2.7	0.005
460	31.5	0.600	2.7	0.005
470	31.0	0.580	2.7	0.005
480	30.0	0.555	2.7	0.005
490	29.5	0.551	2.7	0.005
500	28.5	0.525	2.7	0.005
510	27.0	0.505	2.7	0.005
520	26.5	0.495	2.7	0.005
530	26.0	0.480	2.7	0.005
540	26.0	0.465	2.8	0.005

Run 15

Time (sec)	FI-1 reads	CH_4 botm.	FI-2 reads	CH_4 raffnt.
0	555.0	0.755	21.8	0.360
10	485.0	0.878	4.8	0.384
20	380.0	0.770	31.0	0.386
30	295.0	0.750	17.6	0.387
40	210.0	0.748	16.3	0.407
50	110.0	0.746	15.7	0.409
60	27.7	0.745	15.5	0.410
70	25.6	0.745	15.8	0.412
80	22.0	0.747	16.0	0.413
90	19.5	0.749	16.4	0.386
100	17.8	0.750	17.0	0.290
110	16.2	0.752	17.5	0.246
120	15.1	0.754	18.0	0.232
130	14.2	0.755	18.3	0.230
140	13.4	0.756	18.5	0.250
150	604.0	0.757	18.6	0.282
160	500.0	0.873	5.0	0.305
170	400.0	0.780	35.8	0.334
180	290.0	0.747	20.2	0.358
190	200.0	0.748	18.6	0.378
200	70.0	0.748	18.0	0.401
210	33.0	0.748	18.0	0.403
220	27.0	0.748	18.4	0.405
230	25.6	0.749	19.0	0.407
240	21.8	0.751	19.6	0.310
250	19.8	0.752	20.1	0.243
260	18.4	0.755	20.6	0.223
270	17.3	0.755	21.0	0.238
280	16.4	0.756	21.1	0.257
290	15.8	0.757	21.2	0.310
300	15.3	0.755	21.2	0.338

Run 16

Time (sec)	FI-1 reads	CH_4 botm.	FI-2 reads	CH_4 raffnt.
0	285.0	0.795	33.2	0.386
10	490.0	0.802	4.0	0.388
20	390.0	0.795	28.0	0.390
30	280.0	0.794	25.1	0.392
40	100.0	0.796	24.8	0.394
50	64.0	0.801	24.8	0.393
60	44.0	0.817	24.6	0.395
70	38.0	0.818	24.4	0.396
80	34.0	0.819	23.6	0.398
90	30.5	0.820	22.9	0.358
100	29.5	0.821	22.8	0.260
110	28.0	0.822	22.8	0.225
120	26.0	0.823	23.1	0.222
130	25.0	0.824	23.6	0.200
140	24.0	0.823	24.6	0.198
150	23.0	0.823	25.5	0.196
160	22.0	0.820	26.2	0.176
170	21.5	0.819	26.8	0.174
180	21.0	0.818	26.9	0.174
190	20.5	0.815	27.0	0.205
200	20.0	8.140	27.0	0.253
210	20.0	0.813	27.0	0.305
220	20.0	0.810	27.0	0.345
230	19.5	0.795	27.2	0.373
240	285.0	0.794	27.2	0.375
250	264.0	0.794	8.0	0.388
260	400.0	0.794	1.2	0.399
270	310.0	0.775	28.9	0.397
280	200.0	0.790	26.7	0.396
290	88.0	0.800	26.2	0.394
300	50.0	0.801	26.1	0.392
310	42.0	0.804	25.8	0.393
320	37.0	0.806	25.6	0.360
330	34.5	0.807	25.5	0.300
340	33.0	0.811	25.8	0.230
350	31.0	0.812	26.2	0.205
360	30.0	0.812	27.3	0.198
370	28.0	0.811	8.4	0.173
380	27.0	0.810	29.2	0.170
390	26.0	0.809	29.9	0.168
400	25.5	0.806	30.2	0.180
410	25.0	0.804	30.6	0.240
420	24.0	0.803	30.6	0.298
430	23.5	0.802	30.6	0.340
440	23.0	0.800	30.6	0.370
450	23.0	0.798	30.6	0.379
460	22.5	0.788	30.6	0.381
470	22.5	0.785	30.8	0.382
480	22.0	0.785	30.8	0.385

Run 17

Time (sec)	FI-1 reads	CH_4 botm.	FI-2 reads	CH_4 raffnt.
0	588.0	0.773	27.1	0.382
10	490.0	0.798	8.0	0.383
20	380.0	0.792	3.5	0.385
30	384.0	0.792	23.0	0.386
40	160.0	0.793	20.3	0.386
50	76.0	0.796	20.3	0.386
60	46.0	0.797	20.3	0.386
70	39.0	0.813	20.0	0.387
80	34.0	0.813	19.8	0.390
90	32.0	0.813	19.6	0.392
100	30.5	0.814	19.6	0.350
110	27.5	0.814	19.5	0.250
120	27.0	0.814	19.5	0.219
130	26.0	0.814	19.6	0.217
140	25.0	0.814	19.8	0.195
150	24.0	0.812	20.4	0.191
160	23.0	0.811	21.0	0.180
170	22.0	0.808	21.8	0.168
180	22.0	0.806	22.4	0.165
190	20.5	0.805	22.8	0.163
200	20.5	0.803	23.0	0.162
210	20.0	0.801	23.2	0.193
220	20.0	0.800	23.3	0.230
230	20.0	0.786	23.3	0.280
240	560.0	0.783	23.3	0.330
250	470.0	0.783	8.0	0.350
260	310.0	0.783	1.0	0.358
270	284.0	0.781	25.9	0.358
280	188.0	0.782	23.2	0.374
290	84.0	0.785	22.7	0.375
300	45.0	0.800	22.4	0.375
310	42.0	0.800	22.1	0.379
320	37.0	0.800	21.8	0.381
330	35.0	0.801	21.7	0.348
340	33.5	0.801	21.7	0.280
350	31.5	0.802	22.0	0.220
360	30.0	0.803	22.4	0.195
370	29.0	0.802	23.4	0.172
380	27.0	0.801	24.2	0.168
390	26.5	0.800	24.9	0.144
400	26.0	0.799	25.4	0.144
410	25.0	0.797	25.8	0.144
420	24.0	0.795	26.1	0.182
430	24.0	0.779	26.2	0.230
440	24.0	0.779	26.6	0.280
450	23.5	0.779	26.6	0.335
460	23.5	0.778	26.4	0.350
470	23.0	0.775	26.5	0.370
480	22.0	0.774	26.5	0.375

Run 1N

Time (sec)	FI-1 reads	CH_4 botm.	FI-1 reads	CH_4 top
0	20.6	0.760	35.6	0.162
10	285.0	0.759	2.0	0.163
20	340.0	0.774	32.0	0.165
30	300.0	0.785	2.1	0.166
40	180.0	0.810	12.0	0.167
50	120.0	0.814	16.0	0.190
60	78.0	0.816	18.1	0.200
70	70.0	0.818	19.2	0.260
80	64.0	0.820	12.0	0.250
90	62.5	0.818	18.8	0.200
100	59.0	0.816	20.0	0.190
110	57.5	0.806	18.8	0.187
120	56.0	0.797	19.3	0.185
130	54.0	0.794	19.2	0.166
140	52.0	0.770	19.6	0.162
150	50.0	0.750	18.8	0.138
160	48.3	0.740	20.0	0.136
170	46.7	0.748	12.0	0.134
180	45.0	0.725	35.6	0.117
190	290.0	0.725	4.0	0.117
200	340.0	0.770	35.6	0.118
210	300.0	0.798	3.0	0.118
220	220.0	0.824	-0.2	0.118
230	148.0	0.842	-1.3	0.145
240	90.0	0.841	20.1	0.170
250	76.0	0.843	20.0	0.280
260	68.5	0.845	24.0	0.240
270	66.5	0.847	19.4	0.189
280	65.5	0.847	20.0	0.180
290	64.0	0.845	19.2	0.167
300	62.5	0.844	18.6	0.164
310	61.0	0.841	20.0	0.163
320	60.0	0.823	20.0	0.161
330	58.0	0.817	10.0	0.160
340	56.0	0.813	20.0	0.130
350	53.0	0.790	20.4	0.109
360	50.0	0.773	35.6	0.103

Run 3N

Time (sec)	FI-1 reads	CH_4 botm.	FI-2 reads	CH_4 top
0	50.0	0.781	27.2	0.365
10	410.0	0.830	35.6	0.383
20	400.0	0.830	34.2	0.385
30	315.0	0.840	6.8	0.384
40	180.0	0.867	27.7	0.386
50	112.0	0.869	25.6	0.427
60	80.0	0.871	25.8	0.276
70	72.0	0.873	26.1	0.249
80	63.0	0.875	26.2	0.238
90	65.0	0.878	26.3	0.224
100	62.8	0.879	26.4	0.213
110	61.6	0.879	26.6	0.194
120	60.5	0.879	26.8	0.171
130	58.0	0.876	27.5	0.166
140	55.0	0.874	28	0.147
150	54.0	0.853	27.6	0.14
160	50.0	0.848	27.4	0.138
170	49.0	0.825	26.9	0.136
180	47.0	0.816	26.2	0.134
190	400.0	0.852	35.6	0.168
200	390.0	0.830	34.1	0.169
210	305.0	0.832	13.2	0.202
220	222.0	0.846	8	0.265
230	140.0	0.864	25.8	0.345
240	93.0	0.867	26.3	0.188
250	79.0	0.868	26.4	0.18
260	74.0	0.870	26.1	0.17
270	72.0	0.873	26.5	0.16
280	70.0	0.875	26.7	0.131
290	67.0	0.874	27.3	0.12
300	65.0	0.872	27.7	0.107
310	62.3	0.874	27.8	0.106
320	59.7	0.873	27.8	0.12
330	57.0	0.872	27.2	0.142
340	54.7	0.875	27.1	0.21
350	52.3	0.854	27.1	0.27
360	50.0	0.830	26.8	0.314

Run 4N

Time (sec)	FI-1 reads	CH_4 botm.	FI-2 reads	CH_4 top
0	280.0	0.730	27.4	0.100
10	260.0	0.752	8.4	0.260
20	345.0	0.770	35.6	0.285
30	278.0	0.783	26.6	0.320
40	130.0	0.790	25.1	0.340
50	90.0	0.805	25.8	0.368
60	68.0	0.806	25.4	0.370
70	62.0	0.806	25.7	0.270
80	58.0	0.806	25.7	0.205
90	56.0	0.806	25.7	0.198
100	54.0	0.805	25.8	0.168
110	52.0	0.803	26.0	0.143
120	51.5	0.802	26.3	0.140
130	50.0	0.785	26.0	0.110
140	48.0	0.781	26.8	0.090
150	46.0	0.780	27.3	0.085
160	44.0	0.777	27.5	0.084
170	42.0	0.756	27.5	0.082
180	41.0	0.754	27.6	0.105
190	260.0	0.733	10.0	0.232
200	345.0	0.750	35.6	0.285
210	278.0	0.763	29.2	0.230
220	204.0	0.775	25.8	0.310
230	130.0	0.789	26.2	0.336
240	82.0	0.790	26.3	0.300
250	73.0	0.792	26.0	0.210
260	66.0	0.793	26.3	0.167
270	64.0	0.794	26.4	0.150
280	62.0	0.792	26.6	0.130
290	59.0	0.790	26.8	0.105
300	58.0	0.788	27.3	0.100
310	55.0	0.761	27.6	0.082
320	53.0	0.746	28.0	0.079
330	51.5	0.744	28.3	0.079
340	50.0	0.720	28.2	0.110
350	48.0	0.718	28.1	0.155
360	47.0	0.719	27.5	0.021

Run 5N

Time (sec)	FI-1 reads	CH_4 botm.	FI-2 reads	CH_4 top
0	50.0	0.775	28.2	0.198
10	-0.5	0.790	40.0	0.199
20	380.0	0.850	40.0	0.199
30	295.0	0.850	15.6	0.200
40	200.0	0.867	6.0	0.230
50	116.0	0.868	24.8	0.270
60	78.0	0.887	26.4	0.306
70	70.0	0.888	26.6	0.320
80	65.0	0.887	26.7	0.345
90	62.0	0.889	26.4	0.375
100	60.0	0.890	26.2	0.395
110	58.0	0.890	26.3	0.230
120	56.0	0.888	26.8	0.218
130	54.0	0.886	26.1	0.215
140	51.0	0.865	26.6	0.188
150	50.0	0.864	26.3	0.187
160	48.0	0.845	26.2	0.210
170	46.0	0.820	25.8	0.240
180	45.0	0.808	24.6	0.285
190	-0.4	0.800	40.0	0.318
200	380.0	0.830	40.0	0.321
210	305.0	0.850	19.6	0.321
220	220.0	0.851	4.0	0.348
230	140.0	0.867	24.4	0.360
240	88.0	0.869	25.4	0.376
250	76.0	0.871	25.8	0.350
260	70.0	0.873	25.8	0.200
270	67.0	0.874	25.3	0.198
280	65.0	0.878	26.2	0.197
290	62.0	0.879	26.5	0.194
300	61.0	0.880	26.8	0.193
310	59.0	0.880	26.7	0.192
320	57.0	0.870	25.7	0.250
330	55.0	0.852	26.0	0.300
340	54.0	0.830	25.6	0.328
350	51.0	0.798	25.3	0.364
360	50.0	0.770	25.6	0.385

Run 6N

Time (sec)	FI-1 reads	CH_4 botm.
0	50.0	0.813
10	-0.7	0.840
20	380.0	0.850
30	295.0	0.862
40	196.0	0.874
50	112.0	0.893
60	80.0	0.894
70	72.0	0.896
80	67.0	0.898
90	64.0	0.900
100	61.7	0.901
110	59.3	0.904
120	57.0	0.905
130	52.0	0.904
140	47.0	0.903
150	42.0	0.882
160	42.0	0.882
170	40.0	0.853
180	36.0	0.851
190	-0.5	0.840
200	375.0	0.830
210	320.0	0.845
220	260.0	0.862
230	160.0	0.891
240	96.0	0.890
250	78.0	0.891
260	73.0	0.893
270	69.0	0.891
280	66.7	0.895
290	64.3	0.899
300	62.0	0.900
310	60.3	0.900
320	58.7	0.889
330	57.0	0.880
340	54.7	0.873
350	52.3	0.840
360	50.0	0.876
Other data		
missing		

```
C   THIS PROGRAM  SOLVES THE  BINARY LINEAR  DRIVING FORCE
C   EQUATIONS

      PARAMETER(NEQ=2)
      IMPLICIT REAL*8(A-H,O-Z)
      INTEGER METH,AMITER,IWK(NEQ),IER,K
      DIMENSION Q(50),PARAM(50)
      COMMON AL2,AL1,BL2,BL1,ZETA,BETA,DELTA,THBARA,THBARB
      EXTERNAL FCN,FCNJ

      AL2  =  0.80
      AL1  =  0.0
      BL2  =  0.10
      BL1  =  0.00
      ZETA =(BL2 - BL1)/(AL2 - AL1)
      BETA =  (0.1D+01)
      DELTA=  1.0/5.0
      AOMEGA=0.35
      BOMEGA=0.35
      THBARA=AL1*AOMEGA + (1.0-AOMEGA)*AL2
      THBARB=BL1*BOMEGA + (1.0-BOMEGA)*BL2
     T=0.0
      DO 4 K=1,NEQ
      Q(K)=0.0
   4  CONTINUE
C ******** IMSL VARIABLES ********************
C -------- TFIN = FINAL TIME -----------------
C -------- DTPRNT = PRINT INTERVAL -----------
       TFIN =0.2000
       DTPRNT =0.005
```

```
      NPRINT = INT(TFIN/DTPRNT)
      TOL =1.0E-06
      H=1.0E-06
      METH=2
      MITER=0
      INDEX=1
C
C****************** FOR DIVPAG *******************************
      IER=0
      NPARAM=50
      CALL SSET(NPARAM,0.0,PARAM,1)
      PARAM(1)=H
      PARAM(4)=1000000
      PARAM(12)=METH
      PARAM(13)=MITER
      PARAM(19)=0
      WRITE (7,9)
      WRITE (17,9)
 9    FORMAT (/7X,' TIME          UPTAKE(A)        UPTAKE(B)'/)
      DO 10 K=1,NPRINT
      TEND=DTPRNT*FLOAT(K)
      WRITE(6,*)'  T = ', T, '   TEND = ',TEND
      CALL DIVPAG(INDEX,NEQ,FCN,FCNJ,DUMMY,T,TEND,TOL,PARAM,Q)
      WRITE(7,21)T,Q(1),Q(2)
      WRITE(17,21)T,Q(1),Q(2)
 21   FORMAT (2X,3(F14.7,2X))
 10   CONTINUE
      STOP
      END
```

```
 SUBROUTINE  FCN(NEQ,T,Q,QPRIME)
 IMPLICIT REAL*8(A-H,O-Z)
 COMMON AL2,AL1,BL2,BL1,ZETA,BETA,DELTA,THBARA,THBARB
 DIMENSION QPRIME(50),Q(50)
 INTEGER NEQ
 QPRIME(1)=(15.0/(1.0-THBARA-THBARB))*(  ((1.0-THBARB)*(1.0-Q(1)))
@ + (ZETA * THBARA* ( 1.0 - Q(2))) )
 QPRIME(2)=(15.0*DELTA/(1.0-THBARA-THBARB))*( ((1.0-THBARA)
@ *(1.0-Q(2))) + ((BETA*THBARB) * ( 1.0 - Q(1) )))
 RETURN
 END

 SUBROUTINE FCNJ(N,T,Y,PD)
 IMPLICIT REAL*8(A-H,O-Z)
 INTEGER N
 REAL*8  Y(N),PD(N,N),T
 RETURN
 END
```

Vitae

Name	Mohammad Arshad Sheikh
Date of Birth	September 23, 1968
Home Address	141 Saidpur Scheme II, Satellite Town, Rawalpindi-46300, Pakistan
Educational Record	Awarded B. Sc. degree in Chemical Engineering with honors from University of Engineering and Technology, Lahore, Pakistan (1992). Awarded M. S. degree in Chemical Engineering from King Fahd University of Petroleum & Minerals, Dhahran, Saudi Arabia (1995).
Practical Experience	Served as a Process Engineer at Fauji Fertilizer Company, Rawalpindi, Pakistan in 1993. Returning to a higher rank at the same company in 1996.
Research Publications	1) Sheikh, M. A. and E. Z. Hamad "A Three-Phase Model for Adsorption in Microporous Zeolites". Submitted to *Langmuir*. 2) Sheikh, M. A., M. M. Hassan and K. F. Loughlin "Adsorption Equilibrium and Rate Parameters for Methane and Nitrogen on MAXSORB Activated Carbon". Submitted to *Gas Separation and Purification*. 3) Sheikh, M. A., K. F. Loughlin, M. M. Hassan and A. I. Fatehi "Equilibrium PSA Separation of a Methane-Nitrogen Mixture on MAXSORB Activated Carbon". Submitted to *Adsorption*.